Multivariate Iterative Filtering for Multichannel EEG Signal Processing

Ph.D. Thesis

by

Kritiprasanna Das

Department of Electrical Engineering

INDIAN INSTITUTE OF TECHNOLOGY INDORE

June 2024

Multivariate Iterative Filtering for Multichannel EEG Signal Processing

A Thesis

Submitted in partial fulfillment of the requirements for the award of the degree
of
Doctor of Philosophy

by

Kritiprasanna Das

Department of Electrical Engineering
INDIAN INSTITUTE OF TECHNOLOGY INDORE

June 2024

INDIAN INSTITUTE OF TECHNOLOGY INDORE

I hereby certify that the work which is being presented in the thesis entitled **Multivariate Iterative Filtering for Multichannel EEG Signal Processing** in the partial fulfillment of the requirements for the award of the degree of **Doctor of Philosophy** and submitted in the **Department of Electrical Engineering**, Indian Institute of Technology Indore, is an authentic record of my own work carried out during the time period from **July 2019** to **June 2024** under the supervision of **Prof. Ram Bilas Pachori**.

The matter presented in this thesis has not been submitted by me for the award of any other degree of this or any other institute.

Kritiprasanna Das
06 November 2024

Signature of the student with date

(Kritiprasanna Das)

This is to certify that the above statement made by the candidate is correct to the best of my knowledge.

06.11.2024

Signature of Thesis Supervisor with date

(Prof. Ram Bilas Pachori)

Kritiprasanna Das has successfully given his Ph.D. Oral Examination held on 05 November 2024.

06.11.2024

Signature of Thesis Supervisor with date

(Prof. Ram Bilas Pachori)

ACKNOWLEDGEMENTS

I am deeply grateful to many people who have supported me throughout my PhD journey.

First of all, I would like to express my sincere gratitude to my supervisor, Prof. Ram Bilas Pachori, for his invaluable guidance, continuous support, motivation, and patience throughout my PhD study. His immense knowledge and experience have been crucial in shaping my research and academic development. I consider this a great opportunity to learn from his expertise and perform PhD research under his guidance.

I would also like to thank the members of my PhD Student's Progress Committee (PSPC), Prof. Ritunesh Kumar and Prof. Santosh K. Vishvakarma, for their insightful comments and encouragement, which have significantly improved the quality of my research.

I would like to convey my sincere thanks to the external examiners of the thesis for their constructive and motivating comments.

Special thanks to my colleagues and friends in the Signal Analysis Research Lab (SARL) for creating a stimulating and friendly environment to learn and grow. I would like to appreciate the fine company of my dearest colleagues and friends, especially Pradeep Kumar Chaudhary, Vivek Kumar Singh, Shailesh Bhalerao, Ashok Mahato, Aditya Nalwaya, Nabasmita Phukan, Achinta Mondal, and Maharana Pratap Singh.

My sincere acknowledgment to the Director of the Indian Institute of Technology Indore, for providing me the opportunity to explore my research capabilities at the Indian Institute of Technology Indore. I would like to thank the Head of the Department, Electrical Engineering, for kind support. I am also indebted to the administrative and technical staff at the Indian Institute of Technology Indore, India, whose support has been invaluable in overcoming many logistical and technical challenges during my research.

I express my deepest appreciation to my school teachers, whose early encouragement and dedication laid the foundation for my love of learning. I would also like to thank my undergraduate and postgraduate professors at the Academy of Technology, India (Maulana Abul Kalam Azad University of Technology, formerly known as West Bengal University of Technology) and the National Institute of Technology Arunachal Pradesh, India. Their profound knowledge and commitment to excellence have been instrumental in shaping my academic path.

My heartfelt thanks go to my family for their unconditional support and encouragement. To my parents (Smt. Malati Das and Sri Nabakumar Das), sister (Prajnadipta Das Bag), and brother (Dhritinandan Koley and Benimadhab Bag), who have always believed in me and provided unwavering support throughout my academic journey. It is difficult to express my gratitude towards my parents for their blessings, which have always been my strength. To my spouse, Sudipa Rani Adak, for her love, patience, and understanding during the highs and lows of this endeavor.

I would also like to acknowledge the funding agencies that supported my research, particularly the University Grant Commission, India, for providing the financial resources necessary to complete my work. I would like to thank all those who have contributed to this thesis, directly or indirectly. Your support and contributions have been instrumental in the completion of my PhD.

I extend my deepest gratitude to the omnipotent Supreme Lord for granting me the opportunity, strength, and ability to undertake and successfully complete this research work.

Kritiprasanna Das

Dedicated

to
My Parents

ABSTRACT

The human brain is a highly complex organ that contains 100 billion neurons interacting with each other to perform day-to-day tasks. Electroencephalogram (EEG) is the recording of electrical activity of the brain results from the summations of excitatory and inhibitory postsynaptic potentials of relatively large groups of synchronously firing neurons. The processing of EEG signals has become a cornerstone in neurophysiological research and clinical diagnostics, providing insights into brain function and aiding in the development of brain-computer interface (BCI). EEG provides high temporal resolution with limited spatial resolution. A higher number of electrodes are used to record multichannel dense EEG signals for improved spatial resolution. This thesis extends the univariate adaptive signal decomposition technique, iterative filtering, to multivariate iterative filtering (MIF) for analyzing multichannel signals. Based on MIF, this thesis presents novel methodologies for the analysis of EEG signals, addressing critical challenges such as feature extraction, classification for neurological disease diagnosis, and BCI applications.

The thesis proposed automated neurological disease diagnosis frameworks using MIF algorithms and machine learning frameworks. It introduced multichannel EEG rhythm separation techniques using the MIF algorithm, significantly advancing the development of schizophrenia detection. Additionally, it develops a diagnostic feature based on the area under the Euclidean distance curve obtained from phase-space representation (PSR), which has been successfully used to classify Parkinson's disease EEG signals. The decision level and feature level fusion strategies have been proposed to improve the sensitivity in Parkinson's disease identification.

The thesis has contributed to developing BCI frameworks based on the detection of motor imagery (MI) movement, steady-state visual evoked potential (SSVEP) frequency, and drowsiness from multichannel EEG. The mode-alignment oscillatory modes obtained from MIF enabled extracting features based on common spatial patterns from multichannel EEG signals. These features have proven effective for the MI BCI framework. Canonical correlation analysis (CCA) is traditionally used for identifying SSVEP frequency, which has been suggested as a feature extraction method. The MIF-CCA features have been used to develop a robust SSVEP framework with improved performance in mobile environments. Furthermore, the thesis proposed a joint time-frequency framework based on MIF and discrete energy separation algorithms, which has been used to develop a drowsiness detection framework from EEG. The proposed algorithms have been evaluated using real-time EEG databases. Finally, the thesis concludes the presented work and discusses directions for future research.

The performance of the proposed frameworks has also been compared with the state-of-the-art methods. This thesis contributes to the field of EEG signal processing by presenting innovative methods for multichannel signal decomposition, feature extraction, and classification. The findings offer promising implications for the development of more effective diagnostic tools and interactive brain-computer systems, highlighting the importance of adaptive signal decomposition and machine learning-based techniques in future neurotechnological applications.

Keywords: Brain-computer interface (BCI), drowsiness detection, electroencephalogram (EEG), neurological disease, motor imagery movement detection, multivariate iterative filtering (MIF), Parkinson's disease, schizophrenia, steady-state visual evoked potential (SSVEP).

Contents

List of Figures

List of Tables

List of Abbreviations

Acc	Accuracy
AE	Amplitude envelope
ANN	Artificial neural network
ADHD	Attention deficit hyperactivity disorder
ADMM	Alternating direction method of multipliers
AUC	Area under the receiver operating characteristic curve
BCI	Brain-computer interface
CCA	Canonical correlation analysis
CNN	Convolutional neural network
CSP	Common spatial patterns
CT	Computed tomography
DESA	Discrete energy separation algorithm
ECG	Electrocardiogram
EEG	Electroencephalogram
EEMD	Ensemble EMD
EMD	Empirical mode decomposition
EMG	Electromyogram
EOG	Electrooculogram
ERD	Event-related desynchronization
ERS	Event-related synchronization
EWT	Empirical wavelet transform
ERP	Event-related potential
FBCCA	Filter bank CCA
FBCSP	Filter bank CSP
FBDM	Fourier-Bessel decomposition method
FBSE	Fourier-Bessel series expansion
FBSE-EWT	FBSE-based EWT
FFT	Fast Fourier transform
FL	Frontal lobe

fMRI	Functional MRI
FN	False negative
FP	False positive
FPL	Frontal and parietal lobe
IF	Instantaneous frequency
IMF	Intrinsic mode function
JTFR	Joint TFR
KNN	k-nearest neighbors
LDA	Linear discriminant analysis
LSTM	Long short-term memory
MEG	Magnetoencephalography
MEMD	Multivariate EMD
MEWT	Multivariate EWT
M-FBSE-EWT	Multivariate FBSE-EWT
MI	Motor imagery
MIF	Multivariate iterative filtering
MIF-CCA	MIF-based CCA
MIMF	multivariate IMF
MRI	Magnetic resonance imaging
MSE	Mean square error
MSP	Midline sagittal plane
MVMD	Multivariate VMD
MvFIF	Multivariate fast iterative filtering
NA-MEMD	Noise assisted MEMD
NHTSA	National highway traffic safety administration
NIRS	Near-infrared spectroscopy
PET	Positron emission tomography
PLI	Power line interface
PPG	Photoplethysmogram
PPV	Positive predictive value

PSD	Power spectral density
PSG	Polysomnography
PSR	Phase-space representation
ReLU	Rectified linear unit
REM	Rapid eye movement
SD	Standard deviation
Sen	Sensitivity
SMC	Sensory-motor cortex
Spe	Specificity
SPET	Single photon emission tomography
SSVEP	Steady-state visual evoked potential
STFT	Short-time Fourier transform
SVM	Support vector machine
TFR	Time-frequency representation
TMS	Transcranial magnetic stimulation
TN	True negative
TP	True positive
t-SNE	t-distributed stochastic neighbor embedding
VMD	Variational mode decomposition

Chapter 1

Introduction

A German neuropsychiatrist, Hans Berger, discovered electroencephalogram (EEG) for humans [1]. The EEG is an electrophysiological method for capturing electrical activity generated by a large group of neural populations in the human brain. Due to the exceptional temporal sensitivity of EEG, it is useful for studying dynamic brain activity. EEG is especially helpful for diagnosing patients with epilepsy and probable seizures [2], dementia [3], etc. Nowadays, EEG has been extensively used for research in the areas of neuroscience, cognitive psychology, cognitive science, brain-computer interface (BCI), and neurolinguistics [4, 5, 6].

EEG has also been used for a number of other clinical purposes. For example, EEG can be used to track the level of anesthesia during surgery, to detect motor imagery (MI) movements, etc., because it is so sensitive to detecting quick changes in brain activity. EEG has shown to be very useful for monitoring the depth of anesthesia and for keeping an eye out for prospective issues like ischemia or infarction [7]. The average of EEG waveforms corresponding to a particular task gives rise to evoked potentials and event-related potentials (ERPs). These potentials represent the neural activity of interest that is temporally related to a specific stimulus. In both clinical practice and research, evoked potentials and ERPs are utilized to examine auditory, visual, somatosensory, and higher cognitive functioning.

In the cerebral cortex, the cortical pyramidal neurons, positioned perpendicular to the surface of the brain, are assumed to be the main source of the EEG. The summation of the excitatory and inhibitory postsynaptic potentials of relatively large groups of synchronously firing neurons can be detected by the EEG [1]. Traditional EEG recorded on the scalp or cortical surface can not record the momentary local field potential changes resulting from neuronal action potentials [8, 9].

1.1 EEG Acquisition

The acquisition of physiological signals and images has become necessary in the early diagnosis of various diseases. Examples of few of the recordings of the electrical activity of the human body are electrocardiogram (ECG) [10], electromyogram (EMG) [11], EEG [5, 9], electrogastrogram [12], and electrooculogram (EOG) [13] signals which represent the electrical activity of the heart, muscles, brain, stomach, and eye, respectively. Similarly, magnetoencephalography (MEG) is the measurement of the magnetic field generated due to electrical activity in the neurons of the human brain. There are various imaging techniques also which play an equal role in early or on-time diagnosis of disease, such as sonography (ultrasound imaging), magnetic resonance imaging (MRI), functional MRI (fMRI), computed tomography (CT), positron emission tomography (PET), single photon emission tomography (SPET), and near-infrared spectroscopy (NIRS) [5]. EEG, MEG, and fMRI signals and images capture the physiological and functional changes happening inside the brain. The applications of fMRI as compared to EEG or MEG signals are limited because of the following reasons [14]:

1. fMRI has very low time resolution, i.e., approximately 2 frames/s.

2. fMRI cannot capture various mental activities and brain disorders as they have less effect on the level of blood oxygenation.

3. fMRI is limited access as well costly.

4. Additionally, fMRI demands a sophisticated lab setup.

In contrast with other neuroimaging techniques, EEG has not been limited by the aforementioned limitations. In this paragraph, the evaluation of EEG technology is discussed in short. The very first electrical neural activity was captured with the help of a simple galvanometer. As the pointer variation of the galvanometer was very fine, light was projected on the galvanometer and reflected on a wall with the help of a mirror in order to record or visualize the variations. Lippmann and Marey introduced the capillary electrometer. In 1903, Einthoven introduced the string galvanometer, which is a very sensitive and accurate measuring instrument. The string galvanometer enabled photographic recording and became a standard instrument for a few decades. The recent EEG recording systems consist of a set of components, namely, delicate electrodes, one differential amplifier per channel or electrode, filters, and registers. The multichannel EEG signals captured using the aforementioned systems could be plotted on the paper. After the arrival of this product in the market, researchers felt a need for a system that can digitize (using multichannel analog-to-digital converters) and store it, as analysis of these on computers needed the same [14].

The computerized EEG recording systems are equipped with stimulations, control on the sampling frequency, and availability of some advanced signal processing tools to preprocess the recorded signals. Generally, most of the significant information is present in the 0-100 Hz frequency region; therefore, a minimum sampling rate of 200 samples/s is required. There are few applications of EEG signal processing where high-frequency information is important; hence, flexibility in choosing the sampling rate up to approximately 2000 samples/s is provided in the EEG recording devices.

For the quantization of the EEG signals, the 16-bit quantization is very popular as it maintains the diagnostic information. This makes the archiving volume of the EEG signals very high for applications like epileptic seizure monitoring and sleep EEG records. Therefore, for archiving the longer-duration EEG signals from so many patients, a larger storage facility is required in diagnostic or research centers and hospitals.

The EEG electrodes and their proper functioning play a very important role in the quality of acquired data. There are several types of EEG electrodes used for EEG signal recording, namely, pre-gelled and gel-less disposable electrodes; tin, stainless steel, silver, or gold reusable disc electrodes; saline-based electrodes; electrode caps; needle or cortical electrodes, etc. Ag-AgCl disk electrodes are the most commonly used ones with a diameter of less than 3 mm and have wired leads that can be connected to amplifiers. The cortical electrodes are used for recording invasive EEG signals by implanting them under the skull via minimal invasive operations. The use of high-impedance electrodes or the presence of high impedance between the cortex and the electrodes can lead to severe distortion of EEG signals. Recording of EEG signals with electrodes with impedance less than 5000 Ω provides satisfactory signal quality. Due to very low amplitude (in the range of microvolt), a high gain amplifier is required. A typical EEG amplifier usually provides a voltage gain of 5000 to 50000. The distribution of the potential is non-uniform over the scalp because of the spiral and layered structure of the brain, which may affect the results of the source localization performed using EEG signals.

1.1.1 EEG Acquisition Device

There are numerous commercially accessible EEG recording devices. Based on the application requirement, properly choosing an EEG device is important. These devices can be categorized based on the connectivity with the computer system, electrode connection, etc. [15]. Several parameters, like the number of channels, device and electrode connectivity, amplifier gain, etc., need to be carefully considered for the selection of EEG devices. Advanced wired EEG recording systems with a notch filter, different amplifier gain options are shown in Fig. 1.1.

Figure 1.1: BIOPACK 10-channel EEG recording system.

1.1.1.1 Wired and Wireless EEG

The connectivity of the acquisition device has been established using wired technology or wirelessly using Bluetooth or WiFi. Wired EEG devices provide more stable data transfer with a higher data transfer rate. Wireless EEG devices offer freedom of movement. On the other hand, lack of freedom of movement is a drawback for wired EEG. Due to the loss of wireless connectivity, data loss may happen, and a repetition of the experiment needs to be done. Movements of cables and electrodes introduce artifacts in both devices.

1.1.1.2 Electrode Connection

The proper connection between the electrode and the scalp is of utmost necessity to obtain a good-quality signal. To establish the connection between the electrode and scalp, conductive gel, saline solution, or conductive adhesive paste is used, which reduces the impedance between the scalp and electrodes. A few modern EEG devices also come up with dry electrodes. For short-duration experiments, saline solution-based or dry electrodes are suitable as the setup time of these kinds of electrodes is less. But with time, saline water will dry, and the impedance between the scalp and electrodes will increase, which deteriorates the signal quality. Due to this, conductive gel-based electrodes are preferred for long-duration experiments.

1.1.1.3 Wearable EEG

For a few applications like human-computer interaction, imagined speech recognition-based BCI systems, EEG-based rehabilitation devices, epileptic seizure onset prediction, continuous recording, and monitoring for several days and months are necessary. However, placing electrodes with wires and other bulky accessories reduces the user's comfort and restricts the long-term recording of EEG signals. Recently, researchers have been trying to develop wearable EEG electrodes with reduced channels [16, 17]. A flexible electronic system printed on the scalp, like a tattoo or ear electrode, has been developed for the recording of EEG signals for BCI applications [18].

1.1.2 Conventional EEG Electrode Positioning

In Fig. 1.2, a conventional 10-20 electrode positioning is depicted, which is recommended by the International Federation of Societies for Electroencephalography and Clinical Neurophysiology. It consists of a total of 21 electrodes, including the two earlobe electrodes (A1 and A2), which are used as reference. The name of the electrodes is given based on the cerebral lobe position, e.g., if the electrode is placed on the frontal lobe (FL), then these are named with the letter ‘F’. The electrodes in the left hemisphere are numbered with odd numbers, the right hemisphere electrodes are numbered with even numbers, and the electrodes on the longitudinal fissure are marked using the letter ‘z’ like Cz.

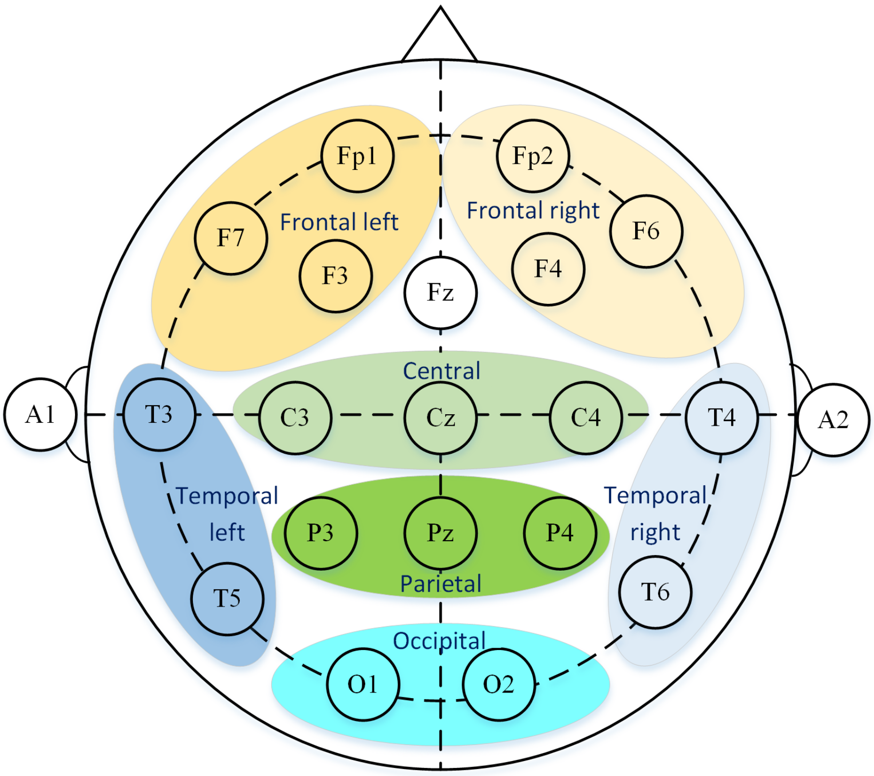

Figure 1.2: 10-20 international standard for EEG electrode position.

To record EEG with higher spatial resolution, a large number of electrodes are required where electrodes are positioned equidistantly in between the above electrodes in a typical 10-20 system. For example, F2 is placed between F4 and Fz. Extra electrodes are sometimes employed to measure the ECG, EOG, and EMG of the eyelid and surrounding muscles, which may help in multimodal applications and artifact removal. Also, for some applications like BCI, fewer number electrodes and even single electrodes are used.

The EEG signal can be recorded in a bipolar (differential) or unipolar (referential) fashion. In bipolar recording, two inputs of the amplifier are attached, with two EEG electrodes placed in different locations on the scalp. Bipolar recordings are suitable for the analysis of localized neural activity. On the other hand, in unipolar recording, one or two reference electrodes are commonly connected to one input of the amplifier, and the other input of the amplifier is connected to the general EEG electrodes like F1 and F2. In literature, the reference electrodes are placed on different locations like Cz, earlobe, mastoid. There are also reference-free EEG acquisition approaches that employ a common average reference.

In a typical EEG recording experiment, the following steps are performed [19]:

1. A technician measures your head and traces your scalp with a special pencil to indicate where the electrodes will be attached.

2. Electrodes will be attached using adhesive conductive paste. Sometimes, an elastic cap with electrodes inside is used to place the electrodes all over the scalp easily.

3. Establish a proper connection between the electrodes and the amplifier for recording the EEG.

A typical experimental procedure for recording EEG signals is shown in Fig. 1.3, where an EEG cap is placed on the subject's head, and the technician is filling conductive electrode gel to establish a proper connection with the scalp. Figure 1.4 shows a 10-channel differentially recorded EEG signal [20].

1.2 EEG Artifacts

Artifacts are undesired signals which adversely affect the signal of interest. It is desirable to prevent artifacts from appearing while recording. However, the EEG signal is, unfortunately, frequently corrupted by physiological and environmental factors other than cerebral activity. An important component of EEG signal processing is removing noise and artifacts, which is typically required for more trustworthy signal analysis. The two

Figure 1.3: EEG cap placement and filling conductive gel.

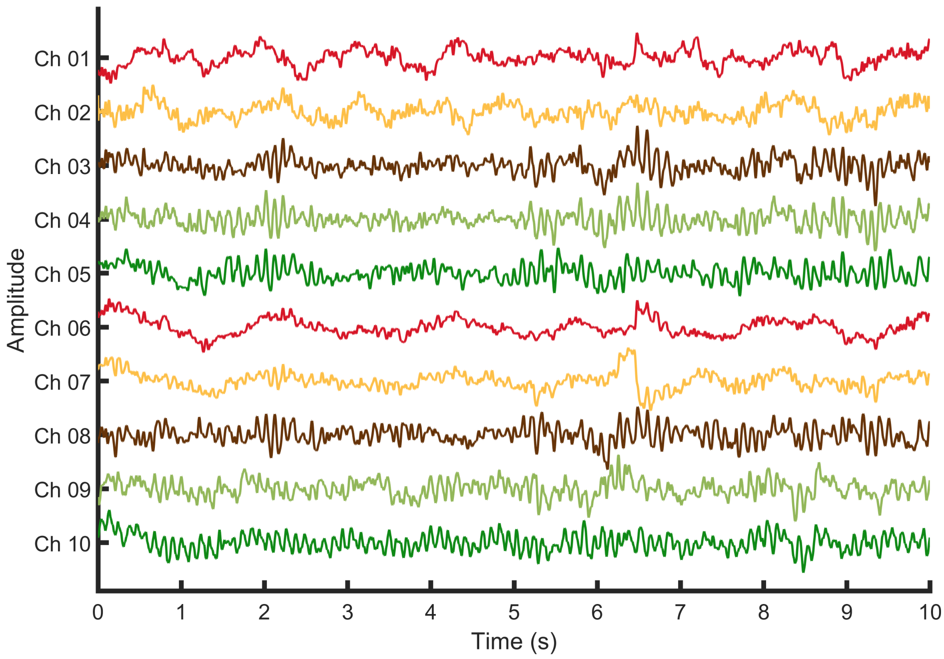

Figure 1.4: EEG signals (Ch i represents i^{th} channel EEG signal, here i varies from 1 to 10).

main types of artifacts are physiological/biological caused by non-cerebral physiological sources and nonphysiological artifacts caused by electrical phenomena or equipment in the recording environment. Physiological artifacts include eye movement, cardiac, glossokinetic, respiratory, pulse, sweat, and muscle and movement artifacts [4]. Power line noise, cable movement, and electromagnetic interference are common environmental artifacts. In the preceding section, we will give a brief overview of artifacts common to EEG.

1.2.1 Physiological Artifacts

1.2.1.1 Ocular Artifact

Significant artifacts are generated by ocular movements in the EEG recordings. Eye movements and blinks are the cause of ocular artifacts. To be more precise, retinal and corneal dipole orientation alterations cause eye movement artifacts, and alterations of contact of the cornea with the eyelid affect ocular conductance, which results in blink artifacts.

Moreover, the ocular artifact spread to the head's surface and was recorded by the EEG electrodes as a result of the volume conduction effect. EOG often has a frequency similar to EEG signals and an amplitude many times greater than EEG, which disqualifies frequency domain filtering as an artifact removal technique [21].

1.2.1.2 Muscle Artifact

Activities from different groups of muscles contaminate EEG, which is known as muscle artifacts. These artifacts can be caused by the subject's talking, sniffing, swallowing, or muscle contraction and stretch close to the signal recording sites. Depending on the muscles are stretched and contracted, the amplitude and shape of the EMG will change. Conceivably, muscle activities detected by EMG have a wide frequency range between 0 Hz and 200 Hz. Obtaining the activity from a single channel measurement is extremely difficult compared to EOG and eye-tracking. As a result, it can be extremely difficult to get rid of EMG artifacts. Significant statistical separation exists between EMG contamination and EEG in both time and space. This suggests that using independent components analysis to exclude EMG contamination would be a good idea.

1.2.1.3 Cardiac Artifact

When EEG electrodes are positioned on or close to a blood vessel, cardiac artifacts may be created due to the expansion and contraction caused by the heart. It is challenging to eliminate these pulse distortions since they can appear in the EEG with a similar waveform and with a frequency of about 1.2 Hz [27]. The electrical activity of the heart, which is known as ECG, can also be contaminated with EEG. As ECG can be monitored with a recognizable regular pattern and recorded separately from brain activity, unlike pulse artifacts, it may be simpler to remove these artifacts by simply utilizing a reference waveform.

1.2.2 Extrinsic Artifacts

In addition to the aforementioned artifacts, EEG measurement is negatively impacted by external sources of artifacts, which include cable movements, misplacement of electrodes, etc. Proper planning and improved signal acquisition can be helpful in minimizing these kinds of artifacts. Another sort of external artifact that influences the EEG data is electromagnetic interference from the environment, which belongs to a specific frequency band. Power line artifact is generated due to the interference by the power source having a frequency of 50/60 Hz [22]. Movement of any part of the recording devices, like electrode wire, can generate artifacts.

1.3 Signal Processing for EEG

EEG signals present a landscape of neural activity of the brain with high temporal resolution. At the same time, EEG suffers from drawbacks like noise prone, high complexity, etc. Due to very low amplitude (in the microvolt range), various physiological and environmental noises easily affect the EEG signal, which degrades the signal-to-noise ratio. Analysis of such noisy EEG signals may lead to erroneous interpretation. Few of these artifacts can be reduced by taking proper measures during recording, but most of them are unavoidable. To improve the signal quality and make it eligible for further processing, artifact removal is a useful pre-processing technique where signal processing has been proven to be a valuable tool. Also, to extract useful information from complex EEG signals and have meaningful interpretation, signal processing is necessary. Many adaptive signal decomposition techniques like empirical wavelet transform (EWT) [23], empirical mode decomposition (EMD) [24], multivariate EWT (MEWT) [2], multivariate iterative filtering (MIF) [25], sparse spectrum-based swarm decomposition [26], Fourier-Bessel series expansion (FBSE)-based EWT (FBSE-EWT) [27] have been used for decomposing the EEG signal and feature extraction. Time-frequency representation (TFR) of EEG signal is also helpful for classification with deep neural network [28, 29, 30]. Instead of using deep learning techniques like convolutional neural network (CNN) for classification, activation, or output from a particular layer or multiple layers are combinedly used as the deep features which can be further classified with the help of machine learning classifier [26]. A general approach for automated classification of EEG signals based on signal processing and artificial intelligence includes signal recording, pre-processing, signal decomposition and feature extraction, and classification, which is depicted in Fig. 1.5.

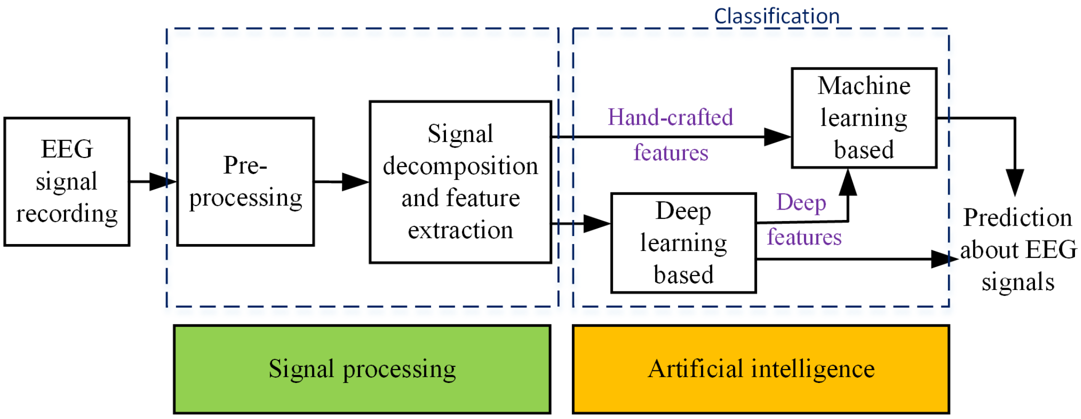

Figure 1.5: A block diagram of a general approach for automated classification of EEG signals.

1.3.1 Artifact Removal

The EEG signals are employed as a cutting-edge diagnostic tool for various neural illnesses, in BCI applications, and in studying fundamental neuroscience because they capture electrical activities produced by brain cells. But oftentimes, undesirable artifacts taint the EEG signals and make it difficult to interpret the neural activity [31, 32, 33]. Signal processing-based techniques have been proposed to remove the artifact effectively.

In this section, we will discuss a state-of-the-art artifact removal technique. A frequency-spatial filtering-based ocular artifact removal technique to remove ocular artifacts has been proposed in [31]. EWT and dictionary-based spatial filtering have been employed to develop the artifact removal framework. An isolated artifact dictionary is formed by selecting the contaminated EEG channels and EWT-based frequency domain filtering. More preciously, the delta rhythms of the highly contaminated channels are taken out and added to an artifact dictionary. Afterward, the ocular artifact is isolated by spatially filtering the delta-rhythms of multichannel EEG data using the developed dictionary. After eliminating the artifact components, the clean EEG delta-rhythm is reconstructed using inverse spatial filtering. In the end, to get the ocular artifact-free signals, the clear delta rhythms are merged with other EEG rhythms. The suggested technique eliminates the ocular artifact while leaving the baseline EEG data unchanged.

1.3.2 EEG Rhythm Separation

Visual examination of EEG data can be used to diagnose various brain illnesses. EEG signals typically have a frequency range of 0.1 to 100 Hz, and based on the frequency content, they can be further divided into five distinct rhythms. These rhythms are delta (0.1-4 Hz), theta (4-8 Hz), alpha (8-13 Hz), beta (13-30 Hz), and gamma (30-100 Hz). Clinical professionals with expertise in this area are familiar with the manifestation of brain rhythms in EEG signals. The amplitudes and frequency of these rhythms vary depending on the human's state, such as awake or asleep. Age also alters the properties of the rhythm waves [34].

1.3.3 Feature Extraction

Due to the complexity of EEG signals, it is highly challenging to extract information from them using the naked eye. These days, we may use sophisticated automatic processing methods to retrieve hidden information from EEG data owing to computers. There exist various ways to represent EEG using features such as time domain features (mean, standard deviation (SD), entropy [25, 35]), frequency domain features (mean frequency, band-power), time-frequency domain features (Shannon entropy, time-varying energy, instantaneous amplitude, and frequency [36, 37]) and synchronisity features, which look to the relationship between two or more EEG channels (coherence, mutual information, correlation), merely to name a few. Deep learning networks have also been used to extract automated or deep features from the EEG signal or TFR of the EEG signal.

1.4 Applications of EEG

A large number of studies suggested that EEG is useful for assessing human mental health states, clinical conditions, imagination, thoughts, etc. EEG finds its applications in various areas like clinical diagnosis, BCI, biometrics, fundamental neuroscience, neuromarketing, custom solutions, etc. [9, 15, 38].

1.4.1 Clinical Applications

EEG is a very useful diagnostic tool used for various neurological disease diagnoses and predictions, including but not limited to epilepsy, dyslexia, Alzheimer's disease, Parkinson's disease, attention deficit hyperactivity disorder (ADHD), sleep disorders, Huntington's disease, anxiety and depression, schizophrenia, level of consciousness. Monitoring EEG signals during neurosurgery helps to complete the procedure smoothly and properly and increases the success rate. A few representative clinical diagnostic applications are described below.

1.4.1.1 Epilepsy

The simultaneous irregular firing of a neuronal population causes epilepsy, which is the second most well-known neurological condition in the brain. Almost 60 million people worldwide are affected by epilepsy. EEG signal is a gold-standard diagnostic tool for epilepsy, but it requires long-term monitoring of the EEG signal. However, it is a laborious and time-consuming task to manually monitor the patient's EEG signal for an extended period. Furthermore, muscle artifacts, background noise, and other neurological symptomatology may contaminate the recorded EEG data. Hence, a system that automatically detects seizures will make it easier to monitor and treat epileptic seizures in real-time [2, 27, 29, 39, 40, 41]. An automated technique for focal and non-foal EEG signal classification using synchrosqueezing transform and CNN is described here.

Madhavan *et al.* [41] proposed an automated classification of focal and non-focal EEG signals. The nonstationary EEG signal is represented in the time-frequency plane using synchrosqueezing transform and wavelet synchrosqueezing transform. The two-dimensional CNN is used to classify the time-frequency matrix of EEG signals into focal and non-focal classes.

1.4.1.2 Sleep Analysis

In sleep apnea, airflow is temporarily stopped or reduced during sleep for a few seconds. This decrease in breathing is accompanied by loud snoring, which could cause the person to feel choked and awakened. Researchers have developed a number of techniques to diagnose sleep apnea. Polysomnography (PSG) has been suggested as the most effective for the analysis of sleep, which monitors several physiological parameters like brain waves, heart rate, breathing pattern, eye movements, blood oxygen level, limb and body movements, snoring sound, etc. Simultaneous recording of these parameters is complicated and creates user discomfort. Also, the analysis of PSG is cumbersome and tedious. There are six stages of sleep for a healthy person: awake, S1, S2, S3, S4, and rapid eye movements (REM) [30]. Precise sleep stage grading can provide clinical information for identifying people with sleep disorders [42]. The automatic detection of sleep stages and sleep apnea from biological signals using signal processing and artificial intelligence-based techniques have been reported in many research [26, 43]. One such method for the sleep stage scoring from EEG signals is described here.

The nonstationary signal analysis technique, namely the Fourier-Bessel decomposition method (FBDM) and deep learning classifier, are used for scoring the different sleep stages from the EEG signal [30]. The FBDM is used to decompose EEG signals into oscillatory modes or Fourier-Bessel intrinsic band functions, which are suitable for obtaining instantaneous frequency (IF) and amplitude envelope (AE) using Hilbert transform. A time-frequency image is obtained from the IF and AE of the EEG signal. CNN has been employed to classify the time-frequency image of EEG signals. Using EEG signals, the developed method has been utilized to categorize six different stages of sleep.

1.4.2 Brain-computer Interface and Rehabilitation Applications

In many pieces of research, EEG signals have been suggested for BCI-based rehabilitation applications, where an alternative communication path has been established between the brain and the outside world.

1.4.2.1 Emotion Recognition

Emotions are essential to human existence and have an impact on daily functions like cognition, decision-making, and intelligence, among many others. A recent trend in the field of human-computer interactions is the development of emotional artificial intelligence. Additionally, emotion has a direct connection to many mental diseases, including depression, ADHD, autism, and game addiction. The importance of understanding emotion has given birth to a new scientific field, affective computing, which primarily deals with identifying and modeling human emotions. Compared to other methods that rely on outward manifestations like facial expression, gesture, or speech signals [7], which may show faked emotions, EEG signals are found to be more compelling for emotion recognition [35, 44, 45, 46].

The multivariate FBSE-EWT (M-FBSE-EWT) has been used for developing an EEG-based emotion detection method where the multichannel EEG signals have been decomposed into narrowband subband signals. Different successive joint instantaneous amplitude and frequency of subband signals are selected to have multiscaling properties in the spectral domain. On the other hand, subband signals are added, and the entropy of the cumulative signals has been computed as temporal multiscale entropies. The spectral and temporal multiscale entropies are smoothened and classified using an autoencoder-based random forest classifier for emotion classification [46].

1.4.2.2 Cognitive Workload Assessment

Studying the mental effort involved in problem-solving is crucial to fully comprehending how the brain allocates cognitive resources to interpret information. Mental effort suggests the quantity of cognitive resources allocated for a particular task. The EEG is an effective physiological signal-based approach for assessing mental workload [47]. An EEG-based mental workload assessment framework is described below.

To induce a different level of mental effort, scientific problems have been given. Based on the complexity of the problem, different levels of mental effort are induced. Power in different EEG rhythms during problem-solving is compared with reference intervals where the subject was not performing any task. The percentage change in rhythm power is quantified: a positive value or increase in band power indicates event-related synchronization (ERS), and a negative value or decrease in band power indicates event-related desynchronization (ERD). This study finds an increase in alpha (lower: 8–10 Hz) desynchronization in the occipital and parietal regions and theta (4–7 Hz) synchronization in the FL. These findings suggest that mental effort due to scientific problem-solving demands cognitive resources like visuospatial processing, working memory, and semantic processing [48].

1.4.2.3 Imagined Speech Identification

Several diseases, for example, pseudocoma or lock-in syndrome, affect the speech generation process, and subjects lose their ability to communicate verbally. In many cases, the brain or central nervous system of such patients works normally. So, the BCI system can be a substitute for reading the commands from the brain itself. Many studies try to decode the EEG signal corresponding to imagined speech, where the subject imagines a vowel or word without articulating. The imagined-speech-based BCI system is useful for a person with a speech disorder not in the central nervous system [24, 49].

A multiscale signal decomposition-based approach has been proposed to classify EEG signals corresponding to five vowels for an imagined speech BCI system. Multivariate fast EMD has been used to decompose the multichannel EEG signals into oscillatory components at different scales. Several statistical features like slope domain entropy, sample entropy, bubble entropy, energy have been computed from the oscillatory modes. Gradient boosting-based machine learning algorithms have been used for classifying the EEG signal [49].

1.4.3 Fundamental Neuroscience

EEG signals have been used to understand the complex neural processing underlying different cognitive processes, brain function, and dysfunction. We have presented a few areas of neuroscience where EEG signals have been used to understand brain functioning.

1.4.3.1 Visual Object Recognition

Computational neuroscientists try to reveal the brain's neural functioning behind visual processing for object recognition by computational and mathematical models. Through a number of phases of linear and nonlinear transformations functioning at a millisecond time frame, the human brain recognizes visual objects. Signal processing and machine learning methods have been used to explain and predict these transformations.

In [50], a large dataset of EEG signals during visualization of 16,740 image conditions are reported for visual object recognition modeling. A total of 82,160 trials for the image conditions were performed. Based on this dataset, visual cognition models have been developed for predicting synthesized EEG signals as a response to an image, identifying the image conditions from synthesized EEG data. This study also shows the effect of varying numbers of trials and image conditions on the visual object identification model.

1.4.3.2 Study of Visual Imagery and Perception

Visual imagery and perception share similar kinds of brain resources, which has been shown by studying the EEG signals during visual imagery and perception [51, 52]. These help biological organisms in cognizing beyond their immediate response to a physically presented stimulus to behave adaptively and with enough flexibility.

Based on multivariate pattern analysis of EEG signal using signal processing and machine learning algorithms, it has been shown that alpha rhythm in parieto-occipital cortex has shared representation for visual imagery and perception [52]. The study was performed on EEG signals recorded from 38 subjects during the visual perception task and visual imagery task. For the visual imagery task, the name of the object to be imagined was uttered to instruct the subject for imagination.

1.4.3.3 Effect of Meditation on Brain

An exponentially growing number of studies are searching for the biological mechanism underlying the beneficial effects of meditation [53]. There exist several pieces of evidence supporting its positive impacts on both physical and mental health. We briefly discussed a study where the effect of meditation on the human brain has been studied with the help of EEG signal analysis.

In [20], the EEG rhythm powers have been used as a marker to analyze the effect of Manta meditation ('Hare Krishna Mahamantra') on the human brain. The EEG rhythm powers were computed using the FBSE before and after the mantra meditation. The alpha band power has increased significantly after meditation, indicating a calm and relaxed state of mind.

1.5 Multivariate Adaptive Signal Decomposition

Adaptive signal decomposition techniques are highly useful in a wide range of applications, as they provide flexible and adaptive methods for separating complex signals into their constituent components. These techniques have gained significant attention due to their ability to handle nonstationary and time-varying signals, where traditional methods may be limited. For example, the Fourier transform represents any signal using sinusoidal basis functions of infinite duration. Almost all the signals of interest are of finite duration, and representing a finite duration signal using an infinite duration basis function is not an effective way. Moreover, the time-varying characteristic of the signal can not be properly captured using the Fourier transform. Signals exhibiting time-varying spectral content cannot be adequately characterized by conventional Fourier analysis [54, 55, 56, 57]. In order to capture the time-varying spectral content, short-time Fourier transform (STFT) has been proposed [58, 59]. A small sliding window (duration of the window is much lower as compared to the signal duration) has been used to select the signal corresponding to a particular time, and spectral content is estimated using Fourier transform for that time [28]. Choosing the proper window length is a major challenge in STFT; there is no thumb rule for choosing the window length. STFT provides uniform frequency resolution for all frequency components. Additionally, the frequency resolution is limited by Heisenberg's boxes [60]. The wavelet transform has been introduced with multiresolution property [61, 62], which uses a time-localized window function (wavelet) for analysis of any signal. Though these methods have been applied for the analysis of various biomedical signals, pre-defined basis functions may not be well suited for the representation of real-time signals. Moreover, the time-frequency localization provided by these methods is limited. The STFT and wavelet transform require the selection of a basis function or mother wavelet. Improper selection of these can badly affect the signal representation. Wigner-Ville distribution has been proposed, which does not require to choose any separate basis function [60].

The aforementioned problems have been addressed in EMD, a data-adaptive signal decomposition technique [63, 64, 65, 66, 67]. In biomedical signal processing, adaptive signal decomposition methods play a crucial role in extracting relevant information from complex physiological signals. Biomedical signals often exhibit nonstationary characteristics, making them challenging to analyze using traditional techniques. Adaptive methods such as EMD and its variants allow the decomposition of biomedical signals into intrinsic mode functions (IMFs), which capture the underlying oscillatory components at different scales [63]. This enables the identification of specific frequency bands or components associated with physiological processes, such as heart rate variability in ECG signals or sleep stages in EEG signals. Overall, adaptive signal decomposition techniques provide versatile tools for analyzing, extracting, and manipulating signals in various domains. By adaptively decomposing signals into their constituent components, these methods enable the extraction of relevant information, removal of noise or interference, and facilitate improved analysis, interpretation, and manipulation of complex signals in diverse applications [28].

EEG signals are highly nonstationary and complex in nature. Adaptive signal decomposition techniques adaptively adjust their basis functions to effectively capture the changing features of the signal. Adaptive methods can offer a more accurate and detailed analysis of the complex EEG signals. Since the last decades after the introduction of adaptive multivariate decomposition techniques, it finds various applications in EEG signal analysis and classification [38, 45, 46, 68, 69, 70].

1.6 Motivations

In recent times, novel approaches have emerged for decomposing multicomponent signals into amplitude frequency modulated components data adaptively [71]. The availability of multivariate (multichannel) data has increased significantly due to advancements in sensor technology. EEG signals provide very high temporal resolution but suffer from poor spatial resolution. Spatial resolution can be improved by using more number of electrodes. However, the processing of these multivariate signals using a univariate signal decomposition, e.g., EMD, EWT, results in a loss of mutual information present in the signal. Processing of these multichannel EEG signals demands multivariate decomposition techniques. As a means to leverage the interdependence among multichannel signals through joint time-frequency analysis, the concepts of modulated bivariate and trivariate data oscillations have been introduced initially, followed by the generalization of these concepts to accommodate an arbitrary number of channels [72, 73, 74]. The univariate signal decomposition techniques have been extended for multivariate signals. The multivariate extensions are developed in such a manner so that they can generate the same number of multivariate oscillatory modes across different channels and have similar frequency components. The existing multivariate decomposition techniques are found to be useful but take a longer time for decomposition. So, a multivariate signal decomposition technique with lower time complexity needs to be developed.

Schizophrenia is a chronic and severe mental illness affecting 20 million people, about 1 percent of the world population worldwide [75], and more than 1 million cases in India. In active states of schizophrenia, it associates with symptoms like dellucinations (fixed false belief), hallucinations (experience of seeing, hearing, tasting, smelling, or feeling that does not really occur), disorganized speech and thinking, abnormal motor behavior (movements that can range from childish silliness to unpredictable agitation or purposeless movements) [76]. Though there is no permanent cure for schizophrenia, many patients do well with minimal symptoms with treatment [76]. Most of the symptoms of schizophrenia will greatly be improved, and the likelihood of recurrence can be diminished. Diagnosis and treatment can be complicated by substance misuse. Before a diagnosis can be made, however, a psychiatrist should conduct a thorough examination to rule out substance misuse or other neurological disorders whose symptoms mimic schizophrenia. This examination may be a lengthy time-consuming procedure and depends on several factors that may give rise to erroneous diagnosis. Accurate prediction of schizophrenia can help a lot to start treatment without delay and also reduce the risk of substance misuse. People with schizophrenia are 2-3 times more likely to die early than the general population [77]. This is often due to physical illnesses such as cardiovascular, metabolic, and infectious diseases, which are treatable if extra care can be taken [78]. For that, the detection of schizophrenia is important. More than 69% of people with schizophrenia are not receiving appropriate care [75], ninety percent of people with untreated schizophrenia live in low- and middle-income countries. Lack of access to mental health services is an important issue. In this scenario, easy, convenient, and cost-effective detection techniques may be beneficial for all humankind.

Parkinson's disease is a progressive, chronic, neurodegenerative disorder that affects movements [79, 80]. Substantia nigra, a specific area of the brain, is predominantly affected by Parkinson's disease where dopamine-producing (dopaminergic) neurons are located [80]. Ten million people suffer from Parkinson's disease worldwide, and more than one million cases per year are reported in India. Only four percent (estimated) of people are diagnosed with Parkinson's disease before the age of 50 years. Behavioral symptoms are hardly apparent and difficult to diagnose in the early stages of Parkinson's disease. Parkinson's disease symptoms might differ from person to person, which complicates the early diagnosis. Signs and symptoms of Parkinson's disease may include slowed movement (bradykinesia), tremors, impaired posture and balance, rigid muscles, loss of automatic movements, urinary disturbances, speech changes, difficulties in writing, etc. [79, 80]. There are currently no definite imaging or biochemical markers for detecting Parkinson's disease [79]. Well-trained neurologists can diagnose Parkinson's disease based on medical history, signs, and symptoms, physical and neurological examinations. Mimicking symptoms from other neurological illnesses can adversely affect diagnosis, so drug misuse may happen during treatment. Early identification of Parkinson's disease is critical for initiating effective treatments and care.

BCI is a state-of-the-art technology that aims to establish a direct communication path between the brain and the computer or external supportive device [69]. Brain activity patterns are analyzed and decoded in order to generate commands for computers. A cognitive process, in which imagination of movement of any part of the body is performed without actually moving it, is known as MI task [69]. EEG signal recorded during an event of performing MI movement is termed as MI EEG which is analyzed to detect the intention in EEG based MI BCI [69, 81]. EEG based MI BCI tries to reveal the features of brain electrical activity during MI movement, which are very important for fundamental neuroscience and related applications, such as noninvasive exoskeletons and bioprostheses controlled by brain, or supportive device for rehabilitation of patients after stroke or trauma [82, 83].

The BCI technology is an effective rehabilitation technique for patients with neuromuscular diseases and supports the daily life of healthy individuals by facilitating an alternate communication path. Steady-state visual evoked potential (SSVEP) is one of the widely used exogenous BCI paradigms due to its strong responses to brain activity [84]. Stimuli flickering at a particular frequency can cause sustained brain response in the occipital area, which is termed SSVEP [84]. The change in the brain response due to the visual stimuli can be detected from EEG signals. Individuals afflicted with neurological conditions or neurodegenerative diseases experience difficulties in controlling their muscles through neural pathways. The SSVEP approach offers a highly effective and reliable means of communication, facilitating the implementation of a non-invasive BCI.

Drowsiness or fatigue is one of the major challenges for road safety, and due to this, severe injuries, economic loss, and even death can happen. Lack of alertness due to an unconscious transition from wakefulness to sleep may lead to serious accidents. There may be several factors like lack of sleep, restlessness, long journeys, mental pressure, or consumption of alcohol behind the fatigue. Nowadays, road traffic is increasing rapidly, which surge the probability of undesired incidents due to drowsiness. In 2018, 2841 deaths and 400,000 (estimated) injuries in crashes are taken place on account of distracted driving, according to a report published by the national highway traffic safety administration (NHTSA) [85]. The onset of fatigue or disengagement mode detection-based alertness monitoring system can force the driver to pay continuous attention, which may help avoid many fatal accidents. Drowsiness detection will also be helpful for aircraft pilots, power-plant controllers, or similar kinds of working environments where automaton reduces the role of humans to passive observation. Still, continuous attention is required to take prompt action when necessary to avoid any accidents.

1.7 Objectives

The EEG signal presents important information about the brain with high temporal resolution. EEG signal is widely used for neurological disease diagnosis and BCI applications. However, manual inspection of long-duration EEG signals is a tedious task. Also required interventions of expert neurologists. The thesis aims to develop EEG signal analysis and classification frameworks based on multivariate analysis. The objectives of the thesis are as follows:

Objective 1: To classify schizophrenia EEG signals based on MIF-based multivariate EEG rhythms

Objective 2: To classify Parkinson's disease from EEG signals using phase-space representation (PSR)-based features

Objective 3: To identify MI movement for BCI application based on MIF-common spatial patterns (CSP) based feature

Objective 4: To detect different flickering frequencies in SSVEP for the BCI framework with improved performance

Objective 5: To develop a framework for drowsiness detection from multichannel EEG signals

1.8 Contributions of the Thesis

A summary of the contributions of the thesis is presented in this section. In particular, we have divided the contributions into two subsections: neurological disease diagnosis framework and BCI applications.

1.8.1 Neurological Disease Diagnosis

We have made contributions in multichannel EEG rhythm separation; feature extraction and dimension reduction; and high-dimensional PSR-based features for the automatic diagnosis of neurological disorders from EEG signals.

Schizophrenia detection framework: An approach based on MIF has been developed for the reliable prediction of schizophrenia from multichannel EEG signals. Multichannel EEG data are decomposed into multivariate oscillatory modes using MIF. An adaptive multivariate decomposition based EEG rhythm separation technique has been proposed. Multivariate oscillatory modes are grouped based on their mean frequency to obtain EEG rhythms, which have been further represented using Hjorth parameters features. These features are ranked based on student t-tests, and significant features are selected. Machine learning classifiers are developed for classifying the EEG signals using these features.

Parkinson's disease detection framework: This chapter presented a novel MIF based framework to extract the oscillatory modes present in the signal adaptively. The oscillatory modes are represented in higher dimensions based on PSR. The Euclidean distance of each point in PSR from the origin is computed to get the Euclidean distance curve. The area under the Euclidean distance curve is proposed as a potential biomarker for Parkinson's disease. The area of Euclidean distance curve-based features is classified using machine learning classifiers. Moreover, three different fusion strategies based on feature level and decision level fusion to get a more reliable Parkinson's disease identification framework. We have evaluated the proposed framework using a real-time EEG dataset.

1.8.2 Brain-computer Interface Applications

MI movement detection: We have proposed a MIF-based MI movement detection framework for BCI applications. MIF has been used to handle the data variability. MIF adaptively decomposes the multichannel EEG data and helps to select the optimum frequency band automatically. The variability in the frequency content across different channels adversely affects the performance. The mode alignments property of MIF enables us to extract CSP-based feature extraction. Then, from each band, CSP features are extracted and classified using a linear discriminant analysis (LDA)-based classifier.

SSVEP frequency detection: We have developed an SSVEP frequency detection framework. MIF is used to analyze the nonstationary EEG signal. MIF extracts narrowband oscillatory modes from EEG signals. Canonical correlation analysis (CCA) has been used widely for SSVEP classification. We have proposed CCA as feature extraction method from each multivariate IMF (MIMF). Different SSVEP frequencies are identified using a support vector machine (SVM) classifier based on the proposed feature representation of EEG signals.

Drowsiness detection: A drowsiness detection framework is developed based on the MIF algorithm. MIF is used to decompose the multichannel EEG signals. The discrete energy separation algorithm (DESA) is used to compute the joint AE and IF for joint TFR (JTFR). The joint marginal spectrum obtained from the JTFR is proposed as a feature and classified using an artificial neural network (ANN) into different mental states.

1.9 Road-map

The thesis contains eight chapters. The outline of the thesis is presented in Fig. 1.6. After introducing EEG signal processing and the importance of multivariate signal decomposition for the analysis of EEG signals, we have reviewed the existing multivariate signal decomposition techniques and presented the proposed MIF techniques (Chapter 2).

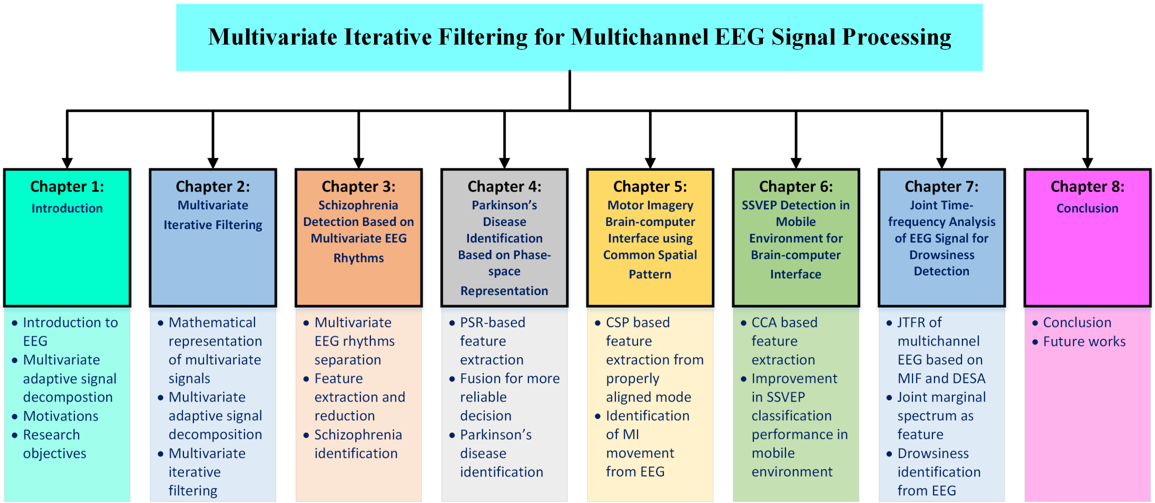

Figure 1.6: Outline of the thesis.

Chapter 3 introduces a novel schizophrenia detection framework. It also presented the results of the experiments and a comparative study with state-of-the-art methods.

Chapter 4 presents the proposed Parkinson's disease detection framework from multichannel EEG signals with the obtained results. The results obtained and comparative performance analysis of the Parkinson's disease detection framework are also included in this chapter.

Chapter 5 presents the developed MI BCI framework for BCI applications based on MIF and CSP. The proposed framework for MI movement identification is evaluated using two databases, and the results and discussion are presented in this chapter.

Chapter 6 presents the proposed SSVEP frequency detection framework based on MIF and CCA. The framework is evaluated in a mobile environment to test the robustness of the SSVEP detection framework.

Chapter 7 introduces a drowsiness detection framework based on the JTFR-based feature and ANN classifier. The performance of the framework and comparative results with the existing framework are presented in this chapter.

Chapter 8 concludes the presented work and as well as discusses future work.

Chapter 2

Multivariate Iterative Filtering

In this chapter, we have described the mathematical representation of multichannel signals, the multivariate extension of adaptive signal decomposition algorithms, and the multivariate iterative filtering (MIF) algorithm. The decomposed oscillatory components for synthetic signal and real-time electroencephalogram (EEG) signal are shown for each algorithm.

2.1 Adaptive Signal Decomposition

The univariate adaptive decompositions like empirical mode decomposition (EMD) [63], empirical wavelet transform (EWT) [67], variational mode decomposition (VMD) [65], iterative filtering [64] have attracted the focus of large research communities from various domains. Though these methods have been used for the analysis of multichannel signals, they face drawbacks like the absence of mode alignment, missing mutual information, and unequal number of oscillatory modes among different channels. One major issue with univariate EMD, mode mixing, has been attempted to solve using a multivariate extension of EMD [86, 87]. The key requirements of multivariate decomposition techniques are:

(1) Mode alignment: Estimation of common frequencies or shared oscillatory patterns across channels provides proper mode alignment to the extracted oscillatory modes.

(2) Equal number of modes: The number of oscillatory components should be the same across different channels.

Proper mode alignment enables the algorithm to identify and characterize the joint instantaneous frequencies in a manner that accounts for variations in different oscillatory modes. By finding the joint instantaneous frequency (IF), we gain valuable insights into the synchronized oscillatory behavior across multiple channels and obtain a comprehensive picture of the oscillatory patterns present in the multichannel signal [2, 74].

The adaptive univariate decomposition techniques like EMD [87], EWT [2], and VMD [88], iterative filtering have been extended to analyze multivariate signals.

2.2 Mathematical Representation of Multivariate Signals

The analysis of univariate modulated oscillations has seen more advanced development compared to the multivariate case [63, 64, 65, 67]. In both scenarios, the initial step involves establishing a model for the underlying structure of the signal. Let us define a multivariate time series $x(t)$ as follows [74]:

$$x(t) = \begin{bmatrix} x^1(t) \\ x^2(t) \\ \vdots \\ x^C(t) \end{bmatrix} \tag{2.1}$$

where C is the number of channels and $x^c(t)$ is the signal corresponding to c^{th} channel. This C-variate signal can also be termed as a multichannel and/or multidimensional signal [71].

The signal can be represented in terms of amplitude-frequency modulated oscillation $u(t) = a(t)e^{j\phi(t)}$ where $a(t) \geq 0$, $\frac{d\phi(t)}{dt} \geq 0$. Many approaches have been explored for univariate signals [89, 90, 91] in order to represent using amplitude-frequency modulated oscillatory components. C-variate monocomponent signal can be written in the form as follows:

$$x(t) = \begin{bmatrix} a^1(t)e^{j\phi^1(t)} \\ a^2(t)e^{j\phi^2(t)} \\ \vdots \\ a^C(t)e^{j\phi^C(t)} \end{bmatrix}$$

In practice, signals are commonly multicomponent, implying that they can be expressed as linear combinations of individual signals or components [92]. A signal $x(t)$ with P-components can be written as,

$$x(t) = \sum_{p}^{P} \begin{bmatrix} u_p^1(t) \\ u_p^2(t) \\ \vdots \\ u_p^C(t) \end{bmatrix} = \sum_{p}^{P} \begin{bmatrix} a_p^1(t)e^{j\phi_1(t)} \\ a_p^2(t)e^{j\phi_2(t)} \\ \vdots \\ a_p^C(t)e^{j\phi_C(t)} \end{bmatrix} \tag{2.2}$$

Let us consider the three-channel synthetic multicomponent signal given as,

$$x_s(t) = \begin{bmatrix} x_{s_1}(t) + 0.4x_{s_2}(t) \\ x_{s_2}(t) + x_{s_3}(t) \\ x_{s_1}(t) + x_{s_3}(t) \end{bmatrix} \tag{2.3}$$

where $x_{s_1}(t)$, $x_{s_2}(t)$, and $x_{s_3}(t)$ are defined as follows:

$$\begin{aligned} x_{s_1}(t) &= 2\sin\left(70\pi t + \pi\sin\left(2\pi t\right)\right) \\ x_{s_2}(t) &= \left(1 + 0.6\sin\left(2\pi t\right)\right)\cos\left(40\pi t\right) \\ x_{s_3}(t) &= \begin{cases} 0, & 0.67 \le t \le 1.35 \\ \sin\left(10\pi t\right), & \text{otherwise} \end{cases} \end{aligned} \tag{2.4}$$

For simulation purposes, a sampling frequency of 100 Hz has been considered for the synthetic signal $x_s(t)$. Figure 2.1 is showing the signal $x_s(t)$ and its components $x_{s_1}(t)$, $x_{s_2}(t)$, and $x_{s_3}(t)$. A resting-state multichannel EEG signal is taken to show the decomposed components based on multivariate decomposition algorithms (shown in Fig. 2.2) [20].

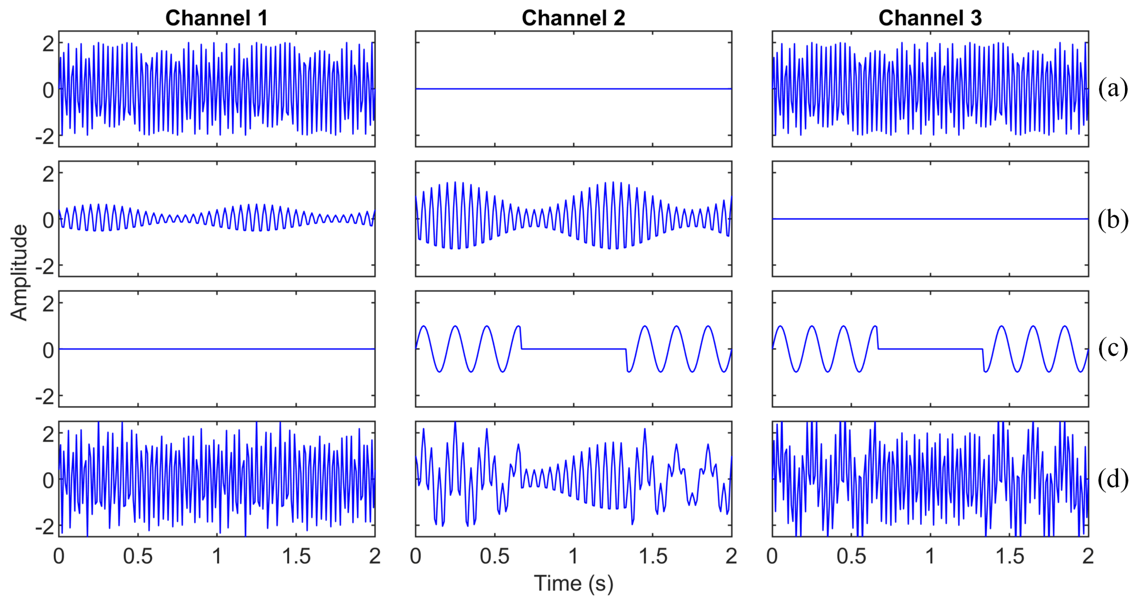

Figure 2.1: (a) $x_{s_1}(t)$, (b) $x_{s_2}(t)$, and (c) $x_{s_3}(t)$ components of (d) synthetic signal $x_s(t)$.

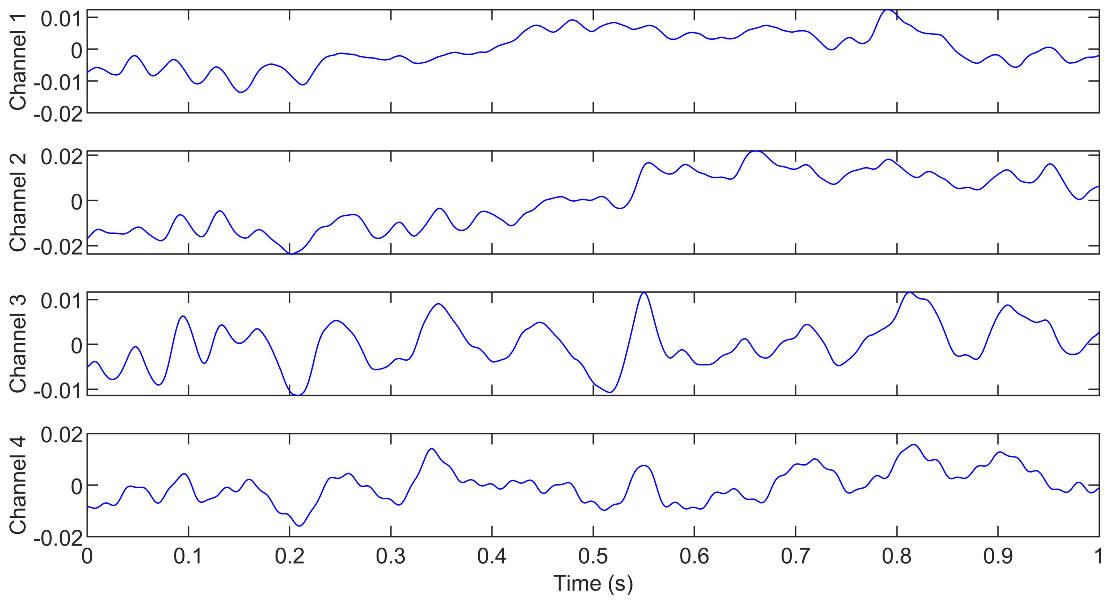

Figure 2.2: Four-channel EEG signals.

2.3 Multivariate Adaptive Signal Decomposition

2.3.1 Multivariate Empirical Mode Decomposition

EMD is a data-driven signal processing technique that has gained significant popularity for analyzing nonlinear and nonstationary signals. It is an adaptive method that decomposes a signal into a set of oscillatory components called intrinsic mode functions (IMFs). EMD provides an automated and effective way to analyze signals with varying frequencies and time-varying characteristics, making it particularly useful in various fields such as biomedical signal processing, image analysis, and environmental signal processing [63].

The primary goal of EMD is to decompose a signal into its underlying components without making any prior assumptions about its properties. Unlike traditional Fourier-based methods that assume signal components to be sinusoidal or stationary, EMD focuses on capturing the local dynamics and extracting the inherent oscillatory patterns present in the signal. This adaptability makes EMD well-suited for analyzing signals with rapidly changing frequencies or complex nonlinear behavior [63].

The decomposition process in EMD starts by identifying the local extrema points (maxima and minima) of the signal. These extrema points are then connected by cubic spline interpolation to form upper and lower envelopes, which bind the signal. The mean of these envelopes, referred to as the local mean, represents the slowly varying trend or the low-frequency component of the signal. By subtracting the local mean from the original signal, the high-frequency components are extracted. The process is iteratively repeated on the obtained high-frequency components, treating them as new input signals until a stopping criterion is met. In each iteration, the local extrema points, envelopes, and local mean are computed specifically for the current input signal. The final result of the decomposition is a set of IMFs, each characterized by a well-defined frequency scale.

The IMFs extracted by EMD satisfy two main criteria: (1) They should have equal numbers of zero crossings and extrema, and (2) the mean value of the envelopes defined by the local maxima and minima should be close to zero. These criteria ensure that the IMFs capture the oscillatory patterns inherent in the signal.

In the literature, several approaches can be found to extend the EMD algorithm for multivariate data, including bivariate EMD [93, 94], rotation invariant EMD [95], trivariate EMD [96], etc. In the context of multivariate signals, the computation of the local mean becomes a critical step since the concept of local extrema is not clearly defined. To address this challenge, Rehman and Mandic [87] proposed a novel approach that involves calculating envelopes and the local mean for multivariate signals by employing real-valued projections along multiple directions on hyperspheres (n-spheres). To extend the concept of EMD, a set of direction vectors has been defined that facilitates the decomposition process in the multivariate domain.

A unit hypersphere (n-spheres) has been sampled using both uniform angular sampling methods and quasi-Monte Carlo-based low-discrepancy sequences to obtain these direction vectors. This approach enables the adaptation of EMD to multivariate signals, allowing for effective decomposition and analysis of complex multivariate data.

The multivariate time series $x(t)$ can be represented as a C-dimensional vector $\{x(t)\}_{t=1}^{T}= \{x_1(t), x_2(t), \ldots, x_C(t)\}$. A set of direction vectors $v^{\gamma_k} = \{v_1^k, v_2^k, \ldots, v_C^k\}$ along the directions $\gamma_k = \{\gamma_1^k, \gamma_2^k, \ldots, \gamma_{C-1}^k\}$ is defined on an $(C-1)$-sphere. The multivariate EMD (MEMD) algorithm is described using the following steps [87]:

Step 1: Select an appropriate set of points for sampling on an $(C-1)$-dimensional sphere.

Step 2: Compute the projection, represented as $\{p^{\gamma_k}(t)\}_{t=1}^{T}$, of the input signal $\{x(t)\}_{t=1}^{T}$ along the direction vector v^{γ_k} for all k (the complete set of direction vectors), resulting in the set of projections $p^{\gamma_k}(t)$ for $k = 1$ to K.

Step 3: Identify the time points $\{t_j^{\gamma_k}\}$ that correspond to the maxima of the set of projected signals $p^{\gamma_k}(t)$ for k ranging from 1 to K.

Step 4: Perform interpolation on the pairs $[t_j^{\gamma_k}, x(t_j^{\gamma_k})]$ to generate multivariate envelope curves $\Delta^{\gamma_k}(t)$ for k ranging from 1 to K.

Step 5: The mean $m(t)$ of the envelope curves for a set of K direction vectors is computed as follows:

$$m(t) = \frac{1}{K} \sum_{k=1}^{K} \Delta^{\gamma_k}(t) \tag{2.5}$$

Step 6: Calculate detail component $d(t)$ as the difference between the original signal $x(t)$ and the mean $m(t)$ of the envelope curves: $d(t) = x(t) - m(t)$. If $d(t)$ satisfies the stoppage criterion [63], apply the same procedure described above to $x(t) - d(t)$, treating it as the new input signal. Otherwise, apply the procedure to $d(t)$ instead.

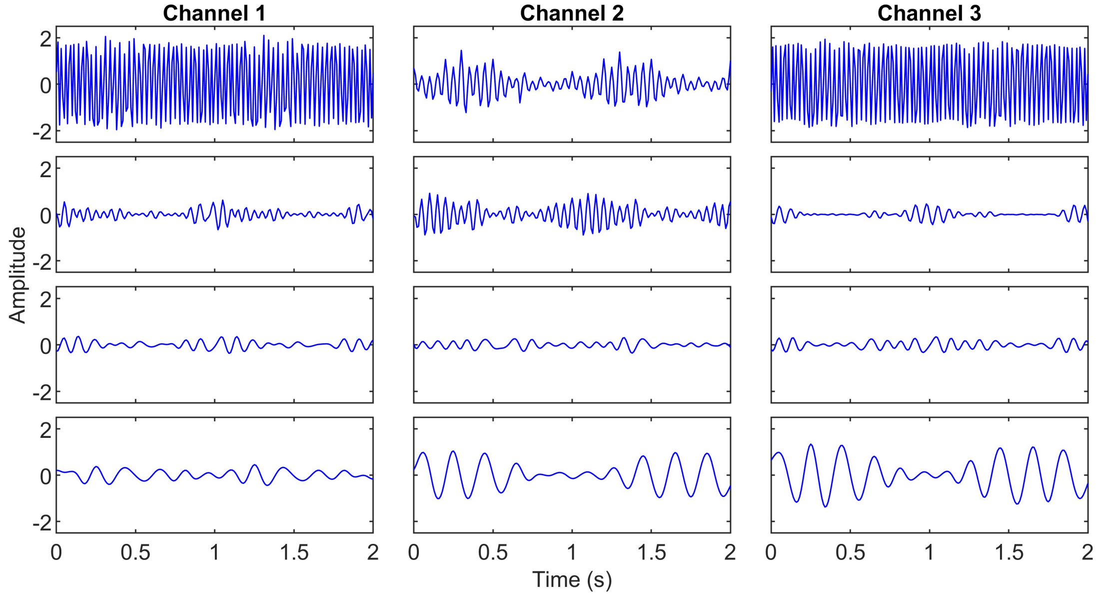

Figure 2.3: MIMFs corresponding to the synthetic signal $x_s(t)$ obtained from MEMD.

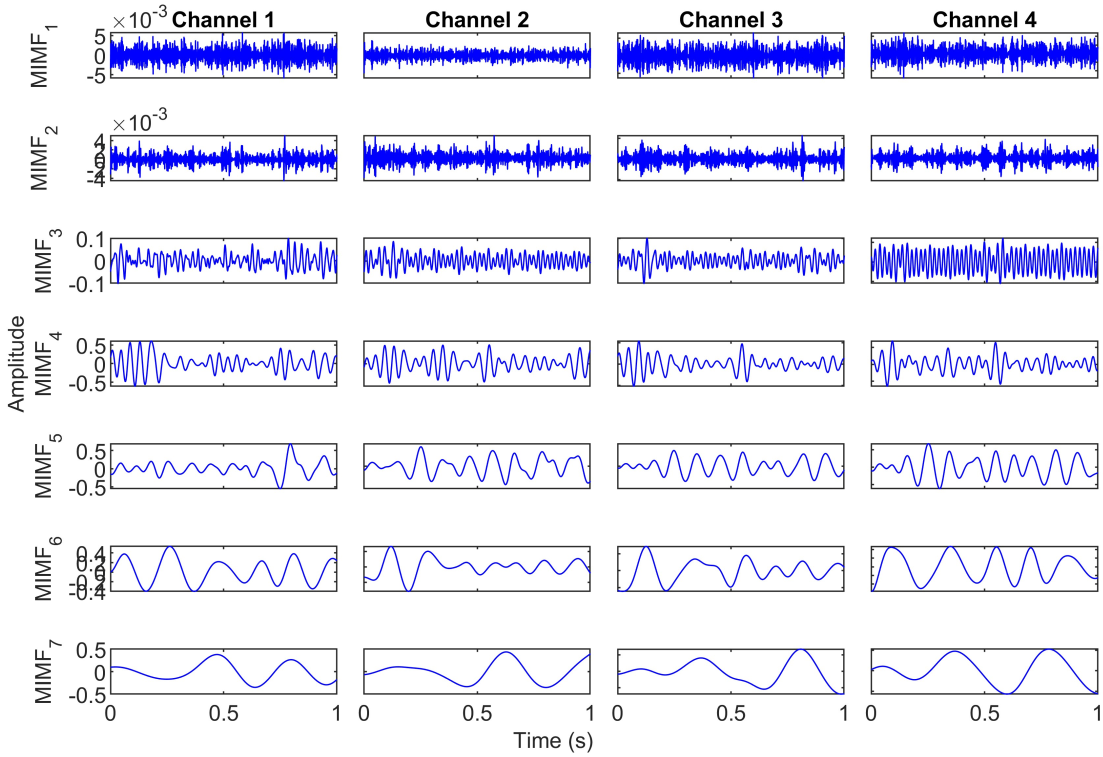

Figure 2.4: MIMFs corresponding to EEG signal obtained from MEMD.

The synthetic signal $x_s(t)$ (defined in Eq. (2.3)) is decomposed using MEMD, and the multivariate IMFs (MIMFs) are shown in Fig. 2.3. The first three MIMFs contained two components x_{s_1} and x_{s_2} of the synthetic signal. MEMD fails to separate x_{s_1} and x_{s_2} components properly and suffers from mode mixing. The EEG signal (Fig. 2.2) is decomposed using MEMD, and the MIMFs are presented in Fig. 2.4. The MEMD algorithm is computationally very complex [25, 70]. The MEMD algorithm is modified to reduce the computational time in fast MEMD [97].

2.3.2 Multivariate Empirical Wavelet Transform

The EWT is a data-driven signal analysis technique that combines the principles of EMD and wavelet analysis. It aims to decompose a signal into a set of localized oscillatory components called empirical wavelets, which capture the local dynamics and spectral characteristics of the signal in both time and frequency domains. Unlike traditional wavelet analysis, the EWT does not rely on predefined wavelet basis functions but derives the wavelets directly from the data. The decomposition process in EWT involves selecting a set of scales or frequencies for each IMF and applying wavelet transforms at those scales. The wavelet transforms are performed using adaptive basis functions derived from the IMF's local characteristics.

The adaptive wavelet-based bandpass filters generated by univariate EWT result in distinct components for multichannel signals corresponding to different channels. The number of components and their frequency ranges may vary across channels, creating an obstacle for multivariate analysis. To adapt univariate EWT for multichannel signals, a new concept for adaptive boundary detection is proposed to extract MIMFs for each channel [2]. This modified boundary detection ensures the MIMFs have similar frequency components across different channels. The steps involved in multivariate EWT (MEWT) for multivariate signal $x(t)$ (defined in Eq. (2.1)) are explained below.

Step 1: To obtain a unique set of boundaries for all channels, authors in [2] calculated the mean spectrum magnitude of multichannel signals acquired from all channels. The mean spectrum magnitude is defined as follows:

$$\hat{X}(f) = \frac{1}{C}\sum_{c=1}^{C}|X^c(f)| \tag{2.6}$$

where the Fourier spectrum of each channel signal $x^c(t)$ is denoted as $X^c(f)$.

Step 2: The mean Fourier spectrum is segmented into N contiguous segments using the EWT boundary detection method [67]. The set of boundaries can be denoted as $\{\Omega_b\}_{b=0,1,\ldots,B}$. It is important to mention that the first boundary frequency (Ω_0) is 0, and the last boundary frequency (Ω_B) is π. Based on these boundaries, the segment can be defined as $[0, \Omega_1]$, $[\Omega_1, \Omega_2]$, ..., $[\Omega_{B-1}, \Omega_B]$.

Step 3: Empirical wavelets are defined as the bandpass filters applied to each segment. To construct the empirical wavelet-based filter for each segment, we draw inspiration from the concept used in the construction of Littlewood-Paley and Meyer's wavelets [62]. The wavelet and scaling functions are defined empirically as, follows: [67]:

$$\textbf{Scaling function: } \chi_b(\Omega) = \begin{cases} 1, & \text{if } |\Omega| \leq (1-\phi)\Omega_b \\ \cos\left(\frac{\pi\Lambda(\phi,\Omega_b)}{2}\right), & \text{if } (1-\phi)\Omega_b \leq |\Omega| \leq (1+\phi)\Omega_b \\ 0, & \text{otherwise} \end{cases} \tag{2.7}$$

$$\textbf{Wavelet function: } \Psi_b(\Omega) = \begin{cases} 1, & \text{if } (1+\phi)\Omega_b \leq |\Omega| \leq (1-\phi)\Omega_{b+1} \\ \cos\left(\frac{\pi\Lambda(\phi,\Omega_{b+1})}{2}\right), & \text{if } (1-\phi)\Omega_{b+1} \leq |\Omega| \leq (1+\phi)\Omega_{b+1} \\ \sin\left(\frac{\pi\Lambda(\phi,\Omega_b)}{2}\right), & \text{if } (1-\phi)\Omega_b \leq |\Omega| \leq (1+\phi)\Omega_b \\ 0, & \text{otherwise} \end{cases} \tag{2.8}$$

where $\Lambda(\phi, \Omega_b) = \kappa\left(\frac{|\Omega|-(1-\phi)\Omega_b}{2\phi\Omega_b}\right)$. Here, the condition on variable ϕ ensures that the scaling and wavelet will have a tight frame, which can be mathematically expressed as $\phi < \left(\frac{\Omega_{b+1}-\Omega_b}{\Omega_{b+1}+\Omega_b}\right)$. $\kappa(p)$ is an arbitrary function as defined below.

$$\kappa(p) = \begin{cases} 0, & \text{if } p \leq 0 \\ \kappa(p) + \kappa(1-p) = 1, & \forall p \in [0,1] \\ 1, & \text{if } p \geq 1 \end{cases} \tag{2.9}$$

Step 4: The approximation and detail coefficients are obtained by taking the inner product of the applied signals $x(t)$ with the scaling and wavelet functions.

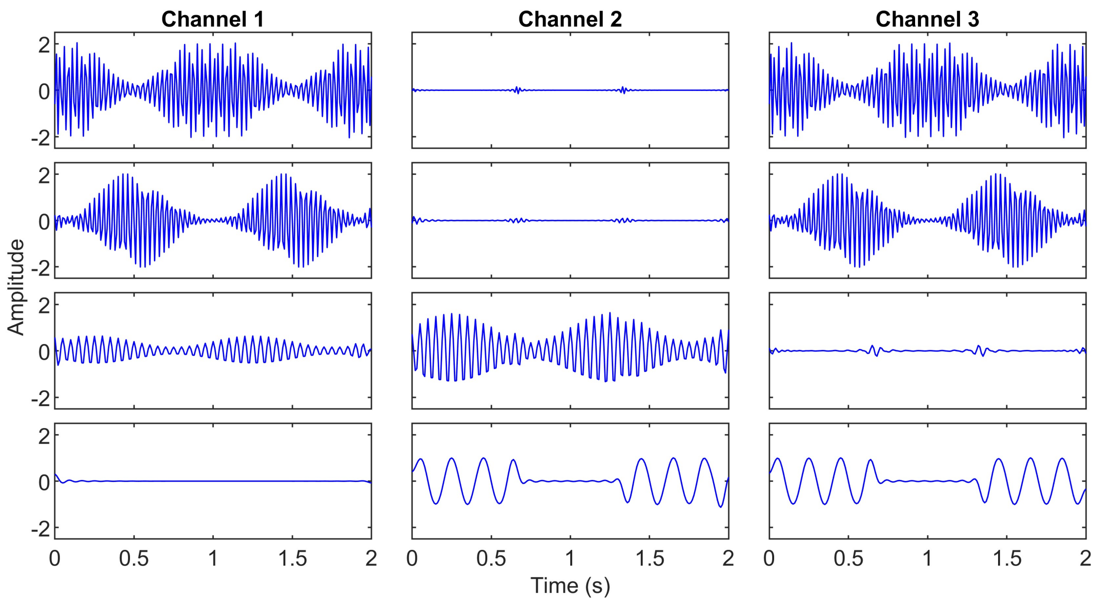

Figure 2.5: MIMFs corresponding to the synthetic signal $x_s(t)$ obtained from MEWT.

The wavelet and scaling functions obtained in the previous step will be the same for all channels; hence, they provide exactly the same number of modes and frequency-aligned modes in all channels. The MIMFs from MEWT for synthetic signal $x_s(t)$ are shown in Fig. 2.5. MEWT divided the first component $x_{s_1}(t)$ into two modes which is known as mode splitting problem. The MEWT-based decomposition result for the EEG signal is shown in Fig. 2.6.

2.3.3 Multivariate Fourier-Bessel Series Expansion based Empirical Wavelet Transform

Similar to the Fourier series, the Fourier-Bessel series possesses orthogonality properties that facilitate signal representation and analysis. This property enables straightforward decomposition and reconstruction of signals using the expansion coefficients [28, 98, 99]. Since nearly all the real-time signals are nonstationary in nature, it is essential to use nonstationary basis functions for their representation. The widely used Fourier transform representation uses sinusoidal functions as basis functions. The Fourier-Bessel representation employs nonstationary Bessel functions as a basis set, which helps to provide a more meaningful representation. The Fourier-Bessel representation of a signal yields unique coefficients, and their length is equal to the length of the signal. In contrast, the Fourier transform provides unique coefficients of length equal to half the length of the signal (for real signal). As a result, the Fourier-Bessel representation can offer double frequency resolution compared to the discrete Fourier transform-based representation. Fourier-Bessel series expansion (FBSE) has been used to represent EEG signals in literature and provided better performance [20, 45, 100, 101].

By leveraging this advantage, the EWT has been improved by using the FBSE [66]. The univariate FBSE-based EWT (FBSE-EWT) is extended for multichannel signal in [46, 66, 99, 101]. The multivariate FBSE-EWT (M-FBSE-EWT) has similar steps to MEWT, described in Section 2.3.2 except for the boundary detection procedure. In M-FBSE-EWT, the FBSE-spectrum is used instead of the Fourier transform-based spectrum. Due to the

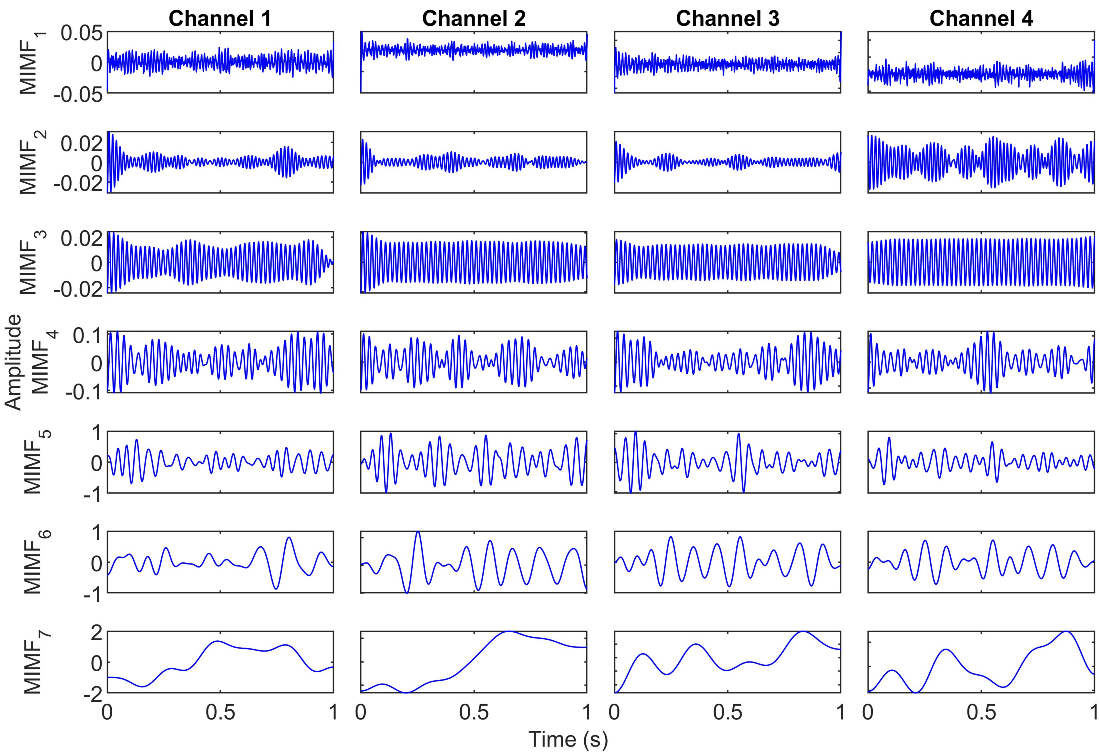

Figure 2.6: MIMFs corresponding to EEG signal obtained from MEWT.

higher resolution of the FBSE spectrum, the signal separation has improved [66]. The FBSE spectrum of signal $y(n)$ can be obtained from the FBSE coefficients of the signal [46, 99]. The FBSE coefficient can be computed as,

$$C_i = \frac{2}{U^2\left(J_1(\beta_i)\right)^2}\sum_{n=0}^{U-1} n y(n) J_0\left(\frac{\beta_i n}{U}\right) \tag{2.10}$$

where, $J_0(\cdot)$ and $J_1(\cdot)$ denote zero and first order Bessel functions, respectively. β_i with i = 1,2,...,U are the positive roots of the zero-order Bessel function ($J_0(\beta) = 0$) arranged in ascending order. The magnitude of the FBSE coefficient $|C_i|$ will provide the FBSE spectrum [66]. For M-FBSE-EWT, the Fourier spectrum in MEWT is replaced with the FBSE spectrum for better separation of components, and the other steps are the same as those in MEWT.

The separated components using M-FBSE-EWT for synthetic signal $x_s(t)$ are shown in Fig. 2.7. All three modes present in the synthetic signal are separated into three MIMFs by M-FBSE-EWT. First, MIMF is an insignificant component that can be discarded based on energy-based thresholding or other thresholding techniques. The M-FBSE-EWT based decomposed components of the EEG signal are shown in Fig. 2.8.

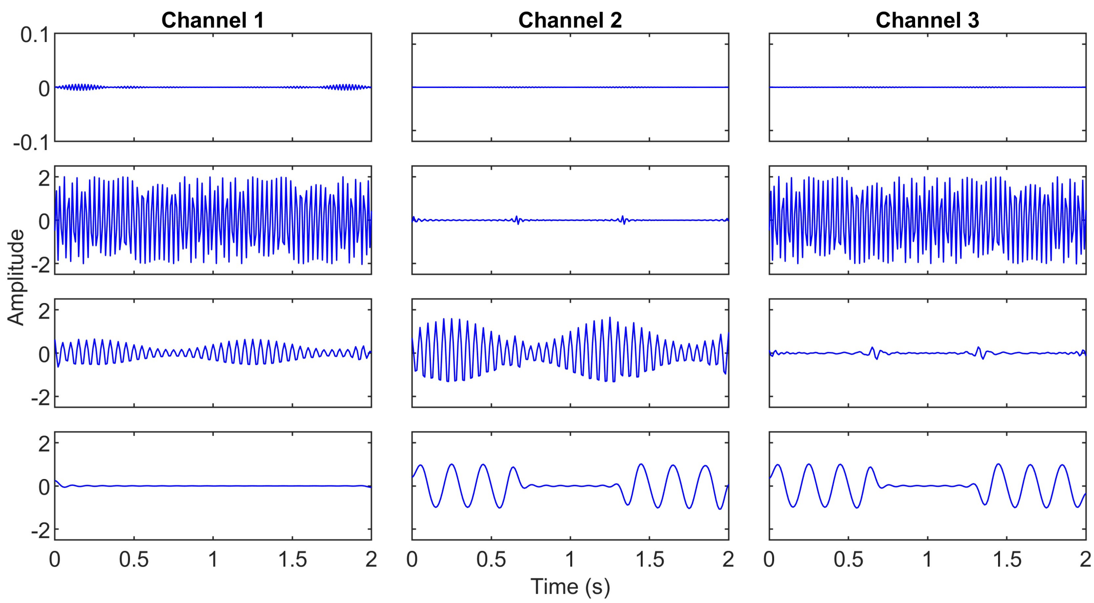

Figure 2.7: MIMFs corresponding to the synthetic signal $x_s(t)$ obtained from M-FBSE-EWT.

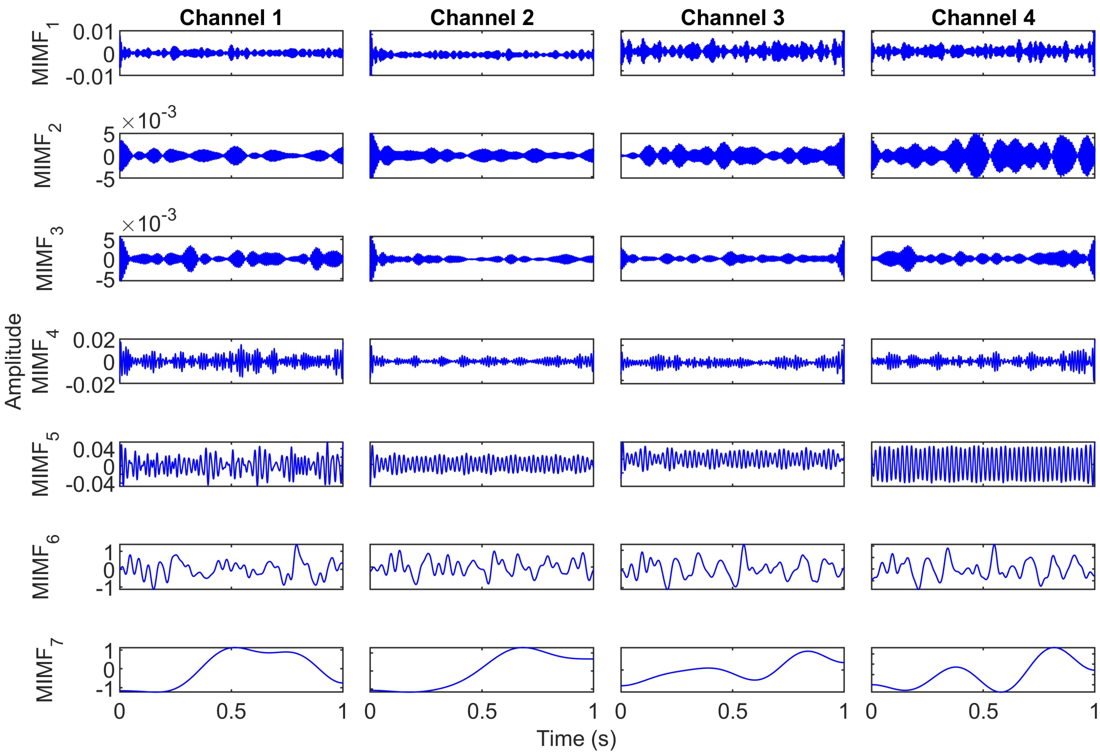

Figure 2.8: MIMFs corresponding to EEG signal obtained from M-FBSE-EWT.

2.3.4 Multivariate Variational Mode Decomposition

VMD is a signal processing technique that decomposes a signal into a set of modes with distinct frequency bands [65]. It is a data-driven approach that provides an adaptive and self-tuning method for analyzing signals with varying frequencies and time-varying characteristics.

The main idea behind VMD is to find a set of modes that best capture the signal while minimizing the cross-mode interference. Unlike traditional Fourier-based methods that assume a fixed set of sinusoidal components can represent the signal, VMD adaptively determines the modes based on the signal's intrinsic characteristics.

The VMD algorithm starts by assuming that the signal can be represented as a sum of K modes, each mode representing a component with a distinct frequency band. The decomposition is obtained by solving an optimization problem that promotes both sparsity and smoothness of the modes. The optimization problem seeks to find the modes that best capture the signal while minimizing the mutual interference between the modes.

To solve the optimization problem, VMD uses a constrained optimization approach. It introduces a constraint on the IF of each mode, which limits the spread of energy in the time-frequency plane. By imposing this constraint, VMD ensures that each mode is localized in both time and frequency domains.

The VMD algorithm iteratively updates the modes and their associated weights until convergence is achieved. At each iteration, the algorithm estimates the modes by minimizing the objective function, which is a combination of data fidelity and regularization terms. The weights represent the importance or energy distribution of each mode in the signal.

Rehman and Aftab [88] proposed an extension of the VMD algorithm to handle multivariate or multichannel data. The proposed multivariate VMD (MVMD) aims to effectively capture multivariate modulated oscillations (joint or common frequency components shared across all channels) present in the signal. In MVMD, the cost function to be minimized is an extension of the cost function used in standard VMD, specifically tailored for multivariate data. The cost function is defined as the sum of bandwidths of all signal modes across all input data channels. This modified cost function takes into account the characteristics of multivariate signals and aims to optimize the decomposition by minimizing the collective bandwidths of the modes across all channels. By minimizing this cost function, the MVMD method aims to achieve an effective decomposition of the multivariate data into distinct modes with minimized bandwidths. A C-variate signal $x(t)$ defined in Eq. (2.1), can be represented using K number of multivariate oscillatory components $v_k(t)$ having center frequency ω_k as,

$$x(t) = \sum_{k=1}^{K} v_k(t) \tag{2.11}$$

where, $v_k(t) = [v_{k,1}, v_{k,2}, \ldots, v_{k,C}]$. The steps involved in the MVMD algorithm to find $v_k(t)$ are presented below.

Step 1: Initialize the center frequency ω_k of the multivariate modes, which can be done in various ways, such as by choosing complete random values.

Step 2: Compute the analytic representation $\hat{v}_k(t)$ of the multivariate signal $v_k(t)$ to obtain the spectrum having a frequency in the positive frequency part only.

Step 3: For each mode obtained in the decomposition, apply a frequency shift to bring the mode's frequency spectrum to the baseband by mixing it with an exponential function tuned to the estimated center frequency of the mode.

Step 4: The estimation of bandwidth is performed by assessing the Gaussian smoothness of the demodulated signal, specifically by considering the squared norm of the gradient. This smoothness measure provides an estimate of the bandwidth of each mode. The resulting constrained variational problem can be formulated as follows:

$$\begin{aligned} &\underset{\{v_{k,c}\}\{\omega_k\}}{\text{minimize}} \left\{ \sum_k \sum_c \left|\left| \partial_t \left[e^{-j\omega_k t} \hat{v}_{k,c}(t) \right] \right|\right|_2^2 \right\} \\ &\text{subject to } \sum_k \hat{v}_{k,c}(t) = x^c(t), \quad c = 1, 2, \ldots, C \end{aligned} \tag{2.12}$$

Step 5: Convert the above-constrained optimization problem into an unconstrained optimization problem by introducing a quadratic multiplier and Lagrangian function, denoted as $\mathcal{L}$. The mathematical expression can be given as,

$$\begin{aligned} \mathcal{L}\left(\{\hat{v}_{k,c}(t)\}, \{\omega_k\}, \{\lambda^c\}\right) = \beta \sum_k \sum_c \left|\left| \partial_t \left[e^{-j\omega_k t} \hat{v}_{k,c}(t) \right] \right|\right|_2^2 \\ + \sum_c \left|\left| x^c(t) - \sum_k v_{k,c}(t) \right|\right|_2^2 \\ + \sum_c \left\langle \lambda^c(t), x^c(t) - \sum_k v_{k,c}(t) \right\rangle \end{aligned} \tag{2.13}$$

Step 6: The complex optimization problem can be efficiently solved using the alternating direction method of multipliers (ADMM) algorithm. ADMM is a powerful optimization technique that decomposes the problem into multiple simpler sub-problems, making it easier to solve [65, 102].

The MIMFs corresponding to the synthetic signal have been shown in Fig. 2.9. It also separates the three components into four MIMFs. The first component x_{s_1} is split into two modes similar to MEWT. The MVMD-based decomposition of the EEG signal is shown

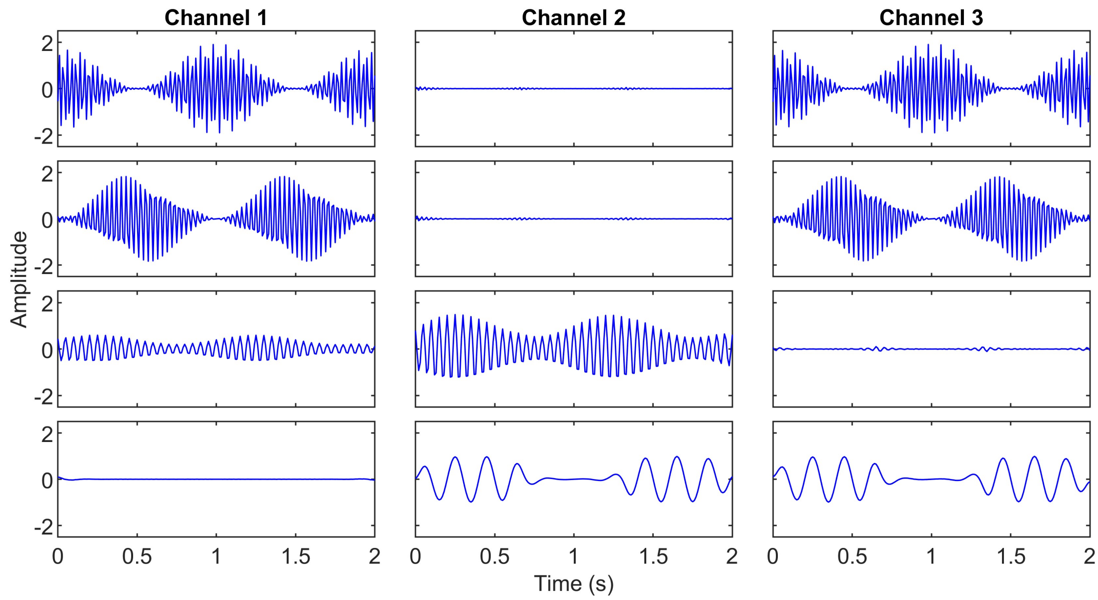

Figure 2.9: MIMFs corresponding to the synthetic signal $x_s(t)$ obtained from MVMD.

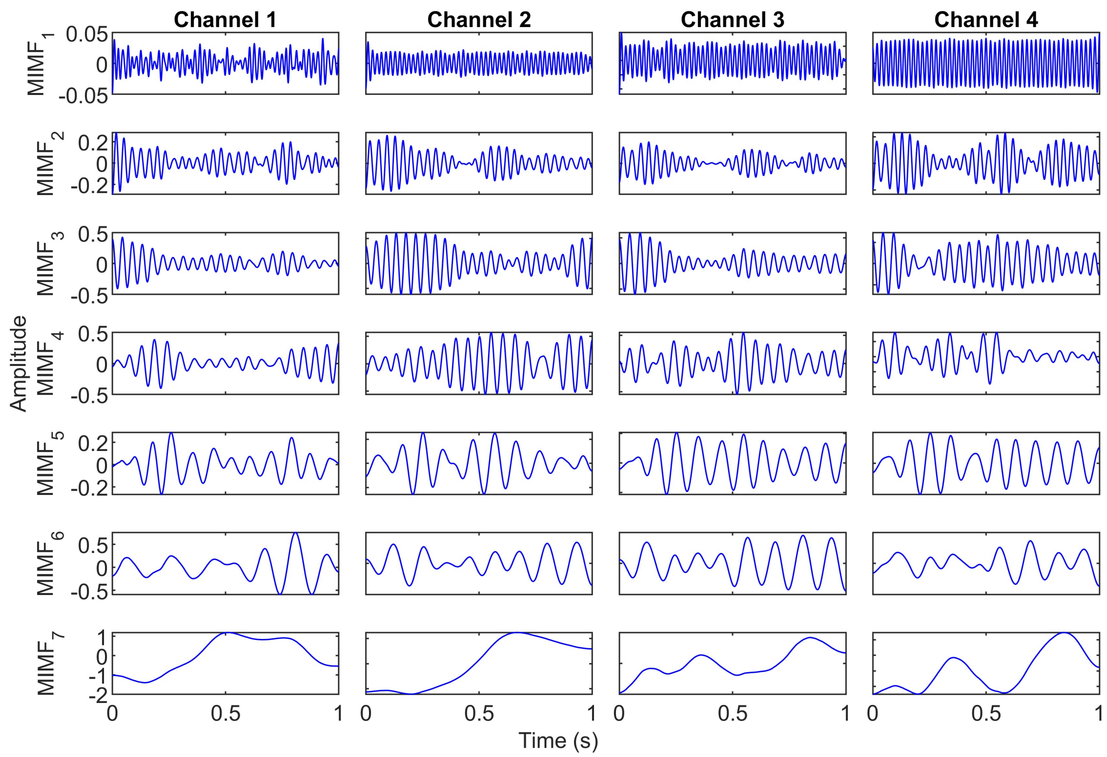

Figure 2.10: MIMFs corresponding to EEG signal obtained from MVMD.

in Fig. 2.10. Liu and Yu have proposed an alternate extension of the VMD algorithm for successive extraction of MIMFs [103].

2.3.5 Others Multivariate Adaptive Decomposition Techniques

In literature, several other univariate adaptive data decomposition approaches have been proposed, like ensemble EMD (EEMD) [104], local mean decomposition [105], singular spectrum analysis [106, 107, 108], local characteristic scale decomposition [109], intrinsic time scale decomposition [110], dynamic mode decomposition [111], nonlinear mode decomposition [112], adaptive local iterative filtering [113], Fourier decomposition method [114]. Several approaches among these techniques have been extended for multivariate data analysis, namely, multivariate nonlinear chirp mode decomposition [115, 116], multivariate singular spectrum analysis [117, 118], multivariate dynamic mode decomposition [119, 120], etc. [121].

2.4 Multivariate Iterative Filtering

Decomposing signals into different IMFs gives access to more meaningful insights into the signals. Lin *et al.* [122] proposed iterative filtering as an alternative algorithm of EMD [63], which addresses the fundamental mathematical issues with EMD, like stopping criteria, the convergence of the sifting process has not been proven [123, 124, 125]. In addition, iterative filtering generates stable IMFs in noisy environments whereas EMD being highly data adaptive generates complete different set of IMFs. The iterative filtering method is briefly described to provide a clear understanding of the proposed MIF.

2.4.1 Iterative Filtering

Iterative filtering extracts the oscillatory components by using a moving average filter designed based on the extrema present in the signal [64]. Iterative filtering extracts the modes from signals one after another, starting from the higher frequency with the help of a moving average filter. Defining a double averaging filter operator as $\Psi(x)$, operates on the input signal $x[k], k \in \mathbf{N}$, and generates a moving average of $x[k]$. The length of the moving average filter at stage j is chosen as follows:

$$L_j = \left\lfloor \frac{\alpha N}{E} \right\rfloor \tag{2.14}$$

where, α is a constant, N is the number of samples in signals, E is the number of extrema in signal. Designing a filter based on the signal properties makes the algorithm data adaptive. Choosing moving average or low pass filter, having compact support is an essential aspect of iterative filtering, for handling nonstationarity and nonlinearity of the signal. Solution of the Fokker-Plank equation can be used as such filter (w is the filter coefficients) with compact support and smoothness. With the help of the moving average operator, let us define a sifting operator $S_j(x)$, such that $S_j(x_n) = x_n[k] - \Psi(x_n) = x_{n+1}$. After n-iteration of sifting operator on signal $x[k]$, it generates first IMF as $I_1 = \lim_{n\to\infty} S^n_{j=1}(x)$. Applying operator $S_{j=2}(x)$ on the residual part after extracting IMF_1, $x - I_1$ gives second IMF. In this way, iterating the process J times gives J^{th} IMF. Iterative filtering has to stop when there are no maxima or minima present in the signal. The iterative filtering is presented in Algorithm 2.1.

Algorithm 2.1 Iterative filtering

Input: x (univariate signal)
Output: IMF

```
IMF = {}
while e ≥ 2 do    //e is the number of extrema of x
    m = 1
    x_m = x
    while stopping criterion (Eq. (2.15)) is not satisfied do
        compute the filter length l_m for x_m(n)
        design moving average filter w_m(n) of length l_m
        x^{m+1}(n) = x^m(n) − Σ_{k=−l_m}^{l_m} x^m(n + k) w_m(k)
        m = m + 1
    end while
    IMF = IMF ∪ {x_m}
    x = x − x_m
end while
IMF = IMF ∪ {x}
```

where, $\overset{m}{x}$ and $\overset{m+1}{x}$ are the intermediate IMFs at m^{th} and $(m+1)^{\text{th}}$ steps of iteration, respectively. At m^{th} step of the sifting process, the length of the filter and filter coefficients are defined as l_m and w_m. The stopping criteria for the sifting process to extract a particular IMF is defined as [64],

$$\frac{\sum_{n=0}^{N-1} |\overset{m+1}{x}(n) - \overset{m}{x}(n)|^2}{\sum_{n=0}^{N-1} |\overset{m}{x}(n)|^2} < \text{Th}, \tag{2.15}$$

When threshold (Th) is chosen as small, then a larger number of sifting steps will be performed, and for a large value of Th, the number of sifting steps will be smaller.

Due to the random nature and low signal-to-noise ratio of EEG signals, univariate decomposition techniques fail to generate unique IMFs across different channels when channel-by-channel analysis is performed. This problem of having different numbers of IMFs and frequency properties across different channels is referred to as the uniqueness problem [69], which may heavily deteriorate the performance of the analysis when multichannel signals are processed in a channel-wise fashion. Any mutual information present among the channels may lost due to univariate processing.

The univariate iterative filtering has been extended for multivariate signals by choosing a unique moving average filter for all channels [25]. We set the length of the moving average filter (used to filter the signals from all channels) based on the maximum value of the extrema of signals from all channels.

MIF is described by the following steps:

Step 1: Define a moving average filter ($a(n)$) of length L based on the extrema present in the signal $x(n) \in \mathbb{R}^{\mathbf{N}\times\mathbf{C}}$, where N is the number of samples [64]. Length L is computed as,

$$L = \left\lfloor \frac{\gamma N}{\max(\mathbf{E})} \right\rfloor \tag{2.16}$$

Here, γ represent a constant, $\mathbf{E}$ vector hold the number of extrema of all C channels ($\mathbf{E} = [e_1, e_2, \ldots, e_C]$, where e_c is the number of extrema for c^{th} channel), and $\max(\cdot)$ is an operator to find the maximum value. The moving average operation can be defined by a operator $\text{MA}(\cdot)$ as,

$$\text{MA}(x) = a(n) * x(n) \tag{2.17}$$

where * denotes the convolution operator.

Step 2: With the help of the moving average operator, the signal $x(n)$ is sifted iteratively, which is defined with an operator $\Xi(\cdot)$ as,

$$\Xi(\overset{m}{x}(n)) = \overset{m}{x}(n) - \text{MA}(\overset{m}{x}(n)) = \overset{m+1}{x}(n) \tag{2.18}$$

The superscript m on $x(n)$ denotes the intermediate signal as m^{th} iteration step. Repeated application of the sifting operator $\Xi(\cdot)$ on the input signal, j times, effectively isolates the fluctuating part of the signal, known as the MIMF. The p-th MIMF I_p, can mathematically expressed as $I_p = \lim_{j\to\infty} \Xi^j(x)$. Here, j represents the number of times the sifting operator operates on the signal $x(n)$, which is ideally infinite. Based on the IMF stopping criterion defined in Eq. (2.15) [63], the iteration can be stopped after finite repetition.

Step 3: Upon subtracting the extracted MIMF from the signal $x(n)$, if the resulting signal still contains oscillatory components, proceed to apply steps 1 and 2 iteratively to extract the remaining MIMFs. Conversely, when there are no oscillatory components present (i.e., the number of extrema is at most one), the remaining signal can be regarded as a trend component $r(n)$. The input signal $x(n)$ can then be expressed as a combination of MIMFs and the trend component as follows:

$$\begin{aligned} x(n) &= \sum_{p=0}^{P-1} I_p\left(n\right) + r\left(n\right) \\ &= \sum_{p=0}^{P} I_p\left(n\right), \quad r(n) \triangleq I_P(n) \end{aligned} \tag{2.19}$$

where P is the total number of MIMFs.

The details of MIF are shown in the Algorithm 2.2. In Algorithm 2.2, the outer loop gives one MIMF after a single iteration, and the inner loop is for properly extracting a particular MIMF. The flowchart of MIF is represented in Fig. 2.11.

The MIF algorithm is used to separate the components of the multichannel synthetic

---

Algorithm 2.2 Multivariate iterative filtering

Input: x (multivariate or multichannel signal)
Output: MIMF

MIMF = $\{\}$, c is number of channel
Compute $\mathbf{E}$ of x, $\mathbf{E} \in \mathbf{R}^{\mathbf{c}\times\mathbf{1}}$ // $\mathbf{E}$ is the number of extrema
while any value in $\mathbf{E} \geq 2$ **do**
    m = 1 // m counts the number of inner loop iteration
    $\overset{m}{x} = x$
    while stopping criterion (Eq. (2.15)) is not satisfied **do**
        Compute $\mathbf{E}$ of x
        Compute the l_m based on maximum($\mathbf{E}$) for $\overset{m}{x}$
        design moving average filter $w_m(n)$ of length l_m
        $\overset{m+1}{x}(n) = \overset{m}{x}(n) - \sum_{k=-l_m}^{l_m} \overset{m}{x}(n+k)w_m(k)$
        $m = m + 1$
    end while
    MIMF = MIMF $\cup$ $\{\overset{m}{x}\}$
    $x = x - \overset{m}{x}$
    Compute $\mathbf{E}$ of x
end while
MIMF = MIMF $\cup$ $\{x\}$

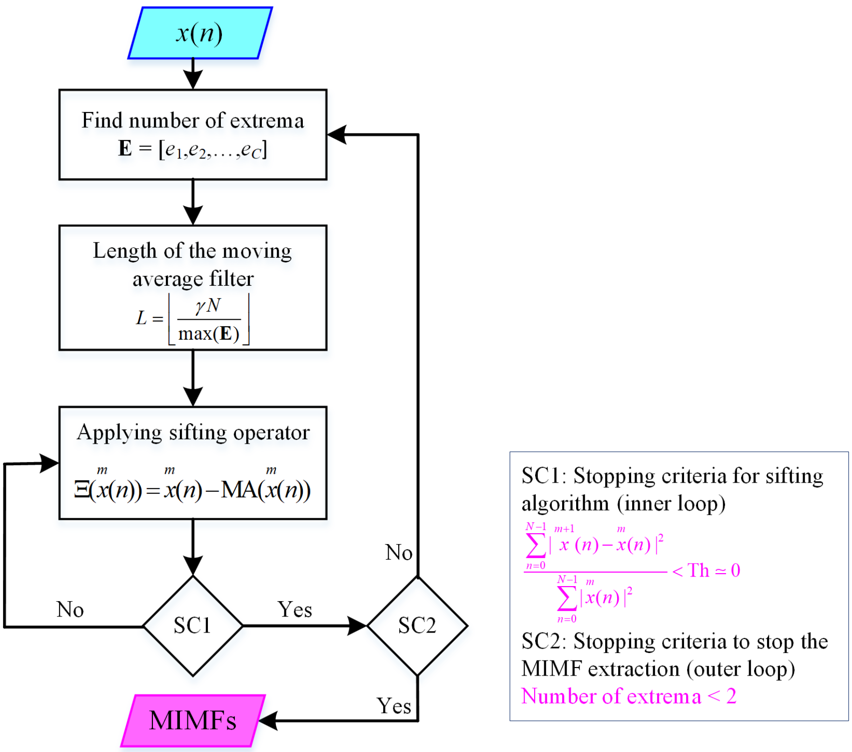

Figure 2.11: Flowchart for MIF.

signal $x_s(t)$ defined in Eq. (2.3) [1]. The obtained modes are shown in Fig. 2.12 The MIF-based decomposed components of the synthetic signal $x_s(t)$ are shown in Fig. 2.12. The first three MIMFs of the MIF algorithm are corresponding to three components of $x_s(t)$. The MIMF$_2$ of channel 3 shows a slight mode mixing problem, where part of the x_{s_1} is mixed with the MIMF$_2$. The MIF-based EEG signal decomposition is shown in Fig. 2.13. Cicone and Pellegrino proposed another extension of univariate iterative filtering in [126].

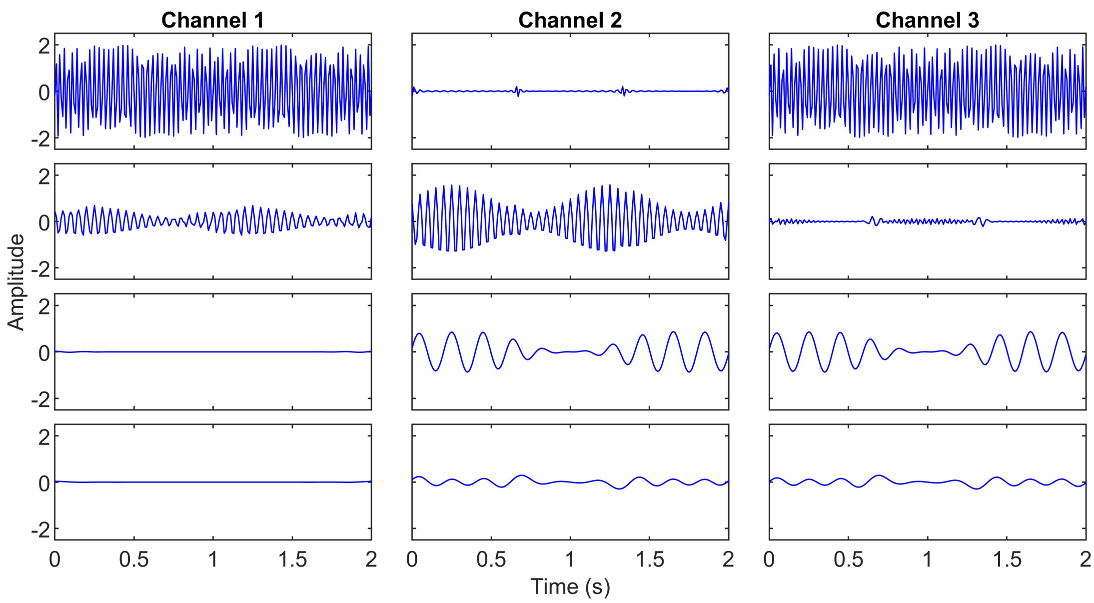

Figure 2.12: MIMFs corresponding to the synthetic signal $x_s(t)$ obtained from MIF.

2.5 Summary

This chapter has introduced the concept of multivariate adaptive decomposition and its usefulness for nonstationary signal processing. The mathematical definition of the multivariate time series is provided. The amplitude-frequency modulated component-based representation of the multivariate signal is mathematically defined. Adaptive signal decomposition techniques can be used to extract these amplitude-frequency modulated components or MIMFs. Various multivariate adaptive decomposition techniques, including MEMD, MEWT, M-FBSE-EWT, MVMD, and MIF, are described with steps. Decomposition re-

[1]https://github.com/kpdas95/MIF

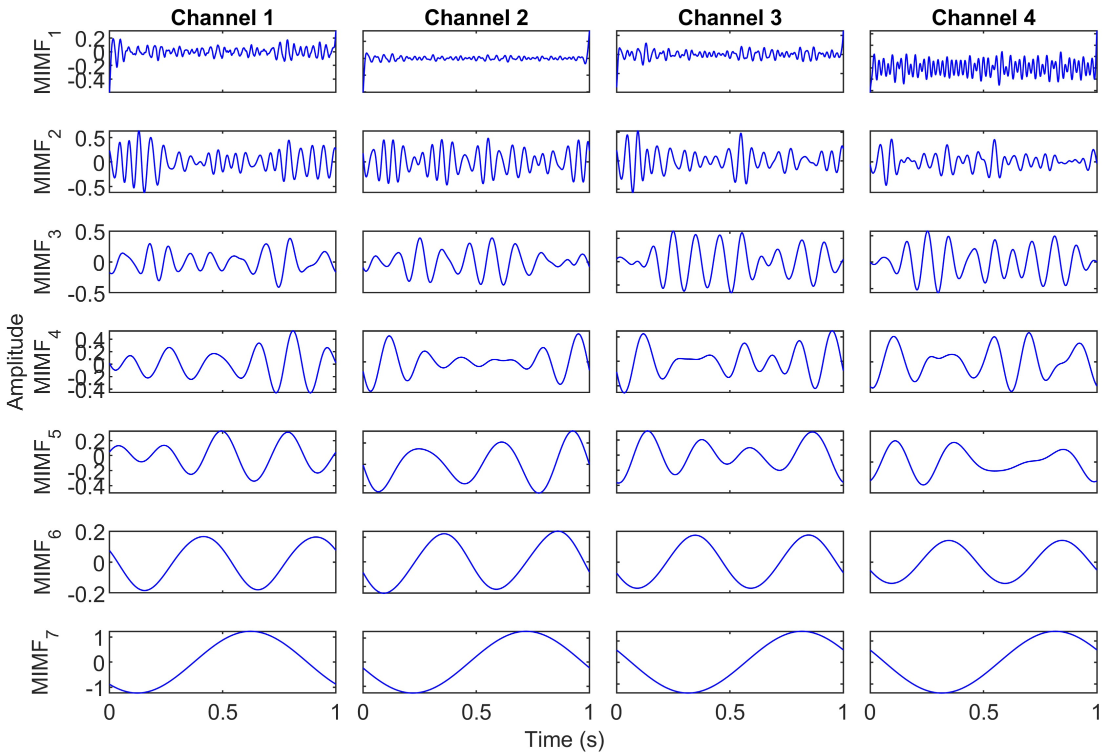

Figure 2.13: MIMFs corresponding to EEG signal obtained from MIF.

sults for both synthetic and real-time EEG signals are presented in the chapter. The area of adaptive multivariate adaptive decomposition is an emerging research area that has applications in almost all areas of science and engineering. In the last decades, it has drawn the focus of researchers from various fields. More research efforts are required to improve various problems like mode mixing, mode splitting in multivariate adaptive decomposition.

Chapter 3

Schizophrenia Detection Based on Multivariate EEG Rhythms

3.1 Introduction

Schizophrenia is a chronic and severe mental illness affecting approximately 20 million people worldwide, including over 1 million cases in India [75]. It is characterized by symptoms such as delusions, hallucinations, disorganized speech and thinking, and abnormal motor behavior [76]. Although no permanent cure exists, many patients can manage their symptoms effectively with treatment, reducing the likelihood of recurrence [77]. Diagnosis can be complicated by substance misuse, requiring thorough psychiatric evaluation to rule out other disorders. Early and accurate prediction of schizophrenia is crucial for timely treatment and reducing risks associated with the illness, including premature death due to treatable physical conditions. Unfortunately, over 69% of people with schizophrenia do not receive appropriate care, particularly in low- and middle-income countries, highlighting the need for accessible, convenient, and cost-effective detection techniques.

Most disorders related to the brain, like Parkinson's disease, Alzheimer's disease, epilepsy, etc., can be assessed by brain imaging techniques (Computed tomography (CT), magnetic resonance imaging (MRI), etc.) [127, 128, 129], or analyzing electroencephalogram (EEG) signals [2, 130, 131, 132]. In the literature, there are several studies that have shown the effectiveness of MRI in the detection of schizophrenia. However, imaging techniques are costly, require sophisticated lab facilities with high-end instruments, and demand more computing resources for analysis. On the other hand, acquiring EEG is inexpensive, non-invasive, possible even in remote locations with minimal instruments, and ease of use makes it another choice over imaging techniques for studying brain functions.

In literature, there are several techniques have been proposed for the detection of schizophrenia based on EEG signals. Kim *et al.* [133] proposed a schizophrenia detection technique, using EEG signals recorded with 21 gold-plated electrodes placed on the scalp, according to 10-20 international system for EEG electrodes placement. The power in different EEG bands was calculated using discrete Fourier transform, and used as features for the classification algorithm. They attained the highest accuracy of 62.2% using this method. Devy-Aharon *et al.* [134] used time-frequency representation (TFR) of EEG signals as classification features, and show 92.0% to 92.9% performance in correctly classifying schizophrenia, using the best five electrodes signal. Santos-Mayo *et al.* [135] use EEG ERP signals of subjects involved in auditory tasks. Brain signals were recorded using Brain Vision Equipment and electrode placement was according to 10-20 international system. EEGLAB was used for preprocessing, and then four frequency domain and ten time domain features were extracted. Linear discriminant analysis (LDA) and mutual information feature selection were used for feature selection. Multi-layer perception provided high classification rates of 93.42% and 92.23%, respectively. Ibanez-Molina *et al.* [136] used Neuroscan SynAmps 32 channel amplifier to collect EEG data in rest and involved in naming task. They concluded that the complexity in the right frontal lobe (FL) was higher in schizophrenia patients in the rest state. Jahmunah *et al.* [137] proposed a method for the detection of schizophrenia based on nonlinear features extraction and obtained an accuracy of 92.19% with a support vector machine (SVM)-radial basis function classifier. In another study, they reported a deep convolutional neural network (CNN)-based feature extraction and classification method with an accuracy of 98.07% [138]. Krishanan et al. [139] decomposed EEG signals into multivariate intrinsic mode functions (MIMFs) using multivariate empirical mode decomposition (MEMD), and extracted five different entropies of MIMFs as a complexity measure. In their proposed method, they have claimed an accuracy of 93.0% using the SVM-radial basis function classifier.

The deep learning-based approach needs more computational resources, large training data, and a longer time to develop. Other feature extraction-based approaches decomposed multichannel EEG data individually using the univariate decomposition method. As a consequence, if there is any mutual information in multichannel data, then that will be lost. In the MEMD-based approach, EEG signal is decomposed into MIMFs using MEMD, which is computationally very expensive for higher dimensional data [87].

Carefully considering the aforementioned issues, we have proposed a MIF based approach for schizophrenia detection. MIF is an extension of univariate iterative filtering for multivariate data. Using MIF, multichannel EEG data is decomposed into MIMFs, and grouped based on mean frequency in order to separate the EEG rhythms. Time domain based features are extracted from EEG rhythms and ranked using student t-test. Finally, the most significant 30 features are chosen for the classification of schizophrenia. We have tested our proposed method of schizophrenia detection on real-time EEG data, which shows promising results.

3.2 EEG Data

We have used a publicly available dataset of schizophrenia from the Institute of Psychiatry and Neurology, Warsaw, Poland, for this study [140]. Dataset contains EEG recordings of 14 patients (seven males with mean age 27.9$\pm$3.3 years and seven females with mean age 28.3$\pm$4.1 years) suffering from paranoid schizophrenia according to international classification of diseases, tenth revision criteria for paranoid schizophrenia. Control group contains 14 EEG recordings of 7 males (Age: 26.8$\pm$2.9 years) and 7 females (Age: 28.7$\pm$3.4 years). EEG were acquired for 15 minutes using 19 channels. Electrodes placement was according to 10-20 international system for EEG electrode placement system. EEG were recorded from the following positions: Fp1, Fp2, F7, F3, Fz, F4, F8, T3, C3, Cz, C4, T4, T5, P3, Pz, P4, T6, O1, O2, FCz (reference electrode) at a sampling rate of 250 Hz.

3.3 Methodology

The proposed approach is briefly depicted in block diagram Fig. 3.1. Major parts of the method are decomposing signal into modes using MIF, groping of modes in order to obtain EEG rhythms, and classifier for detecting schizophrenia EEG patterns. The following subsections illustrate each item of the block diagram briefly.

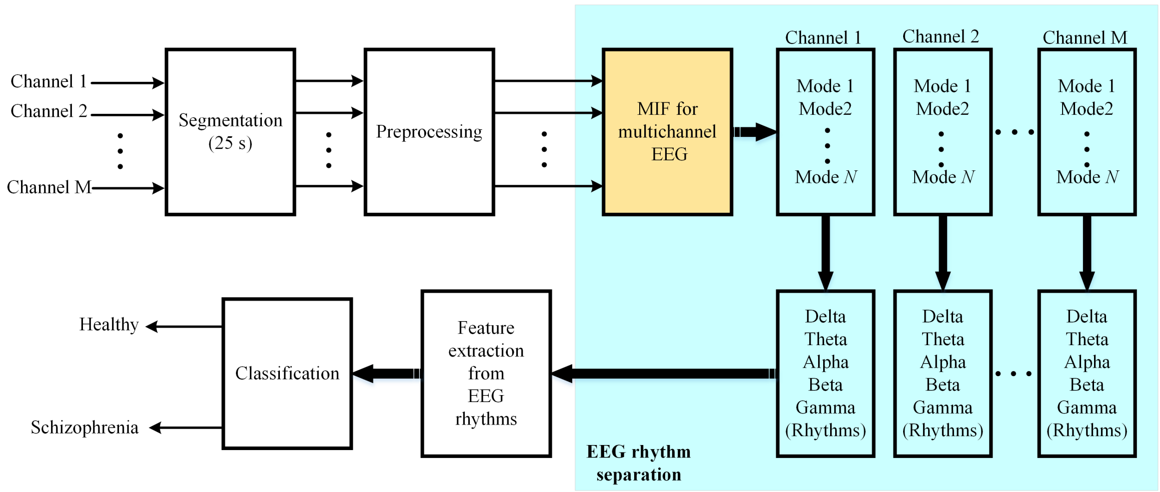

Figure 3.1: Block diagram of proposed MIF based schizophrenia detection.

3.3.1 Data Segmentation and Preprocessing

EEG signals are segmented into 25 s epochs each, with no data overlap. Segmentation gives 1142 EEG patterns of 6250 $\times$ 19 sample points. The healthy group contains 516 EEG patterns, and 626 belong to the other group. A notch filter is employed to remove the power line interface (PLI) artifact from the EEG epoch.

3.3.2 MIF based EEG Rhythm Separation

EEG signal generally lies in the frequency range 0.1 Hz to 100 Hz [141]. EEG signals can be further classified into different bands known as rhythms depending on frequency. EEG rhythms are delta (δ: 0.1-4 Hz), theta (θ: 4-8 Hz), alpha (α: 8-13 Hz), beta (β: 13-30 Hz), and gamma (γ: 30-100 Hz).

Multichannel EEG signals are decomposed into MIMFs using the MIF (described in Chapter 2) algorithm. The EEG signal $x[n]$ can be represented using MIMFs $u_p[n]$ based as follows:

$$x[n] = \sum_{p=1}^{P} u_p[n] \tag{3.1}$$

For a clear visual representation, EEG signals corresponding to three electrodes (Fz, Cz, and Pz) of a healthy subject are chosen and decomposed using the proposed MIF method. Selected decomposed MIMFs, and power spectral density (PSD) obtained using the Weltch method [142] are shown in Fig. 3.2 and Fig. 3.3. An important characteristic of multivariate

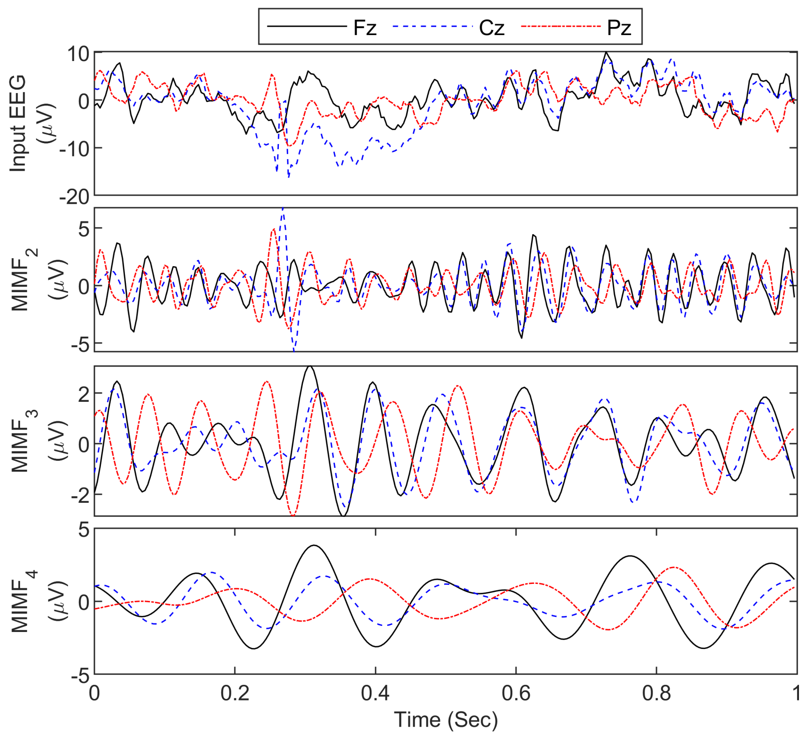

Figure 3.2: MIF decomposition of 3-channel EEG signal: (a) EEG signal and (b)-(c) selected MIMFs (MIMF_2, MIMF_3, and MIMF_4).

decomposition technique is its ability to detect common variability, or joint oscillatory mode (having the same frequency components) in a set of multiple time series. Alignment of mode is necessary for many different data analysis applications [74, 87]. Figure 3.2 shows that MIF has detected the joint oscillations across multiple channels and properly aligned them. MIMF_{2-4} across three selected channels have similar kinds of PSD, which implies modes are properly aligned. Decomposing the multichannel signal separately, using the univariate decomposition technique, will not properly align the similar oscillatory modes into the same numbered MIMFs as in the case of multivariate decomposition [87]. We have implemented the MIMF algorithm using a fast Fourier transform (FFT) based approach described in [143].

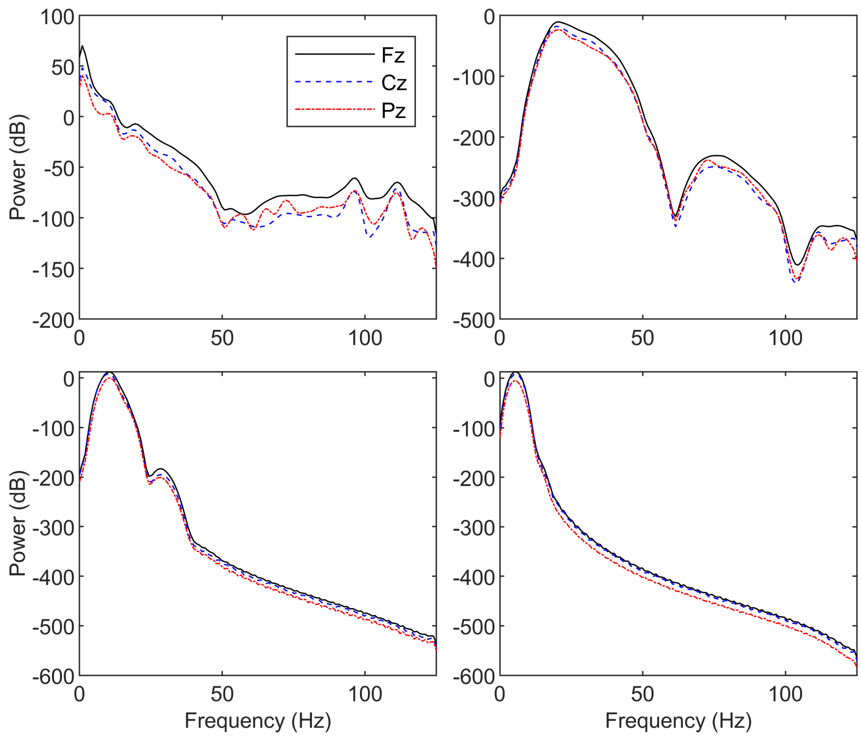

Figure 3.3: PSD of EEG signal (top left) and selected MIMFs (MIMF_2 (top right), MIMF_3 (bottom left), and MIMF_4 (bottom right)).

MIMFs are grouped to separate rhythms from EEG signal, based on mean frequency [144]. Mean frequency, μ_f is defined as follows:

$$\mu_f = \frac{\sum_{K=0}^{\frac{N}{2}-1} f_K |U[K]|^2}{\sum_{K=0}^{\frac{N}{2}-1} |U[K]|^2} \tag{3.2}$$

Where, $U[K] = \frac{1}{N} \sum u[k] \exp(-j\frac{2\pi}{N}Kk)$ is discrete Fourier transform of $u[k]$, and $f_K = \left(\frac{K}{N} f_s\right)$, where f_s is sampling rate of EEG signal.

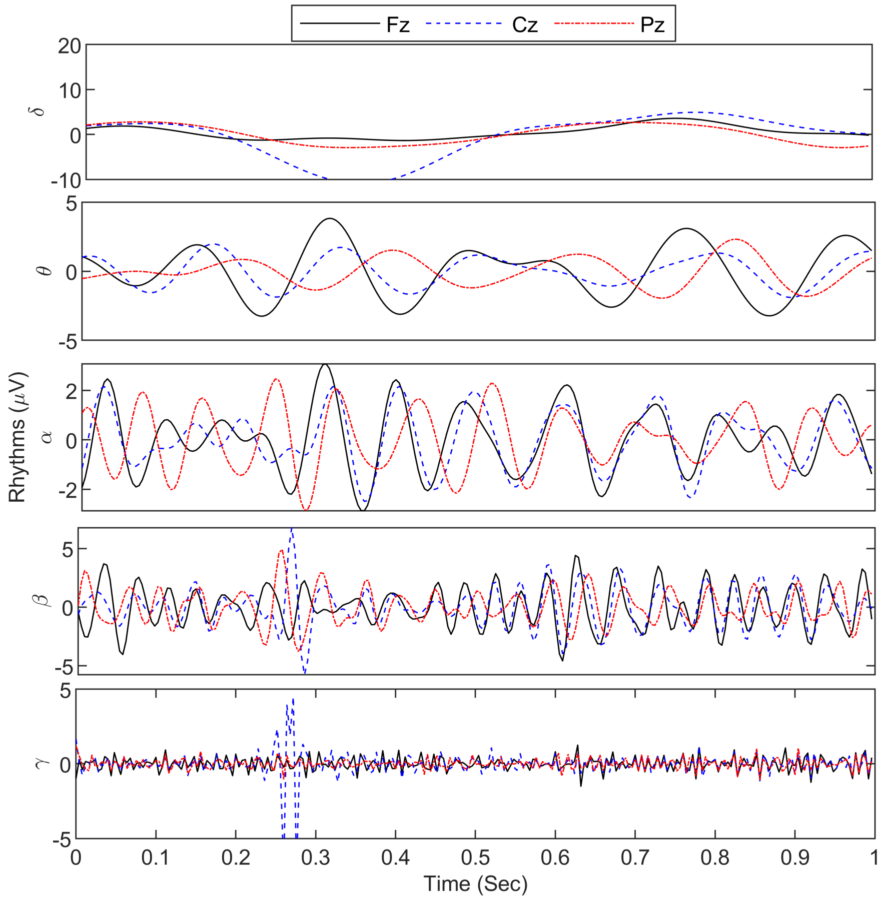

Figure 3.4: EEG rhythms separated using MIF: delta (δ), theta (θ), alpha (α), beta (β), and gamma (γ).

.

EEG rhythms are obtained using the following equations:

$$\text{Delta rhythm}: \quad rh_{\delta} = \sum u_p[k], \qquad 0.1 \text{ Hz} < \text{MF}(u_p) \leq 4 \text{ Hz} \tag{3.3}$$

$$\text{Theta rhythm}: \quad rh_{\theta} = \sum u_p[k], \qquad 4 \text{ Hz} < \text{MF}(u_p) \leq 8 \text{ Hz} \tag{3.4}$$

$$\text{Alpha rhythm}: \quad rh_{\alpha} = \sum u_p[k], \qquad 8 \text{ Hz} < \text{MF}(u_p) \leq 13 \text{ Hz} \tag{3.5}$$

$$\text{Beta rhythm}: \quad rh_{\beta} = \sum u_p[k], \qquad 13 \text{ Hz} < \text{MF}(u_p) \leq 30 \text{ Hz} \tag{3.6}$$

$$\text{Gamma rhythm}: \quad rh_\gamma = \sum u_p[k], \quad 30 \text{ Hz} < \text{MF}(u_p) \leq 100 \text{ Hz} \tag{3.7}$$

where MF(u_p) is mean frequency of $u_p[k]$. EEG rhythms of the EEG signal of Fig. 3.2. are shown in Fig. 3.4.

3.3.3 Feature Extraction and Ranking

In literature, several features like Shannon's entropy [145], approximate entropy [146], largest Lyapunov exponents [147], Hjorth parameters (activity, mobility, and complexity) [148] are used for classification of schizophrenia and healthy groups. For this study, we have tried with several features and got promising results with Hjorth parameters, which measure the statistical properties of signal in the time domain.

3.3.3.1 Hjorth Activity

It is an indicator of signal power and can be calculated by the variance of the signal, as follows:

$$\text{Hjorth}_{\text{Activity}} = \text{var}(x(t)) \tag{3.8}$$

where var$(\cdot)$ denotes the variance operator operating on the signal.

3.3.3.2 Hjorth Mobility

The mobility parameter is an indicator of the mean frequency of signal $x(t)$, and can be defined mathematically as follows:

$$\text{Hjorth}_{\text{Mobility}} = \sqrt{\frac{\text{var}(\frac{dx(t)}{dt})}{\text{var}(x(t))}} \tag{3.9}$$

3.3.3.3 Hjorth Complexity

Complexity is a measure of the nonstationarity of the signal, as it represents the changes in frequency. Defined as,

$$\text{Hjorth}_{\text{Complexity}} = \frac{\text{Mobility}(\frac{dx(t)}{dt})}{\text{Mobility}(x(t))} \tag{3.10}$$

All three above-mentioned Hjorth parameters described above are calculated for five EEG rhythms ($\delta, \theta, \alpha, \beta, \gamma$) corresponding to a set of 19 channels. Each channel gives 15 parameters, combining all the parameters from 19 channels gives a feature vector of dimension 285. The features are then ranked based on the p-value of the student t-test. The best 30 features were selected among 285 features.

3.3.4 Classification

The previous section briefly describes about feature extraction. The robustness of extracted features for the classification of healthy and schizophrenia is exploited using different classifiers, namely SVM, k-nearest neighbors (KNN), LDA, etc. [149].

SVM is developed based on statistical theory by Vapnic [150] for two group classification. A high-dimensional feature space is separated using a linear decision surface. The discrimination functions can be expressed as follows [151]:

$$y(x) = \text{sign}\left[\sum_{p=1}^{P} \alpha_p y_p \phi(x, x_p) + b\right], \tag{3.11}$$

for two class classification problem for a training set of P data points $\{y_p, x_p\}_{p=1}^{P}$, where $x_p \in \mathbf{R}^N$, is the p-th input vector and $y_p \in \mathbf{R}$, is p-th output. In Eq. (3.11), α_p, y_p, $\phi(x, x_p)$, b represent real constant, p-th output, kernel function, bias, respectively. In this study, linear kernel ($\phi(x, x_p) = x_p^T x$), and polynomial kernels ($\phi(x, x_p) = (x_p^T x + 1)^d$, quadrature ($d$=2) and cubic ($d$=3)) are used.

KNN is a non-parametric method for classification [152, 153]. It does not depend on prior probabilities, which makes this algorithm faster. KNN algorithm finds K nearest neighbours of input vector $\mathbf{x} \in \mathbf{R}^N$ from the training data, and then depends on the majority voting it predicts the class of input. In our study, cosine distance is used, and distance (d) between two vectors $\mathbf{x_1}$ and $\mathbf{x_2}$ is defined as follows:

$$d = 1 - \arccos\left(\frac{\mathbf{x_1}}{||\mathbf{x_1}||}.\frac{\mathbf{x_2}}{||\mathbf{x_2}||}\right), \tag{3.12}$$

Moreover, LDA [154] and decision tree [155] were explored. LDA maximizes the ratio of inter-class variance to intra-class variance in the training dataset. In this way, this gives maximum class separation. A decision tree, as the name implies, is used to separate a dataset into classes. During training a tree model is formed which basically partitioned the feature space into smaller subspaces can be represented using tree.

3.4 Results and Discussion

This section presents the results obtained using the proposed MIF-based classification of schizophrenia and healthy EEG signals. As compared to other multivariate decomposition techniques proposed MIF is computationally efficient. For comparing the computational time of the proposed MIF with other existing multivariate signal decomposition algorithms, we have decomposed the same multichannel EEG signal of length 6250 samples (arbitrarily chosen from the used database, and the first 15 channels are used for decomposition) ten times, and the average computation time of each algorithm is shown in Table 3.1. All algorithms were run on a desktop having Intel Core i7 4790 CPU, 3.60 GHz, RAM of 28 GB, windows 10 Education, MATLAB 2019B. MEMD [1] [87] generates 14 MIMFs using default parameter setting in the code. Input parameters for multivariate variational mode decomposition (MVMD) [2] were $\alpha = 2000, \tau = 0, K = 14, DC = 0, init = 1, tol = 10^{-7}$. Multivariate fast iterative filtering (MvFIF) [3] was run with the setting $\alpha = 1$ to keep the number of generated MIMFs similar to MEMD. The decomposition time for the proposed MIF algorithms is approximately 40 times less than MEMD and approximately 300 times

[1] http://www.commsp.ee.ic.ac.uk/ mandic/research/emd.htm

[2] https://www.mathworks.com/matlabcentral/fileexchange/72814-multivariate-variational-mode-decomposition-mvmd

[3] https://github.com/Acicone/MvFIF

less than MVMD. Fast decomposition will help generate decisions faster with less latency. The speed of the brain-computer interface (BCI) frameworks based on the MIF will have a faster data transfer rate between the brain and computer.

Table 3.1: Comparison of computation time of proposed MIF with the existing multivariate algorithms.

Algorithm	Time (s)	Number of MIMFs
MEMD [87]	119.18	14
MVMD [88]	923.27	14
MvFIF ([126])	4.74	20
MIF (proposed)	3.05	21

The most significant thirty features, their mean, standard deviation (SD), and corresponding p-value (obtained using student t-test) are listed in Table 3.2. Features have been named using the convention defined as, location of the EEG electrode then EEG rhythm separated by an underscore sign. For example, Cz_β denotes β rhythm of the location Cz. Boxplot of 10 most discriminant features (Cz_β, Cz_θ, Fz_β, P4_α, F4_β, Pz_β, Pz_α, Cz_α, F3_δ, T3_δ) are shown in Fig. 3.5.

The plot of accuracy versus the number of features used in SVM with the polynomial kernel is shown in Fig. 3.6. Classification accuracy attains maximum value of 98.9% when 30 most significant features are used. Further, adding more features does not increase accuracy. Due to this, only the first 30 features are used for classification to keep the method as computationally efficient as possible.

The performance of the different classifiers used in this study is tested using the following statistical parameters [156]: accuracy (Acc), sensitivity (Sen), specificity (Spe), and positive predictive value (PPV). These parameters are defined by the following mathematical equations:

$$\mathrm{Acc} = \frac{\mathrm{TP}+\mathrm{TN}}{\mathrm{TP}+\mathrm{FP}+\mathrm{TN}+\mathrm{FN}} \tag{3.13}$$

$$\mathrm{Sen} = \frac{\mathrm{TP}}{\mathrm{TP}+\mathrm{FN}} \tag{3.14}$$

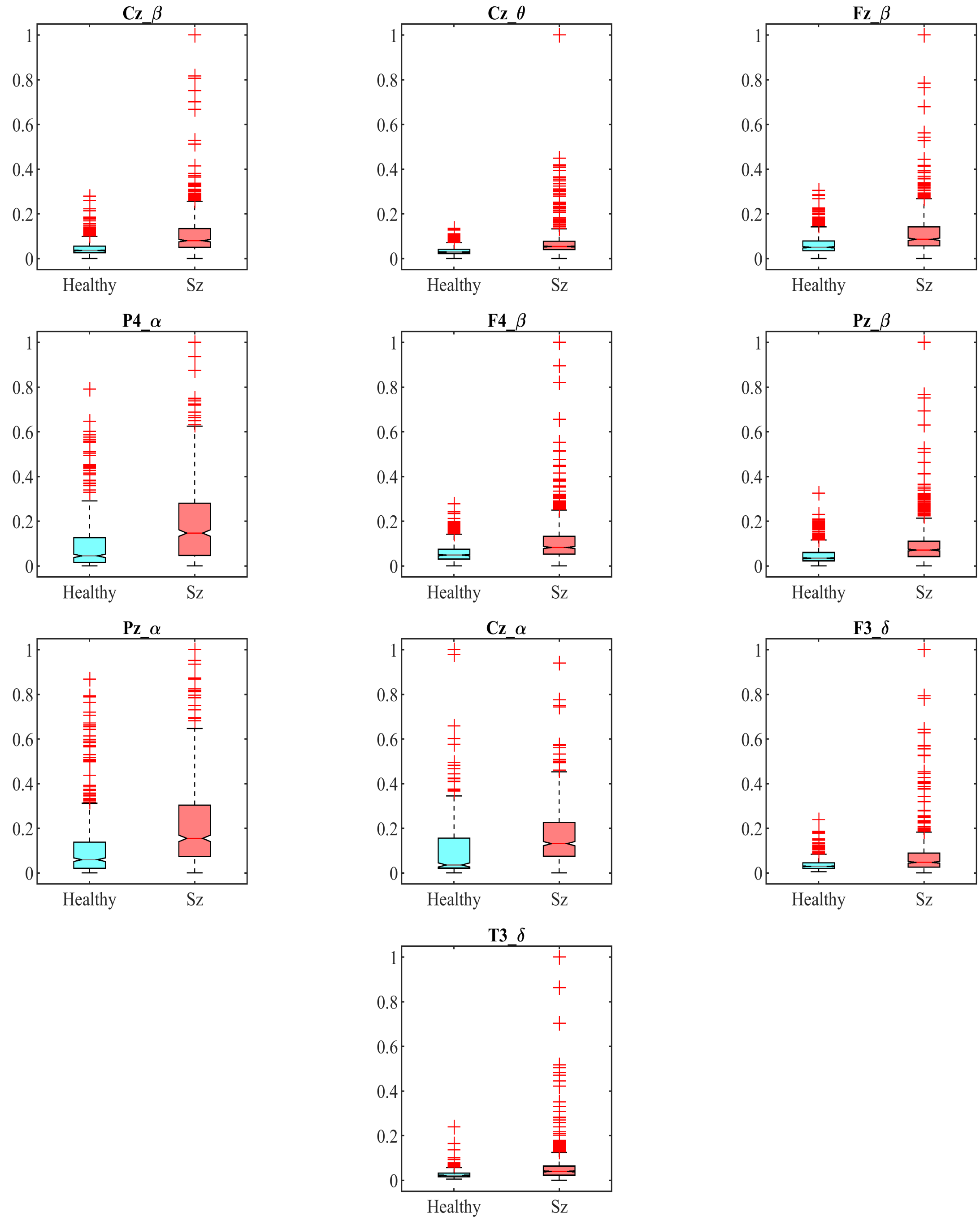

Figure 3.5: Boxplot of 10 most significant features.

Table 3.2: Most significant 30 features chosen using student t-test.

Feature (Location_rhythm)	Healthy (mean±SD)	Schizophrenia (mean±SD)	p-value	t-value
Cz_β	1.89±1.42	4.41±4.14	$2.50e-44$	14.53
Cz_θ	2.09±1.14	4.36±4.31	$2.71e-35$	12.79
Fz_β	2.85±2.08	5.14±4.42	$3.84e-31$	11.93
P4_α	7.02±8.98	14.25±12.91	$9.74e-31$	11.84
F4_β	3.34±2.42	6.14±5.58	$4.99e-30$	11.69
Pz_β	1.88±1.60	3.79±3.84	$7.83e-30$	11.65
Pz_α	8.55±11.31	15.36±12.77	$2.71e-24$	10.39
Cz_α	8.11±9.99	13.65±10.41	$6.77e-23$	10.05
F3_δ	17.54±13.77	36.45±46.77	$8.63e-22$	9.77
T3_δ	8.37±6.19	18.58±25.89	$2.83e-21$	9.64
Cz_δ	7.34±4.10	26.42±50.36	$1.54e-20$	9.45
T3_β	2.80±2.03	4.92±5.34	$2.45e-20$	9.40
Fz_θ	3.31±2.00	5.83±6.63	$1.99e-19$	9.16
P3_α	7.73±9.66	13.26±12.64	$8.48e-19$	9.00
F3_β	3.48±2.32	4.99±3.66	$1.07e-18$	8.97
Pz_δ	6.81±5.78	14.57±21.53	$6.37e-18$	8.76
C4_β	2.28±2.18	4.38±5.85	$4.22e-17$	8.53
Fz_δ	17.42±14.64	36.44±54.23	$4.50e-17$	8.52
C4_α	6.37±6.92	10.00±9.05	$4.47e-16$	8.24
F3_θ	2.99±1.90	4.98±5.85	$6.37e-16$	8.19
P4_β	2.27±2.43	4.37±6.54	$5.64e-14$	7.60
P4_δ	6.62±6.69	23.34±56.73	$4.08e-13$	7.33
T5_α	26.29±30.56	17.34±15.21	$2.39e-12$	7.08
P3_β	1.82±1.77	3.22±4.83	$8.32e-12$	6.90
F7_δ	33.28±28.76	59.12±90.33	$9.97e-12$	6.87
T6_α	28.81±30.20	19.96±19.79	$8.27e-11$	6.55
F4_θ	3.32±2.59	5.34±7.37	$1.09e-10$	6.51
Fp1_β	5.32±3.79	7.80±8.97	$1.63e-10$	6.45
Pz_θ	1.86±1.80	2.74±3.04	$2.24e-10$	6.40
Fp2_β	5.35±3.56	8.41±11.79	$5.24e-10$	6.26

$$\text{Spe} = \frac{\text{TN}}{\text{FP} + \text{TN}} \tag{3.15}$$

$$\text{PPV} = \frac{\text{TP}}{\text{TP} + \text{FP}} \tag{3.16}$$

where true positive (TP) is number of truly detected schizophrenia EEG, true negative (TN) is the number of truly detected healthy EEG, false positive (FP) is number of healthy EEG

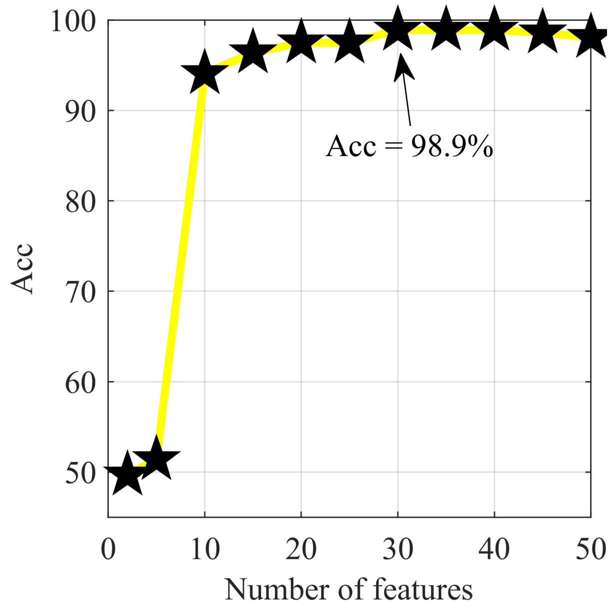

Figure 3.6: Accuracy of SVM (Cubic) classifier with different number of features.

misclassified as schizophrenia EEG, and false negative (FN) is number of schizophrenia EEG is misclassified as healthy EEG.

Table 3.3: Performance parameters of different classifiers used in this study (when proposed MIF is used for EEG rhythm separation).

K-Fold	Classifier	Acc (mean ± SD)	Sen (mean ± SD)	Spe (mean ± SD)	PPV (mean ± SD)	AUC (mean)
5- Fold	SVM-Cubic	97.9±1.1	99.1±1.2	97.0±1.9	96.2±2.5	0.999
	SVM-Quadrature	97.7±0.9	99.0±1.0	96.7±1.6	95.7±2.1	0.999
	SVM-Linear	95.4±2.3	96.2±3.3	94.7±1.9	93.4±2.2	0.994
	Linear discriminant	93.5±3.2	94.0±4.8	93.0±3.3	91.4±3.5	0.985
	KNN	95.6±1.7	96.8±2.4	94.5±3.1	93.3±3.0	0.995
	Decision tree	93.3±2.4	92.6±4.7	93.8±2.5	92.1±3.2	0.981
10- Fold	SVM-Cubic	**98.9±0.9**	**99.0±1.4**	**98.8±1.3**	**98.4±1.9**	**0.999**
	SVM-Quadrature	97.9±1.1	98.8±1.0	97.2±2.0	96.5±2.7	0.999
	SVM-Linear	94.2±2.4	93.6±1.6	94.7±3.5	93.3±4.8	0.989
	Linear discriminant	90.6±3.0	89.7±5.4	91.2±3.0	88.9±4.2	0.974
	KNN	95.3±2.1	95.8±4.0	94.8±3.7	94.0±3.6	0.996
	Decision tree	93.7±2.5	93.6±4.3	93.8±3.6	92.5±4.4	0.984

Note: Bold entries denote the highest values of performance parameters.

Table 3.4: Performance parameters of different classifiers used in this study (when MvFIF is used for EEG rhythm separation).

K-Fold	Classifier	Acc (mean ± SD)	Sen (mean ± SD)	Spe (mean ± SD)	PPV (mean ± SD)	AUC (mean)
5- Fold	SVM-Cubic	96.0±1.5	96.0±2.2	95.9±1.9	95.1±2.1	0.999
	SVM-Quadrature	94.5±2.5	94.5±3.6	94.6±2.8	93.4±3.8	0.998
	SVM-Linear	84.1±2.0	81.8±4.8	86.0±3.1	82.8±3.2	0.923
	Linear discriminant	79.8±3.8	80.5±4.1	79.3±5.0	76.3±3.9	0.896
	KNN	81.6±5.0	81.6±4.6	81.6±6.6	78.7±5.6	0.928
	Decision tree	86.8±2.6	86.8±4.7	86.7±5.6	84.6±4.9	0.966
10- Fold	SVM-Cubic	95.8±1.8	96.1±2.8	95.6±2.5	94.5±3.0	0.999
	SVM-Quadrature	93.2±1.7	93.3±4.5	93.3±3.2	91.6±4.1	0.994
	SVM-Linear	85.0±3.1	82.2±6.5	87.5±3.9	83.8±5.1	0.925
	Linear discriminant	80.1±4.0	81.1±5.0	79.7±5.3	76.0±4.3	0.895
	KNN	83.2±2.1	88.6±3.4	78.5±3.9	78.5±3.8	0.959
	Decision tree	86.1±2.9	87.7±4.2	84.9±5.4	82.3±5.4	0.964

Table 3.3 presents the above-mentioned performance parameters of different classifiers used in this study. Performance parameters of different classifies are shown in Table 3.4 when EEG rhythms separation is done using MvFIF proposed by Cicone and Pellegrino in [126], and all other steps are the same. Accuracy and other parameters for correctly classifying EEG segments corresponding to schizophrenia are better when our proposed MIF algorithm is used for EEG rhythm separation. We have also included the area under the receiver operating characteristic curve (AUC) [157] as another performance measure of the proposed method.

We have analyzed the EEG signal from different lobes to study the effect of schizophrenia on different parts of the brain based on the proposed framework. EEG channels are selected and categorized into five groups based on their position on the brain lobe: Frontal (Fp1, Fp2, F7, F3, Fz, F4, and F8), temporal (T3, T4, T5, and T6), central (C3, Cz, and C4), parietal (P3, Pz, and P4), and occipital (O1 and O2). The 10-fold classification performance for different lobes is showcased in Table 3.5 for the SVM (cubic) classifier. EEG signals from the temporal lobe provide higher accuracy, which may lead to the conclusion that schizophrenia affects the temporal lobe more severely [158].

Table 3.5: The performance of the framework for different lobe's EEG.

Lobe	Acc (mean ± SD)	Sen (mean ± SD)	Spe (mean ± SD)	PPV (mean ± SD)	AUC
Frontal	87.4 ±2.7	87.2 ±5.8	87.9±4.2	85.6±4.7	0.999
Temporal	90.6±2.8	86.2±5.7	94.4±2.2	92.6±3.2	0.999
Central	87.4±3.6	74.9±5.5	97.9±1.3	96.7±2.1	0.999
Parietal	87.4±3.9	75.5±6.6	97.6±1.5	96.3±2.3	0.999
Occipital	77.9±4.2	56.5±7.9	95.3±3.3	91.0±6.0	0.999

Table 3.6: Performance comparison of proposed method with existing methods.

Authors	Methodology	Performance
Oh *et al.* [138] (2019)	Deep CNN	Acc = 98.07%/81.26% Sen = 97.32%/75.0% Spe = 98.17%/87.59%
Jahmunah *et al.* [137] (2019)	Nonlinear feature extraction and SVM-radial basis function classifier	Acc = 92.91% Sen = 93.45% Spe = 92.25%
Krishnan *et al.* [139] (2020)	Entropy feature	Acc = 93.00% Sens = 94.0% Spe = 92.0%
Shalbaf *et al.* [159] (2020)	TFR using continuous wavelet transform and transfer learning using res-net-18-SVM	Acc = 98.6% Sens = 99.65% Spe = 96.92%
Rach *et al.* [160] (2020)	Graph theoretical analysis based feature extraction along with random forest classifier.	Acc = 89.29% Sen = 78.57% Spe = 100% AUC = 0.857
Aslan *et al.* [161] (2020)	Short-time Fourier transform (STFT) based TFR is used as input to CNN	Acc = 97.33% AUC = 0.974
Singh *et al.* [162] (2020)	EEG bands are separated using FFT spectrum, and several features are extracted and used as input to CNN.	Acc = 98.56% Sen = 98.55% Spe = 98.57%
Chandran *et al.* [163] (2020)	Nonlinear feature extraction and long short-term memory (LSTM) technique	Acc = 99.1% Sen = 97.90%
This work	Hjorth features are extracted from EEG rhythms, obtained from EEG signal using MIF based approach. SVM (Cubic) classifier is used for classification.	Acc = 98.9% Sen = 99.0% Spe = 98.8% AUC = 0.999

Table 3.6 presents the comparison of the proposed method with existing methods developed based on this database. For classifying schizophrenia, researchers have explored many different signal processing techniques along with machine learning or deep learning methods. The classification methods proposed by Santos-Mayo *et al.* [135] and Krishnan *et al.* [139] both achieved higher accuracy of about 93.0% using the machine learning

approach. Whereas our proposed method provides a classification accuracy of 98.9%. In addition, Krishanan *et al.* [87, 139] have used MEMD for decomposing multichannel EEG data, which is a computationally complex algorithm for higher dimensional data. Both deep learning-based approaches proposed by Oh *et al.* [138], Shalbaf *et al.* [159], and others achieve higher accuracy, around 98.0%, which is similar to our model's accuracy. However, deep learning-based models are computationally expensive and demand a longer time to be developed as compared to the machine learning-based approach. Hence, our proposed method of detecting schizophrenia is competent to be used as a diagnostic tool.

3.5 Summary

In this chapter, we have proposed a method for the classification of schizophrenia and healthy EEG signals. A novel extension of iterative filtering is developed for multivariate data. Iterative filtering in its original form aims to decompose a single channel multi-components signal into univariate modulated oscillations. MIF decomposes multichannel EEG signals into MIMFs. MIMFs are grouped according to mean frequency in order to obtain different EEG band signals, namely delta, theta, alpha, beta, and gamma rhythms. From each band, Hjorth parameters are extracted and used as features for classifiers. Different classifiers like SVM, KNN, LDA, and decision trees are used to evaluate the performance of features and obtain an accuracy of 98.9% with the SVM (Cubic) classifier.

Comparison of our proposed method with the existing works shows significant improvement in Acc, Spe, and Sen. Other deep CNN-based approaches achieved a similar level of accuracy as our method. But, machine learning based approach is computationally efficient than deep learning based approaches. Thus, the proposed method can be proved as a more realistic and reliable method in predicting schizophrenia and help a medical practitioner to provide better treatment to schizophrenia patients such that they can live a better life.

Chapter 4

Parkinson's Disease Identification Based on Phase-space Representation

4.1 Introduction

Several researchers tried to detect Parkinson's disease using different imaging techniques such as magnetic resonance imaging (MRI), ultrasound of the brain, positron emission tomography (PET) scans, electroencephalogram (EEG), etc. [79]. The conventional subjective method for Parkinson's disease diagnosis is time-consuming and prone to errors [164]. Positron emission tomography (PET), functional MRI (fMRI) based techniques have shown promising performance, but these require high computational facilities, sophisticated instruments, and laboratory setup. EEG signal processing-based methods have several advantages over other neuroimaging techniques, like cost-effectiveness, non-radioactivity, etc.

In the literature, several methods for Parkinson's disease detection from EEG signals have been proposed. Jeong *et al.* [165] proposed a Parkinson's disease detection method based on the wavelet decomposition technique. Relative wavelet energy and wavelet coherence are used as features for classification based on (linear discriminant analysis) LDA. They found that relative wavelet energy was increased for lower frequencies, and the value was lower than in healthy subjects. Liu *et al.* [166] developed a Parkinson's disease detection framework using sample entropy features extracted from three-level discrete wavelet transform subbands. Naghsh *et al.* [167] used a fast Fourier transform (FFT)-based spectrum of EEG signals to diagnose Parkinson's disease. They used independent component analysis to choose the EEG source from the basal ganglia region of the brain. The alpha and beta band powers of the EEG sources in the basal ganglia region are probable indicators of Parkinson's disease. Betrouni *et al.* [168] have proposed a method based on spectral power analysis and k-nearest neighbors (KNN) classifier to classify the different stages of Parkinson's disease, which achieved an accuracy of 84.0%. Oh *et al.* [169] classified the EEG signals belonging to healthy and Parkinson's disease patients using deep convolutional neural network (CNN). They have reported classification accuracies of 88.25% 88.31%. Loh *et al.* [170] developed Gabor transform and deep neural network-based method for Parkinson's disease detection. Their methods obtained an accuracy of 99.46%. Anjum *et al.* [171] used linear predictive coding for EEG with the power spectral density (PSD) for the identification of Parkinson's disease. Jackson *et al.* [164] showed phase-amplitude coupling between beta and broadband gamma (50-150 Hz) is a useful metric for diagnosing Parkinson's disease. Waveform shape measure metrics like sharpness and steepness ratios are also used to categorize EEG signals into healthy and Parkinson's disease classes. George *et al.* [172] reported a decrease in cortical beta-band coherence and an increase in beta band power after dopaminergic medication, generally used to treat Parkinson's disease. Authors in [173] proposed a Parkinson's disease detection framework based on CNN and long short-term memory (LSTM) networks to incorporate structural features and context dependency.

Several methods in literature have used the Fourier transform for the analysis of EEG signals [167, 168]. However, Fourier transform-based methods are not suitable for the analysis of nonstationary signals due to the use of complex sinusoidal basis functions with infinite duration to represent any signal [28]. To capture the time-varying properties, time-localized basis functions are required. Wavelet transforms use a predefined set of basis functions, which also fail to provide proper representation.

By considering the aforementioned issues in existing methods, we have proposed a multivariate analysis-based method for the detection of Parkinson's disease. Multivariate iterative filtering (MIF) has been used to decompose the multichannel EEG data into multivariate oscillatory modes, which are further represented in higher dimensions through phase-space representation (PSR). The area under the Euclidean distance curve obtained from the PSR has been extracted as features. The support vector machine (SVM) and KNN-based machine learning classifiers have been developed to classify the extracted features into Parkinson's disease and healthy categories.

EEG signals are prone to several artifacts, and analysis of artifact-contaminated segments can be misleading. The existing Parkinson's disease detection frameworks have analyzed a single small segment of EEG data for identifying Parkinson's disease. To reduce the effect of artifacts, instead of using a single segment, we have used multiple mini-segments for decision-making. Information fusion is used to obtain a more reliable final decision. Information fusion is typically classified into three types based on the level of abstraction of data processing: data-level fusion, feature-level fusion, and decision-level fusion [174]. In this chapter, we have proposed feature-level and decision-level fusion strategies to get the final decision from multiple mini-segments.

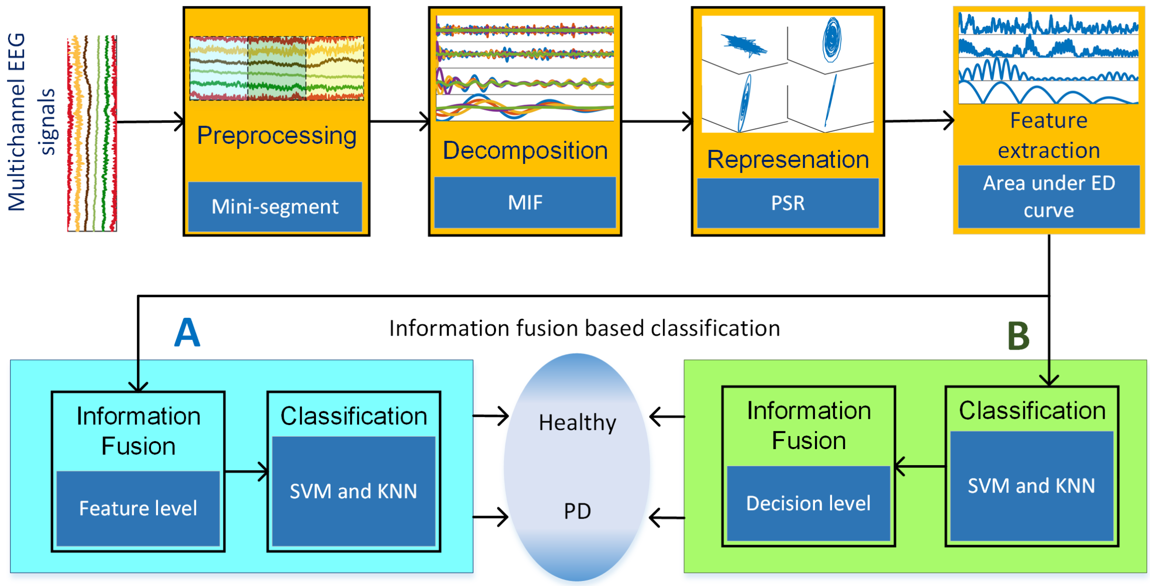

Figure 4.1: Block diagram of the proposed framework for Parkinson's disease detection from EEG (Note: PD denotes Parkinson's disease).

The main contributions of the chapter are as follows:

1. The characteristics of the EEG signal have been studied using MIF for Parkinson's disease detection.

2. A data-adaptive signal decomposition-based framework has been developed for the

detection of Parkinson's disease from EEG signal.

3. PSR-based feature has been proposed for the classification of EEG signals.

4. Different fusion strategies have been proposed for obtaining more reliable decisions with high sensitivity.

4.2 Database

We have used a publicly available database for evaluating the proposed Parkinson's disease detection framework. The EEG data corresponding to 15 Parkinson's disease patients and 16 healthy subjects were collected at a sampling frequency of 512 Hz [164]. The Parkinson's disease patients were suffering from mild to moderate Parkinson's disease (between stage II and III on the Hoehn and Yahr scale) [172]. For Parkinson's disease subjects, EEG signals are recorded with two conditions: medications on and off. A 32-channel Biosemi ActiveTwo bio amplifier is used to record the EEG data for at least 3 minutes. During the data recording, subjects were instructed to sit steadily and to fixate on a cross shown on a screen. Data were filtered using a highpass filter of cut-off frequency 0.5 Hz. EEG signals corresponding to a healthy subject and a Parkinson's disease patient are shown in Figs. 4.2 (a) and (b), respectively. For more details about the dataset used in this study, please refer to [164].

4.3 Methodology

The proposed framework for Parkinson's disease detection, as illustrated in Fig. 4.1, used MIF to decompose the multichannel signal into narrowband multivariate intrinsic mode functions (MIMFs), adaptively. PSR is used to extract features from MIMFs. Finally, using a machining learning classifier and information fusion techniques, the EEG signals are classified into two groups: Healthy and Parkinson's disease. Each step is described below.

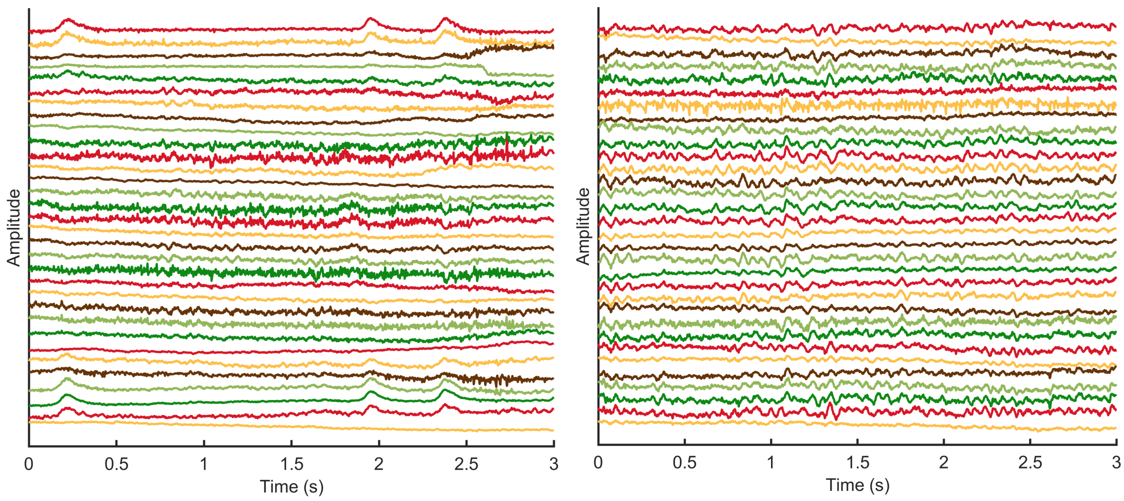

(a) (b)

Figure 4.2: EEG signals corresponding to (a) healthy and (b) Parkinson's disease subjects.

4.3.1 Preprocessing

In the preprocessing stage, we have partitioned the continuously recorded EEG signals into 3 s EEG epochs. A notch filter centered around 60 Hz has been used in order to remove power line noise. EEGLAB toolbox [175] has been used for notch filtering. The 3 s epoch is further divided into mini-segments having different window lengths (W) of 1 s (512 samples) or 1.5 s (768 samples) for information fusion-based classification. We get 3 mini-segments for 1 s length and 2 mini-segments for 1.5 s length. The EEG segments are z-score normalized before further processing.

4.3.2 Signal Decomposition based on MIF

The signals associated with biological systems are generally complex, nonlinear, and nonstationary in nature. Due to lower time-frequency localization and using predefined basis functions, conventional signal processing techniques like Fourier transform, wavelet analysis tools fail to provide an effective representation of bio-signals. The EEG signals are decomposed into narrowband oscillatory components using MIF algorithms described in Chapter 2. For the proposed framework, we have considered Th as 0.001 for the stopping criteria of the MIF algorithm.

4.3.3 Phase-space Representation (PSR)

PSR has been used for representing physiological signals to get more insights. PSR is an effective tool for mapping the signal in such a way that the dynamics of the signal or how the signal has evolved forward in time can be easily observed [176, 177, 178].

A signal $x[n] = \{x[1], x[2], \ldots, x[L]\}$ of length L, can be represented mathematically in the form of PSR vector as follows: $x_{\text{PSR}}(k) = [x[k], x[k+l], \ldots, x[k+(D-1)l]]$, where k will vary in the range 1 to $L-(D-1)l$. l and D denote time lag and embedding dimension of PSR, respectively [179]. The PSR vector can be written in expanded form as,

$$
\begin{aligned}
x_{\text{PSR}} &= \begin{bmatrix} x_{\text{PSR}}(1) \\ x_{\text{PSR}}(2) \\ \vdots \\ x_{\text{PSR}}(L-(D-1)l) \end{bmatrix} \\
&= \begin{bmatrix} x[1] & x[1+l] & \cdots & x[1+(D-1)l] \\ x[2] & x[2+l] & \cdots & x[2+(D-1)l] \\ \vdots & \vdots & \ddots & \vdots \\ x[L-(D-1)l] & x[L-(D-1)l+l] & \cdots & x[L] \end{bmatrix}
\end{aligned} \tag{4.1}
$$

The PSR is a useful representation to depict the nature of nonlinearity, whether the signal is chaotic or not, etc.

4.3.4 Feature Extraction

We have computed the Euclidean distance between all the points in PSR and the center of PSR, which is termed the Euclidean distance curve. The mathematical expression for the Euclidean distance curve can be expressed as follows:

$$\text{Ed}(k) = \sqrt{x^2(k) + x^2(k+l) + x^2(k+(D-1)l)} \tag{4.2}$$

The area under the Euclidean distance curve is computed based on numerical integration using the trapezoidal method [180]. The area under the Euclidean distance curve extracted from the MIMFs corresponding to all channels is used as features. The norm of the Euclidean distance curve is used for feature representation in [181].

4.3.5 Classification

We have used SVM and KNN classifiers to evaluate the effectiveness of the proposed feature space for detecting Parkinson's disease from EEG signals. SVM classifier has been successfully used in EEG signal processing-related applications [25, 182]. Vapnic *et al.* [150] have developed the statistical theory behind the SVM classifier for binary classification. A linear decision surface is used to discriminate a high-dimensional feature space.

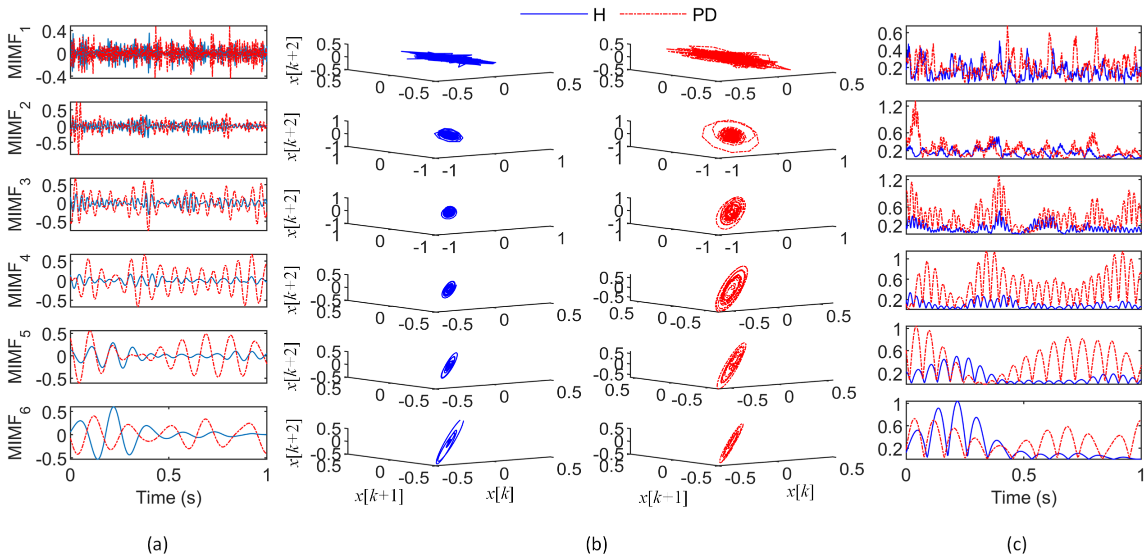

Figure 4.3: (a) EEG signals, (b) 3-D PSRs, and (c) Euclidean distance curves corresponding to healthy and Parkinson's disease subjects (Note: H denotes healthy and PD denotes Parkinson's disease).

KNN is a supervised and non-parametric classifier that classifies a given data point based on the majority of its surrounding data points [152]. The working principle of KNN includes two steps: finding the k nearest neighbor based on distance metrics like Euclidean distance, cosine distance, etc., and assigning the class to the new data point based on the majority in the neighbor. Here, we consider Euclidean distance and $k = 1$ for the KNN classifier.

4.3.6 Fusion for Decision

Classification results from a single small segment of signals may provide an erroneous decision due to the presence of a short-duration artifact. Multiple segment-based fused classifications may improve the system's performance. Artifact-affected segments can be one possible cause of misclassification, which can be avoided by using multiple segments for decisions. Here, we proposed several fusion strategies for multi-segment classification at different levels, like feature-level and decision-level. In feature-level decision fusion, the extracted features from different segments are averaged, and a single classifier is developed based on the averaged feature vector. This fusion strategy is named as fusion model 1 (M1). The fusion model M1 can help to reduce the effect of sudden changes in signal due to the appearance of noise.

In decision-level fusion, multiple classifiers are trained for each mini-segment feature. Then, the classification outputs for mini-segment data are fused using Boolean logic, AND and OR logic, which are named as fusion models 2 (M2) and 3 (M3), respectively.

4.4 Results and Discussion

In this section, we have presented the results obtained for the proposed MIF-PSR-based Parkinson's disease detection method. Additionally, we have discussed the results and compared the performance with the state-of-the-art methods for Parkinson's disease detection.

In the preprocessing stage, a total of 1018 and 1990 3 s epochs are obtained for healthy and Parkinson's disease classes, respectively. We have combined the medications on and off data epoch to form the Parkinson's disease class. MIF is used to decompose the multi-channel EEG epoch into oscillatory components. Figure 4.3 (a) shows decomposed MIMFs corresponding to EEG signals (shown at the top of Figs. 4.2 (a) and (b) for healthy and Parkinson's disease subjects, respectively). Only the first six MIMFs are selected for feature extraction as they give discriminant features, as observed in the preliminary experiment. All MIMFs have been represented individually in n-dimension PSR. Figure 4.3 (b) shows 3D PSRs of MIMFs, shown in 4.3 (a). The Euclidean distance between each point and the center of the PSR is computed, which is shown in Fig. 4.3 (c). The area under the Euclidean distance curve is computed and used as a feature for training classifiers. A total of 192 features are obtained from the MIMFs of 32-channel EEG data (32 channels $\times$ 6 MIMFs). Based on information fusion strategies (M1, M2, and M3), SVM and KNN classifiers are developed for the identification of Parkinson's disease.

A group of statistical measurements, including accuracy (Acc), sensitivity (Sen), and specificity (Spe), are used to assess the classification performance of the proposed framework. These parameters are defined in Eqs. (3.13)-(3.15).

Here, true positive (TP) denotes the Parkinson's disease EEG segments truly detected as Parkinson's disease, false negative (FN) denotes the Parkinson's disease EEG segments classified as healthy, true negative (TN) denotes truly predicted healthy EEG, and false positive (FP) refers to healthy EEG segments classified as Parkinson's disease segments.

Table 4.1: Performance measures (in %) of MIF-PSR for various embedding dimensions of PSR and mini-segment lengths.

D	Parameters	$W = 512$						$W = 768$					
		M1		M2		M3		M1		M2		M3	
		SVM	KNN	SVM	KNN	SVM	KNN	SVM	KNN	SVM	KNN	SVM	KNN
2	Acc	98.27	95.11	96.38	90.16	95.15	89.56	98.27	95.08	96.91	92.32	96.84	92.49
	Sen	98.99	96.28	94.87	86.63	99.80	99.70	98.99	96.28	96.28	90.80	99.70	99.10
	Spe	96.86	92.83	99.31	97.05	86.05	69.74	96.86	92.73	98.13	95.28	91.26	79.57
3	Acc	98.20	95.05	96.34	89.93	95.05	89.59	98.24	95.05	96.97	92.22	96.81	92.49
	Sen	99.05	96.23	94.82	86.28	99.80	99.70	98.99	96.23	96.33	90.85	99.70	99.10
	Spe	96.56	92.73	99.31	97.05	85.76	69.84	96.76	92.73	98.23	94.89	91.16	79.57
4	Acc	98.20	95.05	96.31	89.83	95.05	89.79	98.17	95.01	96.97	92.35	96.78	92.59
	Sen	99.05	96.13	94.77	86.13	99.80	99.70	98.94	96.13	96.33	90.90	99.70	99.10
	Spe	96.56	92.93	99.31	97.05	85.76	70.43	96.66	92.83	98.23	95.19	91.06	79.86
5	Acc	98.24	95.05	96.38	89.86	95.01	89.79	98.17	95.05	97.01	92.39	96.78	92.72
	Sen	99.05	96.13	94.87	86.23	99.80	99.65	98.99	96.13	96.38	90.90	99.70	99.10
	Spe	96.66	92.93	99.31	96.95	85.66	70.53	96.56	92.93	98.23	95.28	91.06	80.26
6	Acc	98.24	95.05	96.34	89.86	94.98	89.76	98.24	95.11	97.01	92.45	96.81	92.69
	Sen	99.05	96.08	94.82	86.23	99.75	99.75	99.05	96.18	96.38	91.01	99.70	99.10
	Spe	96.66	93.03	99.31	96.95	85.66	70.24	96.66	93.03	98.23	95.28	91.16	80.16
7	Acc	98.14	95.05	96.34	89.99	94.98	89.76	98.20	95.18	97.04	92.45	96.88	92.69
	Sen	98.94	96.08	94.82	86.33	99.75	99.75	99.05	96.23	96.43	91.06	99.75	99.10
	Spe	96.56	93.03	99.31	97.15	85.66	70.24	96.56	93.12	98.23	95.19	91.26	80.16
8	Acc	98.14	95.08	96.34	90.03	95.01	89.83	98.20	95.18	97.04	92.49	96.84	92.69
	Sen	98.94	96.13	94.82	86.38	99.75	99.70	99.05	96.23	96.43	91.01	99.75	99.10
	Spe	96.56	93.03	99.31	97.15	85.76	70.53	96.56	93.12	98.23	95.38	91.16	80.16
9	Acc	98.17	95.08	96.38	90.09	95.05	89.83	98.27	95.15	97.07	92.52	96.81	92.65
	Sen	98.94	96.13	94.87	86.43	99.75	99.70	99.05	96.23	96.48	91.06	99.75	99.10
	Spe	96.66	93.03	99.31	97.25	85.85	70.53	96.76	93.03	98.23	95.38	91.06	80.06
10	Acc	98.17	95.15	96.38	90.03	95.05	89.93	98.24	95.15	97.11	92.55	96.84	92.59
	Sen	98.89	96.18	94.87	86.33	99.75	99.70	98.99	96.23	96.53	91.06	99.75	99.10
	Spe	96.76	93.12	99.31	97.25	85.85	70.83	96.76	93.03	98.23	95.48	91.16	79.86

The performance measures of the classifiers obtained for different parameters, including PSR embedding dimension (D) and length of the mini-segment (W), are showcased in Table 4.1. A five-fold cross-validation scheme is used to evaluate the performance of the classifiers. Fusion model M1 provides the highest accuracy of 99.27% (Sen: 98.99% and Spe: 96.86%) for mini-segment length and PSR embedding dimensions of 512 samples and 2, respectively. PSR with two dimensions and a mini-segment length of 512 samples provides 99.80% Sen for the classification of Parkinson's disease with an accuracy of 95.15%. A high sensitivity will ensure that any patients suffering from Parkinson's disease will not be wrongly diagnosed as healthy subjects. For this model, the specificity has decreased to 85.76%, which may lead to the diagnosis of a healthy person with Parkinson's disease. This model will be useful for primary screening purposes. Further confirmation needs to be taken from an expert, and proper treatment can be started.

Table 4.2 shows the performance when Parkinson's disease medication on and medication off-state have been considered as two different classes. The proposed framework based on model M1 with embedding dimension 4, mini-segment length 512, and SVM classifier archives an Acc of 94.95%, Sen of 94.77%, and Spe of 96.77%.

In the literature, most of the studies used PSR realized in lower dimensions like two or three dimensions due to the possibility of easy visualization [177, 181]. However, in this chapter, we have analyzed the performance of the proposed MIF-PSR with higher dimensional PSR. The time taken to obtain the PSR and compute the area feature is calculated for all the epochs. The mean and standard deviation (SD) values for feature computation time are shown in Fig. 4.4 (a) for different embedding dimensions. The computation time has gradually increased for the higher embedding dimension of the PSR. Figure 4.4 (b) shows the evaluation of accuracy with the embedding dimension of PSR. We have not found any significant improvement in classification accuracies for higher dimensions, but the computation time has increased. The results, shown in Table 4.1 and Fig. 4.4, present evidence that lower dimension PSR is also useful to differentiate between the dynamics of MIMFs corresponding to healthy and Parkinson's disease EEG signals. So, for the Parkinson's disease detection application, lower-dimensional PSR features can also be used due to the lower computational complexity compared to higher-dimensional PSR-based features.

The effect of varying time lag parameters (l) on the accuracy of the Parkinson's disease

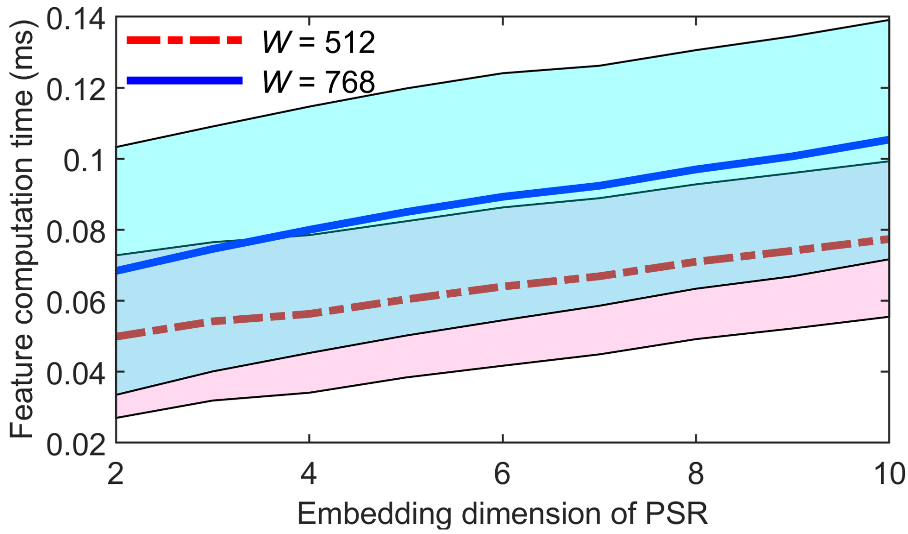

(a)

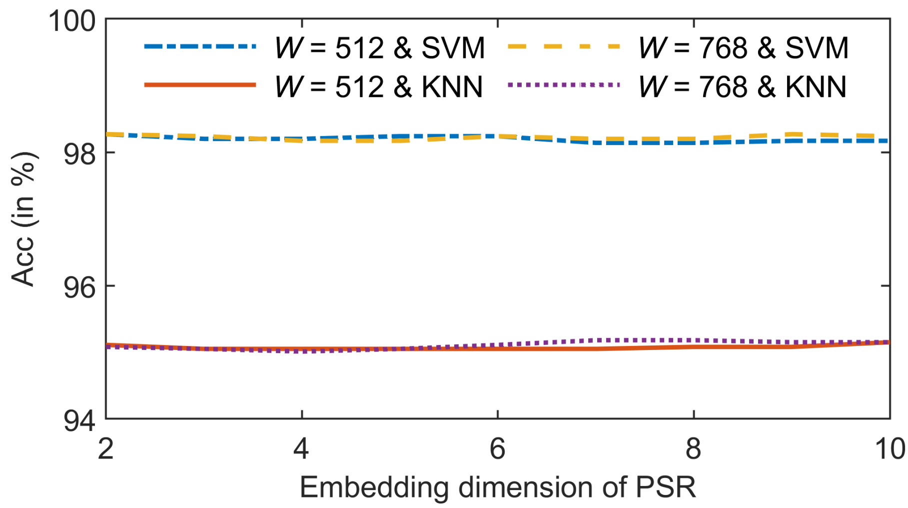

(b)

Figure 4.4: (a) Feature computation time for different embedding dimensions of the PSR (the bold lines show the median of computation time, and the shaded area shows the interquartile range of feature computation time) and (b) evaluation of accuracy (for M1 fusion model) with embedding dimensions of the PSR.

detection framework is assessed by choosing l between 1 to 700 or the maximum possible value ($L - (D-1)l > 0$). The evaluation of accuracy with increasing time lag is illustrated in Fig. 4.5. The accuracy remains the same up to a certain range of time lag parameters. So, we chose time lag l as 1 in the proposed framework.

The proposed MIF-PSR Parkinson's disease detection framework fused information

Table 4.2: Performance measures (in %) of MIF-PSR for various embedding dimensions of PSR and mini-segment lengths for model M1.

D	Parameters	$W = 512$		$W = 768$	
		SVM	KNN	SVM	KNN
2	Acc	94.85	89.13	94.88	89.16
	Sen	94.67	86.82	94.77	86.72
	Spe	96.67	94.44	96.72	94.49
3	Acc	94.91	89.10	94.85	89.10
	Sen	94.77	86.82	94.77	86.62
	Spe	96.77	94.39	96.72	94.44
4	Acc	94.95	89.13	94.91	89.20
	Sen	94.77	86.52	94.87	86.62
	Spe	96.77	94.49	96.72	94.54
5	Acc	94.88	89.20	94.91	89.30
	Sen	94.77	86.52	94.87	86.62
	Spe	96.67	94.59	96.72	94.69
6	Acc	94.85	89.16	94.85	89.39
	Sen	94.67	86.42	94.77	86.72
	Spe	96.67	94.59	96.67	94.69
7	Acc	94.85	89.06	94.81	89.36
	Sen	94.77	86.32	94.77	86.62
	Spe	96.62	94.49	96.62	94.69
8	Acc	94.85	89.10	94.88	89.43
	Sen	94.77	86.42	94.87	86.62
	Spe	96.62	94.54	96.62	94.79
9	Acc	94.85	89.10	94.91	89.43
	Sen	94.77	86.42	94.97	86.62
	Spe	96.62	94.54	96.62	94.79
10	Acc	94.88	89.16	94.91	89.39
	Sen	94.77	86.42	94.97	86.62
	Spe	96.72	94.59	96.67	94.74

from multiple mini-segments to generate a final decision. A short-duration artifact can affect the decision of the whole segment when we analyze the whole segment at a time. To illustrate this, an EEG epoch (only noise-contaminated channels are shown) of a Parkinson's disease patient is shown in Fig. 4.6. The EEG epoch is divided into three mini-segments of length 512 samples which are separated using red dashed lines. It can be observed that the first and second mini-segments are affected by artifacts. The classifier fails to predict these initial two mini-segments (highlighted using red boxes) as Parkinson's disease EEG. The last mini-segment has been successfully predicted as Parkinson's disease, which has been highlighted using a green box. The final decision for the EEG epoch has been obtained by the proposed M3 fusion strategy, which correctly marked the 3 s segment as Parkinson's disease EEG. On the other hand, when the whole EEG epoch (shown in Fig. 4.6) is used for prediction, due to the presence of artifacts, the epoch has been classified as a healthy

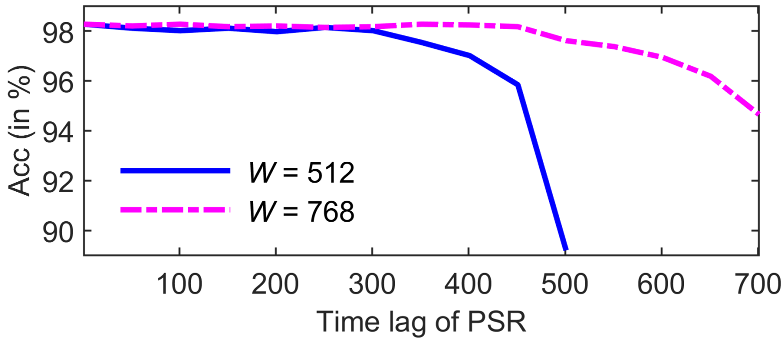

Figure 4.5: Evaluation of Acc (for M1 fusion model) with time lag of the PSR.

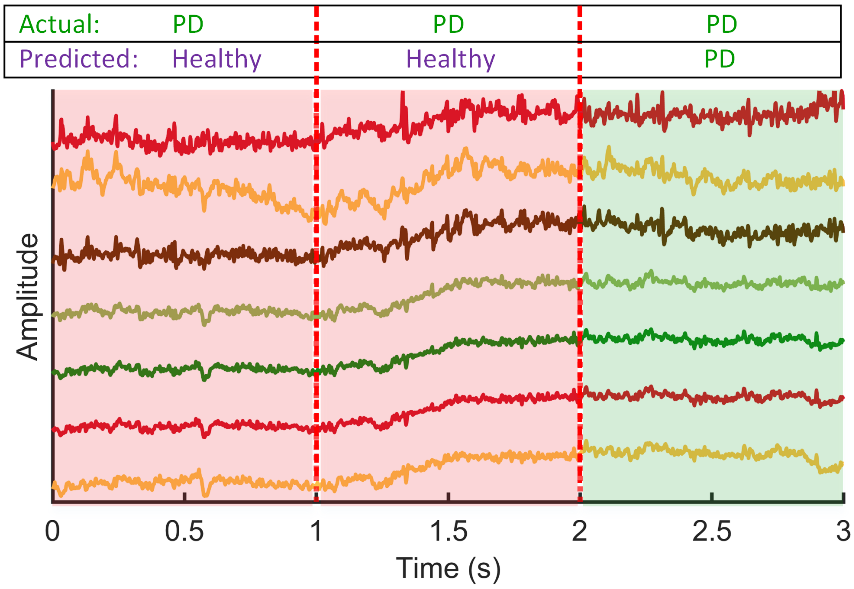

Figure 4.6: EEG signals corresponding to Parkinson's disease subject divided into three mini-segments of window length 512 samples (vertical red dashed lines are separating the mini-segment). (Note: PD denotes Parkinson's disease)

epoch. The proposed fusion model M3 helps in increasing the Sen of the Parkinson's disease identification framework. High Sen is very important for the disease screening process [183].

The performance comparison between using the original EEG signal and MIF-based decomposed component is presented in Fig. 4.7 to show the usefulness of MIF. The average of the performance obtained for different PSR dimensions is shown in Fig. 4.7. Also, univariate iterative filtering is used to decompose the multichannel EEG signal in a channel-wise manner, and the performance is evaluated. The number of decomposed components are

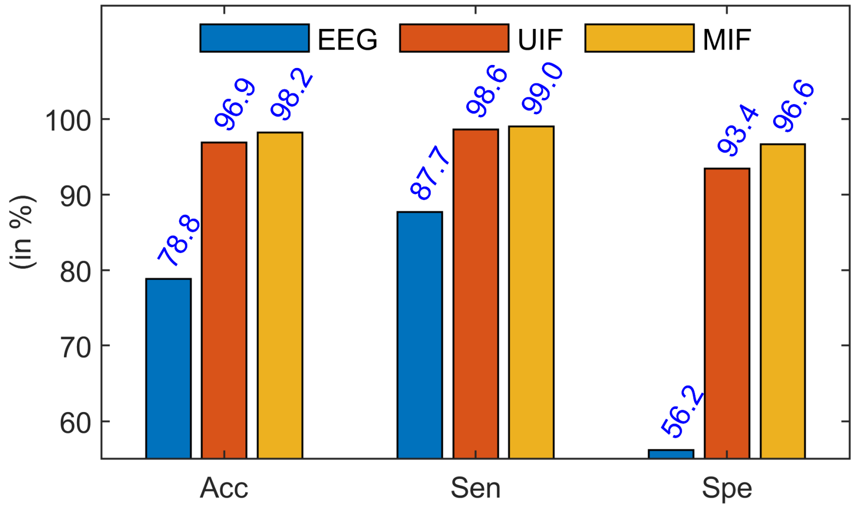

Figure 4.7: Performance comparison between EEG and MIMF (for M1 fusion model). (Note: UIF denotes univariate iterative filtering)

kept as six same as MIF decomposition. The iterative filtering does not guarantee the same number of oscillatory modes in all channels. When iterative filtering provides a number of oscillatory modes less than six, we consider a constant zero signal to obtain the same number of oscillatory modes in all channels. All the statistical parameters Acc, Sen, and Spe have increased significantly for MIF-based decomposed components. An uneven number of modes in different channels and improper mode alignment are two major drawbacks of univariate signal decomposition [25].

The proposed features (average over all epochs) for different MIMFs corresponding to healthy and Parkinson's disease classes are shown using topoplot in Fig. 4.8. The difference between the average feature between the healthy and Parkinson's disease subjects' EEG is shown in the bottom row. The color in the topoplot represents the value of the variable (feature/difference of feature). The higher color difference in the topoplot between healthy and Parkinson's disease classes signifies the feature's discrimination ability. Features corresponding to the fourth and fifth MIMFs are showing visible differences between healthy and Parkinson's disease subjects in the central, temporal, and occipital lobes of the brain. The features corresponding to the second and third MIMFs show a clear difference in the FL of the brain.

Figure 4.2 shows the EEG segments corresponding to healthy and Parkinson's disease

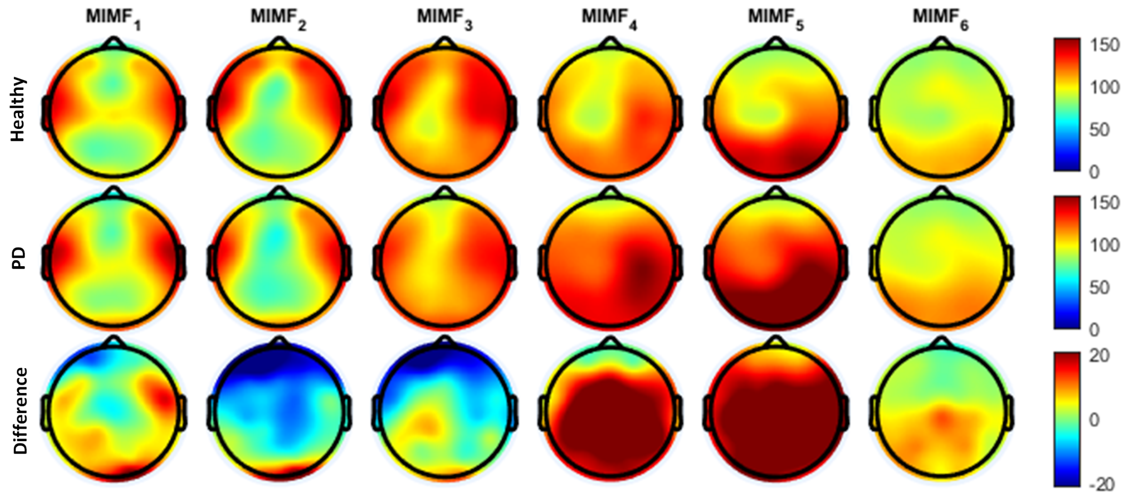

Figure 4.8: Topoplot of the extracted features corresponding to healthy and Parkinson's disease subjects and their difference for different MIMFs. (Note: PD denotes Parkinson's disease)

patients. A neurologist can level the EEG signals by correlating the symptoms of the patients whether the EEG segments belong to Parkinson's disease or not. It is not possible to infer any visual difference from the EEG signals belonging to the two classes. The features derived from the EEG signals are ranked based on two-sample t-tests. The five most significant features corresponding to healthy and Parkinson's disease subjects are shown using a boxplot presented in Fig. 4.9. The feature values corresponding to the Parkinson's disease EEG segments are higher than the healthy EEG segments. The proposed features make it easy to see the visual difference between healthy and Parkinson's disease classes. Hence, the interpretability of the feature can directly help to understand the classes of EEG signals. This feature can be used as a diagnostic feature. Moreover, it can be observed that all five significant features lie in the central region of the brain. A similar finding has been obtained from the topoplot also, presented in Fig. 4.8.

The proposed MIF-PSR-based technique is compared with the state-of-the-art methods to assess its superiority and effectiveness in Parkinson's disease detection in Table 4.3. For classifying Parkinson's disease, researchers have used signal processing algorithms along with machine learning or deep learning classifiers. Our proposed framework is based on a machine learning classifier but provides similar performance to deep learning classifiers. The machine learning methods are computationally less complex but need to be fed with

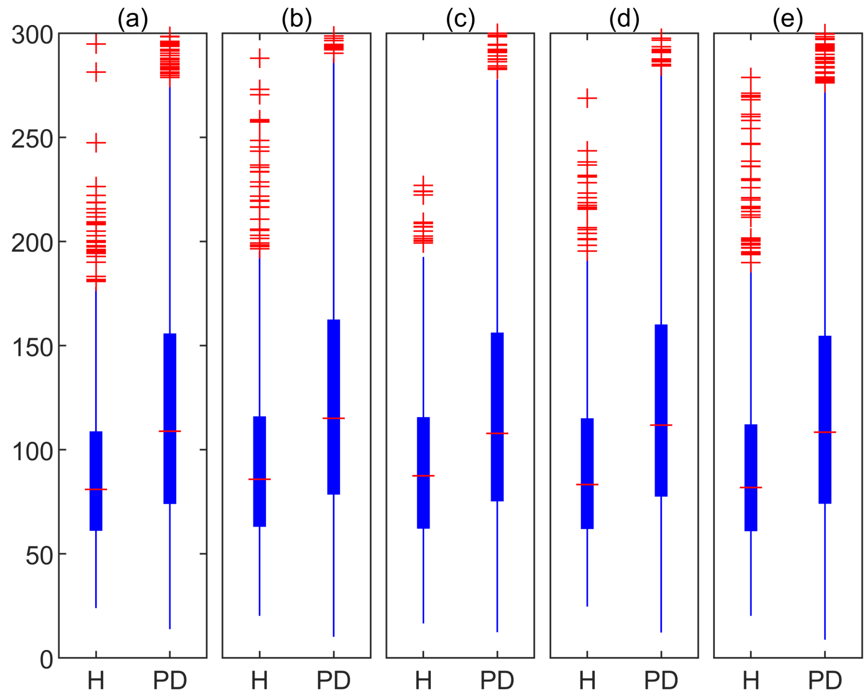

Figure 4.9: Features corresponding to healthy and Parkinson's disease EEG segments: (a) MIMF_5 of Cz channel, (b) MIMF_4 of Cz, (c) MIMF_4 of C3 channel, (d) MIMF_4 of CP1 channel, and (e) MIMF_5 of C3 channel. (Note: H denotes healthy, and PD denotes Parkinson's disease)

hand-crafted features. Depending on the features chosen, accuracy may be adversely affected. The deep learning-based classifiers extract automatic features from the data, but the deep network demands more computational resources as compared to the machine learning classifiers.

The proposed framework has used 32-channel EEG data for Parkinson's disease detection. In the future, channel selection based on the significance can be incorporated with the proposed framework, which may be helpful in reducing the effort of recording EEG signals, achieving a computationally less complex framework.

The automated Parkinson's disease detection system will be helpful in detecting the disease with less manual effort in rural areas where there is generally limited access to neurologists and movement disorder specialists. In urban areas, hospitals are available, but due to the high number of patients coming to avail of health-related services, the workload of the doctors and healthcare providers is very high. The proposed system can be an assistive tool

Table 4.3: Comparative performance of the proposed Parkinson's disease identification framework with existing methods.

Authors (Years)	Dataset	Methodology	Performance measures
Jeong *et al.* [165] (2016)	Subjects: 52 (Healthy: 26 & PD: 26)	Relative wavelet energy and wavelet coherence with LDA	Acc = 79.18% Sen = 81.84% Spe = 76.49%
Liu *et al.* [166] (2017)	Subjects: 42 (Healthy: 25 & PD: 17)	Sample entropy of subbands extracted using discrete wavelet transform and three-way optimal center constructive covariance	Acc = 92.86%
Naghsh *et al.* [167] (2020)	Subjects: 20 (Healthy: 10 & PD: 10)	FFT based PSD and fine Gaussian SVM classifier	Acc = 95.00%
Oh *et al.* [169] (2020)	Subjects: 40 (Healthy: 20 & PD: 20)	CNN having thirteen layers	Acc = 88.25% Sen = 84.71% Spe = 91.77%
Loh *et al.* [170] (2020)	Subjects: 31 (Healthy: 16 & PD: 15) *	Gabor transform and deep neural network	Acc = 99.46%
Anjum *et al.* [171] (2020)	Subjects: 82 (Healthy: 41 & PD: 41)	Linear predictive coding EEG algorithm	Acc = 85.70% Sen = 85.70% Spe = 85.70%
Li *et al.* [173] (2023)	Subjects: 55 (Healthy: 30 & PD: 25)	CNN and LSTM based hybrid deep neural network	Acc = 98.60% Sen = 97.10% Spe = 97.60%
Proposed work	Subjects: 31 (Healthy: 16 & PD: 15)	MIF and PSR-based feature extraction and SVM classifier with information fusion model M1 (window length of 512 samples)	Acc = 98.27% Sen = 98.99% Spe = 96.86%
		Fusion model M3 (window length of 512 samples)	Acc = 95.15% Sen = 99.80% Spe = 86.05%

Note: * denotes the same database as used in our study.

for doctors to make efficient diagnoses, thereby improving patient outcomes and alleviating the burden on healthcare professionals.

4.5 Summary

In this chapter, we have proposed a computer-aided method for detecting Parkinson's disease from EEG signals based on MIF and PSR-based features. Also, a detailed exploration to find suitable parameters for the framework is performed. The multichannel EEG signals are decomposed into multivariate oscillatory modes using MIF, which is represented in higher dimensions based on PSR. The proposed area feature is computed from different MIMFs and channels of EEG signals. The method is validated using a publicly available dataset. The SVM classifier achieves an accuracy of 98.27%, sensitivity of 98.99%, and specificity of 96.86% based on feature-level information fusion with a window length of 512. Based on the decision level feature fusion M2 with a window length of 512 samples, we have obtained 99.80% sensitivity with an accuracy of 95.15%. The experimental results show the efficacy and reliability of the Parkinson's disease detection system. The comparative study between the proposed method and existing methods shows significant improvement in classification performance. The proposed biomarker for detecting Parkinson's disease will be helpful in reducing the manual effort of healthcare service providers by providing automatic, accurate diagnostics.

Chapter 5

Motor Imagery Brain-computer Interface using Common Spatial Pattern

5.1 Introduction

Different experimental techniques, including Functional magnetic resonance imaging (fMRI) [184], electroencephalogram (EEG) [69, 82, 185], magnetoencephalography (MEG) [186], transcranial magnetic stimulation (TMS) [187], positron emission tomography (PET) [188] etc., are used to study motor imagery (MI) brain-computer interface (BCI). Among these techniques, EEG is the most widely used technique and is continuously gaining more interest for BCI systems because it is noninvasive, has the potential for mobility in user, has high time resolution, comparatively low cost, and lastly, recording is possible outside the lab environment with minimum instrument requirements.

A fast-growing number of studies indicates that mu (8-12 Hz) and beta (18-25 Hz) rhythms of EEG are the neurophysiological basis for MI BCI, observed in the sensory-motor cortex (SMC) area of the brain [69]. A study carried out by Nikouline *et al.* [189] has reported suppression of mu rhythms at both the ipsilateral and contralateral somatosensory cortex due to somatosensory stimuli while Pfurtscheller *et al.* [190] demonstrated changes of EEG activity, due to voluntary movements, in low-frequency bands including mu and beta rhythms. Several studies attempted to develop an MI BCI system based on analyzing band powers of mu and beta rhythms [189, 191]. However, most of the studies so far have employed Fourier analysis. Fourier transformation tries to decompose any signal using a predefined set of orthogonal basis functions, namely sine-cosine wave. In most cases, biomedical signals are characterized by short, impulse-like events that represent transitions between different phases of a biological cycle, e.g., the activation potential of the neuron. Complex biological systems produce highly nonlinear and nonstationary signals; due to that, the usefulness of a fixed basis function-based algorithm is less appropriate. These approaches extracted frequency bands using bandpass filtering of the data. But, unfortunately, MI responsive frequency bands vary across subjects and even for different trials of the same subject [69, 192]. To address this issue, researchers go for subject-specific frequency bands selection based on manual visualization or set to unspecified broadband.

Data adaptive techniques like empirical mode decomposition (EMD) [63], variational mode decomposition (VMD) [65, 193], iterative filtering [64] may be the solution to the problems associated with Fourier transform or wavelet analysis. EMD-based techniques were proposed for MI BCI to resolve issues like nonlinearity and nonstationarity of the EEG signal. But multichannel EEG data decomposed by univariate EMD generates intrinsic mode functions (IMFs) for different channels having varying frequency properties, which is known as the uniqueness problem [69].

Park *et al.* [69] overcame this problem by using multivariate EMD (MEMD) [87] technique, which decomposes data into set of data-adaptive basis termed as multivariate IMF (MIMF). Gaur *et al.* [185, 194] also used MEMD along with common spatial pattern (CSP) for developing MI BCI systems. All the above approaches have combined the selected MIMFs based on their relevance to reconstruct EEG signal. Several parameters like classification accuracies, mean, and median frequency of MIMFs were used for determining the relevance of a particular MIMF. A study, performed by Ang *et al.* [192], tried to find most appropriate frequency bands for MI BCI.

In MI-based BCI using EEG, CSP is the most popular method of discriminant feature extraction [195, 196, 197]. CSP is a data-driven supervised algorithm that analyses multichannel EEG data associated with two different classes. This signal is then projected into a new space, in such a way that the variance of the projected signal corresponding to one class of MI task will be maximized, simultaneously it will be minimized for the other class of MI task. However, the performance of CSP depends on the operational frequency bands, which are selected manually or set to a broad frequency range in most of the previously developed applications. Due to subject-to-subject or even trial-to-trial variability of frequency band affected by MI task, these methods suffer from poor performance. Jin *et al*. [198] proposed a CSP based MI BCI technique where they have used Demster-Shafer theory for internal feature selection. This method suppressed the outliers, which may adversely affect the performance. In another CSP based MI BCI approach, Jin *et al.* [196] used correlation based channel selection method to select more relevant channels. CSP is very sensitive to outliers; for that, Jin *et al.* [199] developed feature optimization and outlier detection techniques. The effectiveness of CSP depends on the selection of frequency bands. Therefore, a poorly selected frequency band can adversely affect the classification performance.

To overcome the aforementioned issues, we have proposed an MI BCI algorithm based on MIF and CSP. Instead of choosing an arbitrary broadband signal or any user-specific particular band, MIF automatically extracts the different oscillatory modes from the signal. The MIF algorithm is able to properly align the oscillatory modes into the same numbered MIMF across different channels, which allows us to use CSP successfully. CSP features are ranked and classified using the linear discriminant analysis (LDA) classifier. The main contributions of the chapter are the following:

1. The adaptive signal decomposition property of MIF is explored to analyze nonstationary MI BCI EEG signals.

2. A data-adaptive signal decomposition-based optimal frequency bands selection framework for MI BCI application is proposed.

3. An LDA classifier is developed for MI BCI application, based on the CSP features extracted from the multivariate oscillatory component of the multichannel EEG signal.

5.2 Dataset

We used BCI competition IV 2a (dataset 1) and BCI competition III-IIIa (dataset 2) EEG datasets to validate our proposed model for MI BCI [200]. Dataset 1 consists of EEG data from nine different subjects who were imagining of left-, right-hand, both feet, and tongue movement. For each of the four classes of MI movement, 72 trials were recorded. Two sessions, consisting of 288 trials (72×4), recorded from each subject on different days, one is used for training the model and another is used for evaluating the performance of the model.

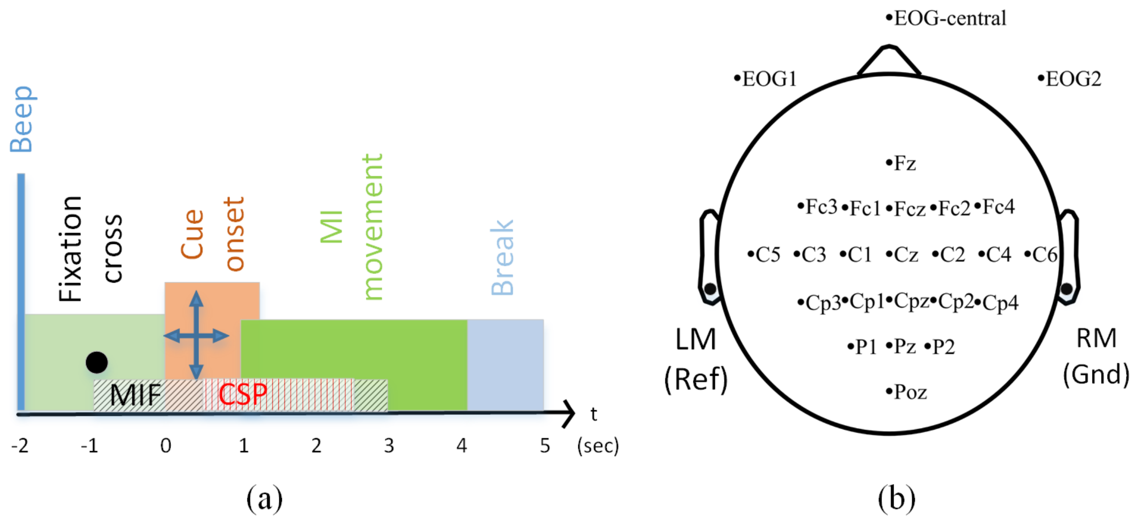

Figure 5.1: (a) Timing scheme of MI BCI experiment, (b) Electrode position (LM: left mastoid and RM: Right mastoid).

A fixation cross appeared on the black screen 2 s prior to cue onset. A cue in the form of an arrow pointing to left, right, down, or up corresponding to four classes was displayed. The timing scheme of the experiment is shown in Fig. 5.1 (a). EEG signals were recorded using 22 Ag/AgCl electrodes monopolarly using the montage shown in Fig. 5.1 (b). Electrodes were placed according to 10-20 international standards for EEG electrode position. Right mastoid (RM) and left mastoid (LM) are used for connecting ground (Gnd) and reference (Ref) electrodes, respectively. An additional three electrooculogram (EOG) channels were recorded for artifact processing related to eye movement. The signals were acquired at a sampling rate of 250 Hz, and bandpass filtered between 0.5-100 Hz. For more detail about the dataset refer to [200].

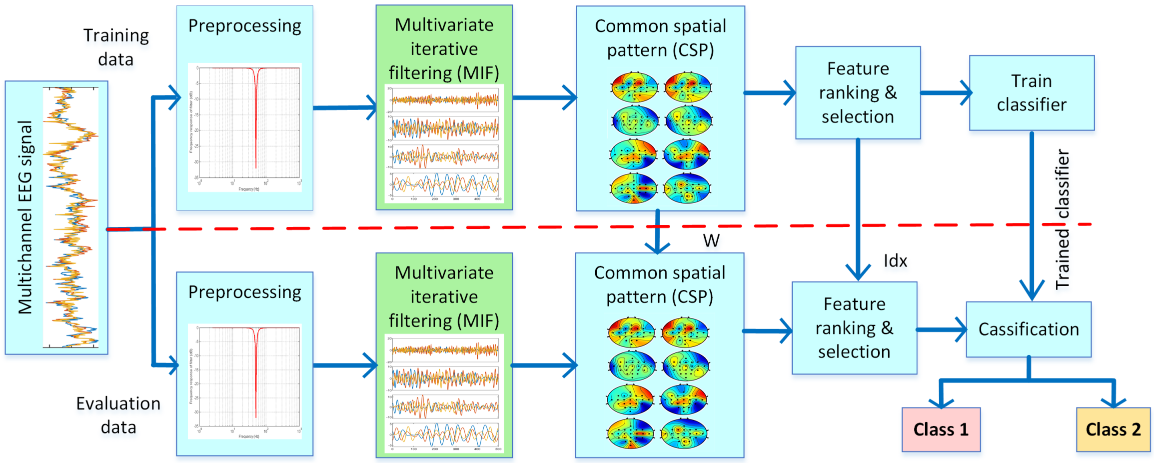

Figure 5.2: Block diagram of proposed MIF based MI BCI algorithm (MIF-CSP).

In dataset 2, sixty channels of EEG data were recorded at the sampling rate of 250 Hz from three subjects. EEG signals were corresponding to four different MI tasks and each class has 60 trials (for subject k3 each class has 90 trials). For more detail about the dataset, refer to [201].

5.3 Methodology

In this section, a brief description of all the steps involved in the proposed MIF-CSP method is given. Figure 5.2 shows the block diagram of the MIF-CSP algorithm.

5.3.1 Preprocessing

The continuous EEG signals are segmented into trials having signal of duration -1 s to 3 s based on the cue onset at 0 s. We have considered the signal of 1 s before the cue onset to avoid any edge artifact that may arise due to filtering of the signal. We visually check the spectrum of the EEG signal; for a few participants, the power line interface (PLI) [25] is very prominent. To get rid of PLI, we employ a notch filter at the frequency of 50 Hz. The training set trials marked as artifacts were removed as CSP are very sensitive to noise and a little perturbation may affect the performance adversely. But for evaluation, we keep all the trials even those are contaminated with artifacts to check the robustness of the proposed method. All the preprocessing steps were performed with the help of an open-source EEG signal processing package EEGLAB [175].

5.3.2 Signal Decomposition

As previously mentioned, biological systems generate complex, nonlinear, and nonstationary signals. Predefined basis based signal analysis tools like Fourier analysis, wavelet analysis tools are not effective due to lower time-frequency localization. We have used a data-adaptive signal decomposition technique, namely MIF, for the analysis of MI EEG signals. The convergence of IMF extraction process or stability of iterative filtering is mathematically proved in [64], and we have graphically demonstrated the same. We have shown the mean square error (MSE) between the original signal and the reconstructed signal at different iteration steps (different numbers of IMFs are used to reconstruct the signal) in Fig. 5.3. It can be observed that MSE is reducing monotonously or converging when IMFs are added iteratively one by one as part of signal energy covered by the IMFs, is increasing. After the sixteenth iteration steps, the MSE has become very small or negligible where the iteration process can be terminated. In MIF-CSP framework, Th in stopping criteria of MIF

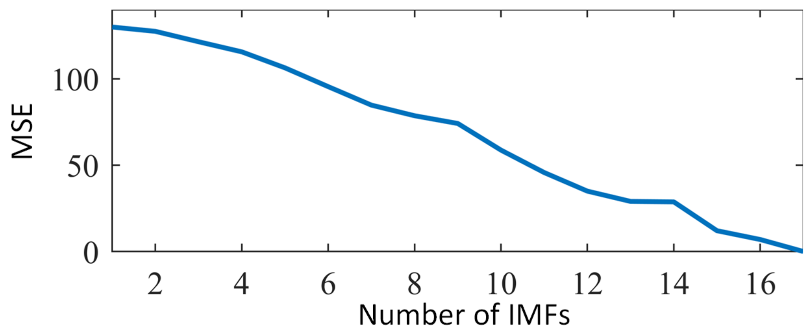

Figure 5.3: Convergence of MIF.

algorithm is set to 0.001 [64].

5.3.3 Common Spatial Pattern (CSP)

Scalp EEG signal, having very poor spatial resolution due to volume conduction, is hard to analyze [9]. It becomes even more challenging when the signal of interest is dominated by some other strong rhythms from nearby sources (e.g., sensory-motor rhythms are dominated by the EEG rhythms from the occipital lobe). Different spatial filters like small Laplacian [191], large Laplacian [191], common average reference [202], CSP [81, 191, 203] were studied to improve the spatial resolution of EEG.

In several MI BCI applications, CSP and its variants are frequently used for discriminant feature extraction [69, 191]. CSP targets to extract a spatial pattern such that it will maximize the variance of the projected signal corresponding to the positive class and minimize the same for the negative class.

Here, we present an overview of the CSP algorithm for EEG data represented by a $C \times N$ matrix, where C is the number of channels and N is the number of samples. The normalized spatial covariance matrix, $C_x \in \mathbf{R}^{C \times C}$, corresponding to $X \in \mathbf{R}^{C \times N}$ can be computed using Eq. (5.1).

$$C_x = \frac{XX^T}{\text{tr}(XX^T)} \tag{5.1}$$

where, tr(X) is the trace or sum of the diagonal elements of X and $(\cdot)^T$ denotes transpose operator. The average covariance matrix $\bar{C}_{d\in[1,2]}$ for a task belonging to class 1 or class 2 is obtained by taking an average of the covariance matrix of task trials. The composite covariance matrix, C_s is given by the sum of the covariance matrix of individual class as,

$$C_s = \bar{C}_1 + \bar{C}_2, \tag{5.2}$$

C_s is factored as $C_s = V_s \lambda_s V_s^T$, where V_s has eigenvectors in its column and λ_s is diagonal matrix of eigenvalues. The variances in the space spanned by V_s are equalized to unity by whitening transformation given by the following equation [191]:

$$\text{Wh}(C_s) = PC_sP^T, \text{where } P = \sqrt{\lambda_s^{-1}}V_s^T, \tag{5.3}$$

where Wh($\cdot$) denotes whitening transformation operator.

Secondly, let $S_1 = P\bar{C}_1P^T$ and $S_2 = P\bar{C}_2P^T$ then S_1 and S_2 will share common eigenvectors B as defined in Eq. (5.4).

$$B^TS_1B = \lambda_1, B^TS_2B = \lambda_2 \quad (\lambda_1 + \lambda_2 = I), \tag{5.4}$$

The final spatial filter is given by $W^T = (B^TP)$. EEG signal can be projected using derived CSP filter W as,

$$Z = W^TX, \tag{5.5}$$

each column vector w_j $(j = 1, 2, \cdots, C)$ of inverse of W^T is termed as spatial filter. The variance of the spatially filtered signal, Z, is used as a feature for classifying the two MI EEG data. The first and last m row vectors are corresponding to largest eigenvalues in λ_1 and λ_2 will have maximum difference in the variance between two groups. The variance features are computed as follows:

$$f_p = \log\left(\frac{\text{var}(z_p)}{\sum_{i=1,\cdots,m}(\text{var}(z_i)) + \sum_{i=C-m+1,\cdots,C}(\text{var}(z_i))}\right), \tag{5.6}$$

where, z_p is the p^{th} row vector of spatially filtered signal Z and var($\cdot$) denotes variance operator. The MIMFs corresponding to time segment 0.5-2.5s are used for CSP feature extraction. For each MIMF, we have extracted six CSP features by considering $m = 3$. Detailed steps for extracting CSP features are described in Algorithm 5.1. The value of r can be set in between 4 to 8 as the lower frequency MIMFs will not lie in the EEG frequency range (0.1-100 Hz).

Algorithm 5.1 CSP feature extraction from MIMFs

Input: MIMF$_{d\in[1,2]}$
Output: F$_{\text{CSP}}$ (CSP features)
1: **for** r = 1 **to** R **do** //R is the number of MIMFs
2: Calculate covariance matrix C_r from r^{th} MIMF for classes 1 & 2 (Eq. (5.1))
3: Design CSP filter W_r (Eqs. (5.2)-(5.4))
4: Transform MIMF$_r$ (Eq. (5.5))
5: F$_{\text{CSP}}$ = extract $2m$ features using Eq. (5.6)
6: **end for**

5.3.4 Feature Ranking and Classification

CSP features are ranked based on the p-value of the student t-test. In the preparatory experiment, we considered both the support vector machine (SVM) and LDA classifiers. LDA classifier provides higher accuracy, so we have selected LDA classifier.

5.3.4.1 Linear Discriminant Analysis (LDA)

LDA is generally used for reducing the dimensionality of the data as well as maintaining most of the discriminatory information [154]. LDA classifier tries to fit a linear boundary between two classes. For EEG based MI BCI application, LDA is widely used for both classification [81] or choosing an optimum set of features. Lets say, two classes C_1 and C_2, having n-dimensional sample points $x = [x_1, x_2, \cdots, x_n]$, are to be separated by a linear boundary, $y = w^T x$, ($(\cdot)^T$ is transpose operator). For best discrimination of the two classes, the mean of the two classes should be separated maximally, and variance should be minimum after projecting on the boundary [81, 154]. To achieve this, the ratio of mean separation to the within class variances, $J(w)$ has to be maximized. $J(w)$ is defined in Eq. (5.7).

$$J(w) = \frac{w^T(\mu_1 - \mu_2)^2 w}{w^T S_1 w + w^T S_2 w}, \tag{5.7}$$

where numerator is corresponding to the separation of mean between two classes and denominator is corresponding to within class variance of two classes. Mean μ_i and standard deviation (SD) S_i for class $i \in \{C_1, C_2\}$ are defined by following equations:

$$\mu_i = \frac{1}{N_i} \sum x, \tag{5.8}$$

where N_i is the number of samples in the class i.

$$S_i = \sum (x - \mu_i)(x - \mu_i)^T, \tag{5.9}$$

$J(w)$ will be maximum when w is w_{max} defined by following equation:

$$w_{\text{max}} = (S_1 + S_2)^{-1}(\mu_1 + \mu_2), \tag{5.10}$$

where w_{max} is the weight vector which provides the optimum projection direction, as well as the linear separability will be preserved. Decision boundary constructed based on the computed weight vector w_{max} is used in Fisher's LDA [154] to classify data using feature vector x as, $y = w_{\text{max}}^T x + b$, where b is the bias or threshold. Based on the sign of y, the features are assigned to a particular class.

5.4 Results and Discussion

In this section, we have showcased the obtained results for the proposed method for MI BCI classification. The four different MI tasks available in the dataset are classified using six different binary classifiers. We decompose multichannel EEG signals into oscillatory modes or MIMFs using MIF. EEG signal and corresponding four MIMFs for subject A03T ('T' in 'A03T' denotes training session data), when performing left hand MI task, are shown in Fig. 5.4. CSP is employed to extract the most discriminant features from the oscillatory

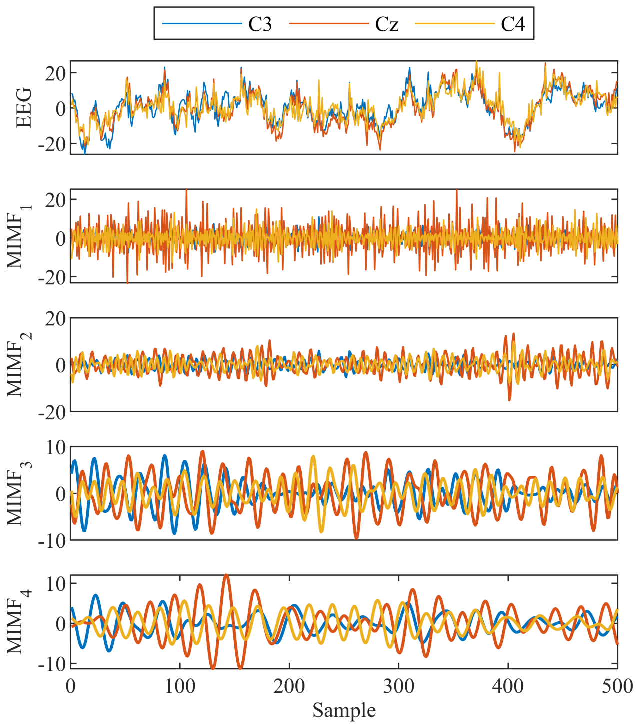

Figure 5.4: EEG signals and four MIMFs for subject A03T during left hand MI task. For clear visualization, EEG signals corresponding to three channels (C3, Cz, and C4) are shown.

modes. Covariance matrices corresponding to left and right hand MI task, the weight of the spatial filters, and the spatially filtered MIMFs (MIMF_2 and MIMF_3) of EEG signals are shown in Fig. 5.5. These features are ranked using student t-test, which is used for feature ranking for EEG based classification problem [25]. We have trained an LDA classifier using all the trials provided in the training set. The trained model is evaluated using a completely different set of trials provided in the evaluation set.

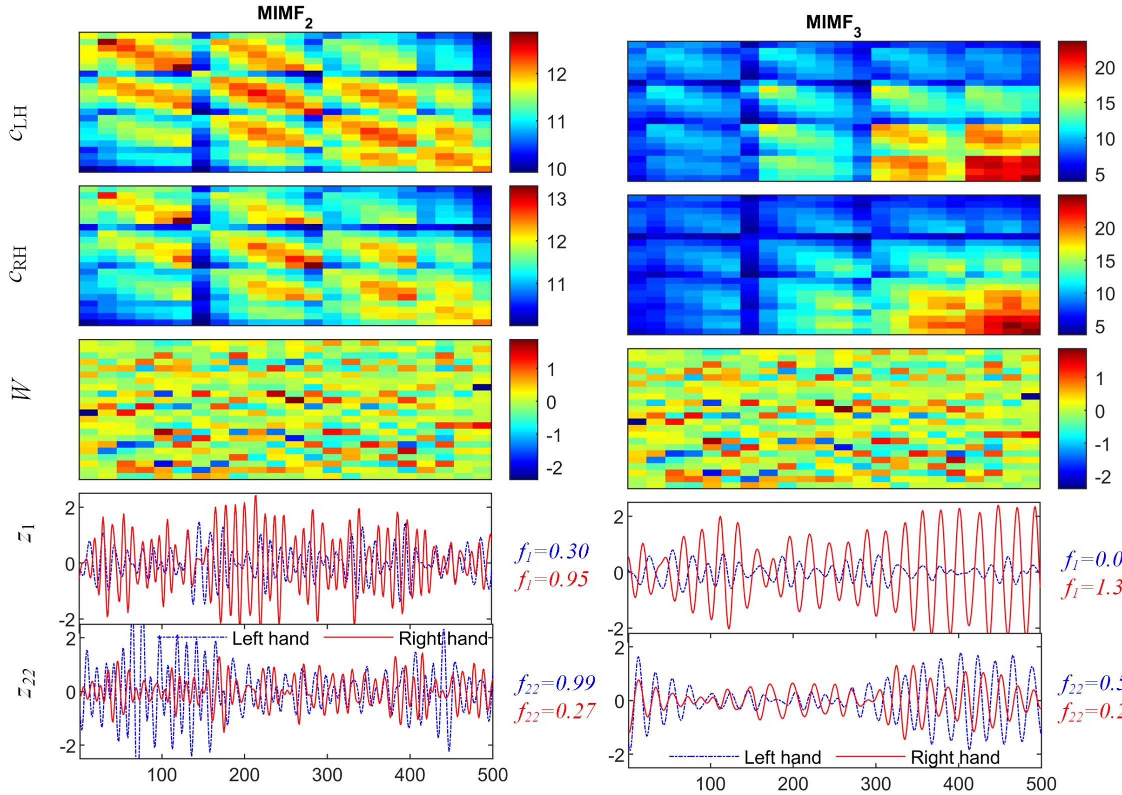

Figure 5.5: CSP based spatial filtering of EEG signals of subject A03T. Note: c_{LH} and c_{RH}: covariance matrices obtained for left and right hand MI tasks, W: spatial filter, z_1 and z_{22}: spatially filtered signals corresponding to first and twenty-second row, respectively, and f_1 and f_{22}: variance features of first and twenty-second row.

Fig. 5.6 shows the evaluation of classification accuracies, when different numbers of features are used, for six different classifiers. We have chosen a minimum number of most significant features which can achieve maximum accuracy in subject specific fashion, which may reduce the flexibility of the proposed framework. To make the framework more general, the number of features (N_f) can be chosen subject independently, based on the average accuracy. The average accuracy over all the subjects is shown in Fig. 5.6. Table 5.1 presents

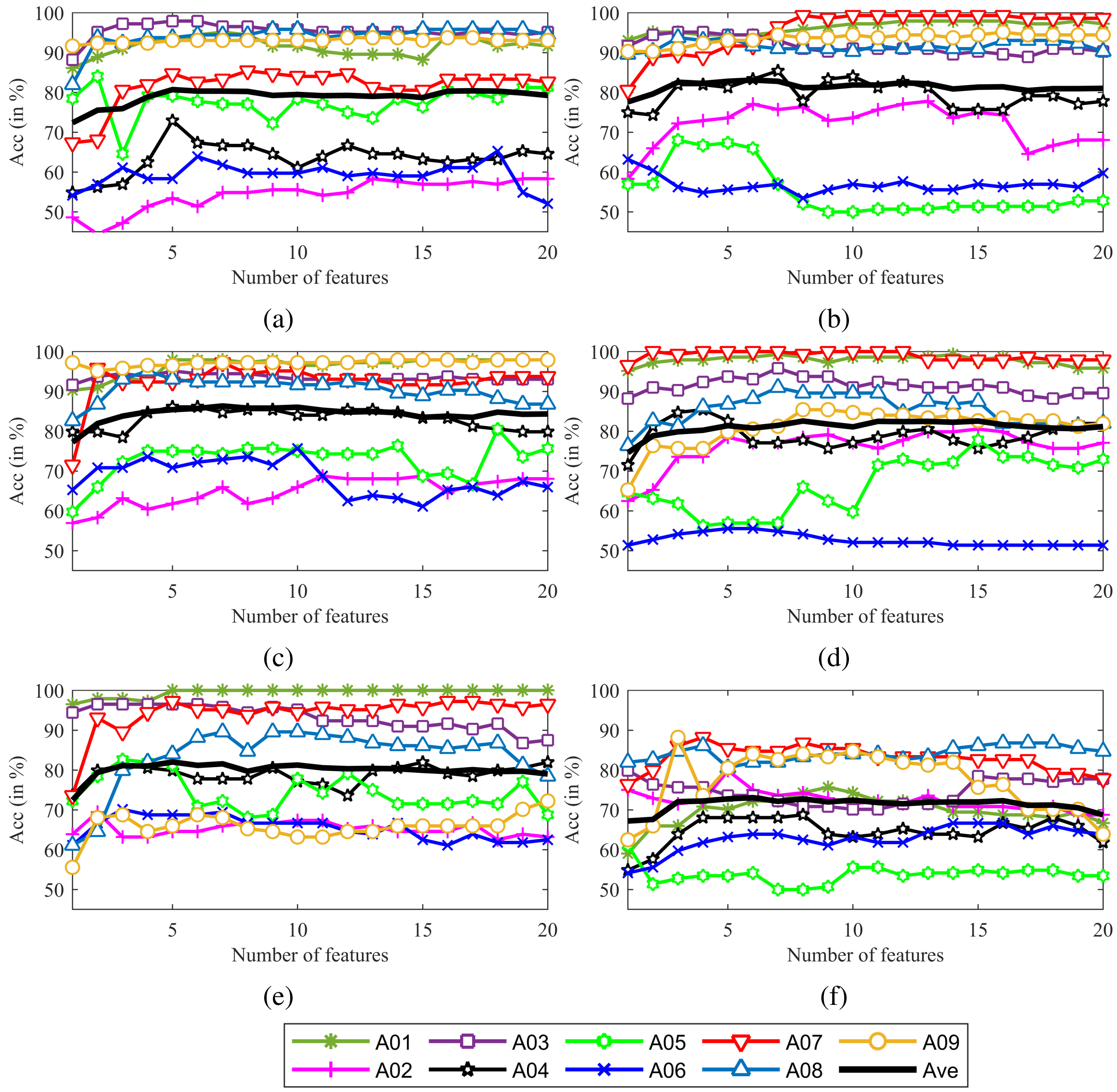

Figure 5.6: Evaluation of classification accuracies when different number of features are used, (a) left versus right hand, (b) left hand versus feet, (c) left hand versus tongue, (d) right hand versus feet, (e) right hand versus tongue, and (f) feet versus tongue.

the subject-wise accuracies and number of features used for classification of different combinations of MI tasks (left- versus right-hand (L&R), left hand versus feet (L&F), left hand versus tongue (L&T), right hand versus feet (R&F), right hand versus tongue (R&T), and feet versus tongue (F&T)). Additionally, the last row of Table 5.1 presents the accuracies when N_f is chosen subject independently. When N_f is chosen in a subject-independent fashion, then the algorithm becomes more general but with the cost of reduced accuracies. Based on the application requirement, N_f can be chosen in subject specific manner or subject-independent fashion. The variability in the performance of different subjects may arise for various reasons, such as changes in recording conditions and variability of the subject's attention to perform the MI task.

Table 5.1: Classification accuracy (in %) obtained for proposed method on BCI competition IV 2a dataset.

Subject	L&R		L&F		L&T		R&F		R&T		F&T	
	Acc	N_f	Acc	N_f	Acc	N_f	Acc	N_f	Acc	N_f	Acc	N_f
A01	95.14	7	97.92	12	97.92	5	99.31	7	100.0	5	75.69	9
A02	58.33	13	77.78	13	68.75	11	80.56	15	69.44	2	79.86	5
A03	97.92	5	95.14	3	95.14	5	95.83	7	96.53	2	79.86	1
A04	79.92	5	85.42	7	86.11	5	85.42	4	81.94	15	68.75	8
A05	84.03	2	68.06	3	80.56	18	77.78	15	82.64	3	61.11	1
A06	65.28	18	63.19	1	75.69	10	55.56	5	70.14	3	66.67	14
A07	85.42	8	99.31	8	97.22	7	100.0	2	97.22	5	88.19	4
A08	95.83	9	93.75	3	95.14	4	90.97	7	89.58	7	86.81	16
A09	93.75	12	95.14	16	97.92	13	85.42	8	72.22	20	88.19	3
Average	83.18	-	86.19	-	88.27	-	85.65	-	84.41	-	77.24	-
SD	14.50	-	13.49	-	10.98	-	13.78	-	12.07	-	9.95	-
SI	80.71	5	83.10	6	86.34	7	82.56	8	82.02	5	73.07	6

N_f: Number of features, SI: Subject independent

MIF-CSP is also evaluated using another publicly available dataset to show the generality of the algorithm. Accuracies for different MI tasks are tabulated in Table 5.2, which lie in a similar range to dataset 1. For subjects k3 and l1, MIF-CSP provides accuracy around 80.0% , but for k6, MIF-CSP shows comparatively lower (by 2-40%) classification performance.

An extensive experimental comparison is presented with the following state-of-the-art MI BCI algorithms.

CSP [191]: EEG signals corresponding to time segment 0.5-2.5 s after cue appeared are band-passed at 4-40 Hz, and CSP features are extracted for classification.

FBCSP [192]: EEG signals corresponding to time segment 0.5-2.5 s after cue onset are separated into several bands using bandpass filter. EEG signals between the band 4 Hz and

Table 5.2: Classification accuracy (in %) obtained for proposed method on BCI competition III IIIa dataset.

Subject	L&R		L&F		L&T		R&F		R&T		F&T	
	Acc	N_f	Acc	N_f	Acc	N_f	Acc	N_f	Acc	N_f	Acc	N_f
k3	100.0	1	96.67	7	97.78	3	98.89	2	100.0	18	87.78	1
k6	60.00	1	61.67	18	88.33	2	75.00	9	85.00	2	85.00	12
l1	93.33	7	96.67	3	96.67	1	91.67	1	88.33	1	58.33	12
Average	84.44	-	85.00	-	94.26	-	88.52	-	91.11	-	77.04	-
SD	21.43	-	20.21	-	5.16	-	12.25	-	7.88	-	16.26	-
SI	81.67	1	82.96	19	93.33	2	87.04	11	90.19	2	74.07	12

N_f: Number of feature, SI: subject independent

40 Hz are separated into non-overlapping subbands of 4 Hz.

S-wLTL [204]: Azab *et al.* used transfer learning approach to reduce the calibration time and requirement of large training data. CSP features are used to train a logistic regression classifier.

MEMDBF-CSP [185]: Gaur *et al.* proposed an MI BCI algorithm, in which EEG signal are filtered with the help of MEMD technique. Relevant IMFs are automatically selected to reconstruct based on the median frequency of the IMF. CSP features of the reconstructed EEG signal are used to classify using both LDA and SVM classifiers. We have shown the results for LDA classifier as it provides slightly higher accuracy.

SS-MEMDBF-RG [194]: EEG signal are filtered and enhanced using MEMD based filtering by selecting MIMFs, based on their mean frequency. Sample covariance matrices are used as features, and different MI tasks are classified with the help of Riemannian geometry.

SW-LCR [81]: Another approach, proposed by Gaur *et al.*, uses a sliding window to get rid of the inconsistency associated with the varying activation time of the task from trial to trial. They have extracted nine time frames using a sliding window of length 1 s from bandpassed (8-30 Hz) EEG signal. Different LDA classifiers are trained for each time frame, based on the CSP features corresponding to that frame. The final prediction is done based on the decision-level fusion of the intermediate predictions from nine classifiers. Fusion is done in two ways: largest consecutive repetition (SW-LCR) of a particular class is chosen or maximum number of repetitions (SW-Mode) of a particular class in the sequence of intermediate prediction. SW-LCR and SW-Mode provide average accuracy of 80.02% and 79.78%, respectively. Accuracies of SW-LCR for each individual subject are shown in Table 5.3.

TSGSP [205]: Temporally constrained sparse group spatial pattern tries to optimize both the frequency band and time window to increase the classification accuracy. In this method, predefined overlapping frequency bands were extracted from different time instants with the help of a sliding window. Optimized CSP features are extracted and selected for classification using a linear SVM classifier.

Table 5.3 summarizes the classification accuracies obtained from the above-described algorithm. The proposed method provides an average accuracy of 83.18% for L&R MI movement, which is higher than the existing state-of-the-art MI BCI algorithm. The highest accuracy in L&R MI task classification is provided by MIF-CSP for four subjects. For a fair comparison, we have performed feature ranking and classification in a similar way to MIF-CSP for both CSP and filter bank CSP (FBCSP) methods. Table 5.4 showcased the average accuracy of MI tasks other than L&R MI task. TSGSP only studied the classification accuracy for L&R and F&T MI tasks.

Table 5.3: Comparative performance (Acc in %) of MIF-CSP for L&R MI task from BCI competition IV 2a dataset.

Subject	CSP [191]	FBCSP [192]	S-wLTL [204]	MEMDBF-CSP [185]	SS-MEMD-RG [194]	SW-LCR [81]	TSGSP [205]	MIF-CSP
A01	84.03	65.28	90.00	90.78	91.49	86.81	87.00	95.14
A02	59.03	57.64	55.00	57.75	60.56	64.58	64.70	58.33
A03	95.14	72.22	93.00	97.08	94.16	95.83	93.80	97.92
A04	74.31	52.08	60.00	70.69	76.72	67.36	74.30	79.92
A05	54.86	60.42	68.00	61.48	58.52	68.06	90.40	84.03
A06	57.64	55.56	60.00	70.37	68.52	67.36	63.90	65.28
A07	72.22	89.58	73.00	72.14	78.57	80.56	91.40	85.42
A08	95.83	88.89	98.00	97.76	97.01	97.22	95.80	95.83
A09	93.06	86.81	83.00	94.62	93.85	92.36	81.30	93.75
Average	76.23	69.83	75.60	79.19	79.93	80.02	82.50	**83.18**
SD	16.60	15.10	16.00	15.85	14.99	13.45	12.20	14.50

Note: Bold entries denote the highest values of Acc.

Table 5.4: Comparative performance (Acc in %) of MIF-CSP for other MI tasks from BCI competition IV 2a dataset.

Methods	L&F	L&T	R&F	R&T	F&T
CSP	82.33	85.49	83.18	83.02	73.38
FBCSP	71.91	73.77	71.22	72.61	66.74
SS-MEMD-RG	85.50	84.30	85.43	**85.75**	74.78
SW-LCR	83.64	86.19	84.64	83.49	72.99
TSGSP	82.50	-	-	-	**84.00**
MIF-CSP	**86.19**	**88.27**	**85.65**	84.41	77.24

Note: Bold entries denote the highest values of Acc.

Unlike, the previous approaches for MI BCI application where adaptive decomposition techniques like EMD, ensemble EMD (EEMD), or MEMD are used for the reconstruction of EEG signal by selecting a few relevant IMFs or MIMFs and combining them, we use MIF to get oscillatory modes or frequency bands separated out from which event-related desynchronization (ERD)/event-related synchronization (ERS) activity can be detected. Improvement in classification accuracies suggested the usefulness of using oscillatory modes, present in the signal, for CSP feature extraction instead of selecting predefined frequency bands extracted narrowband using bandpass filtering. This data-adaptive approach for selecting the frequency band also addresses the problem of frequency variability across subjects or trials.

EEG signals are prone to different kinds of noises, so a robust selection of frequency bands is necessary to ensure the reliability of the analysis method. Moreover, different cognitive tasks affect a particular band, which presents a requirement to detect that particular band. To handle different cognitive tasks in steady-state visual evoked potential (SSVEP) based BCI application, ensemble task related component analysis with temporally local weighting time filter was proposed by Jin *et al.* [206]. A study on human emotion based on fMRI performed by Li *et al.* [207] shows that the neural representation changes for the same state of emotion due to auditory only, visual only, and audiovisual stimuli. The performance of the proposed MIF-CSP algorithm may prove that data adaptive MIF can handle changes in EEG signal due to small perturbations in the condition of a cognitive task.

ERD is the phenomenon of blocking alpha rhythms due to motor or sensory behaviors [1]. The opposite of ERD, namely an increase in alpha rhythmic activity, is called ERS.

Frequency range (bandwidth), defined by energy coverage of 99% of total signal energy of MIMFs, for subject A03, are shown in Fig. 5.7 with the help of box plots. Frequency ranges of alpha rhythm are highlighted using the cyan band in Fig. 5.7. MIMF$_3$ and MIMF$_4$ overlap in the alpha frequency band. From Fig. 5.4, it can be noticed that after cue onset (around 200 samples), the amplitudes of MIMF$_3$ and MIMF$_4$ have faced a decrease in amplitude which implies the occurrence of ERD. MIMFs clearly show the occurrence of ERD than EEG signals.

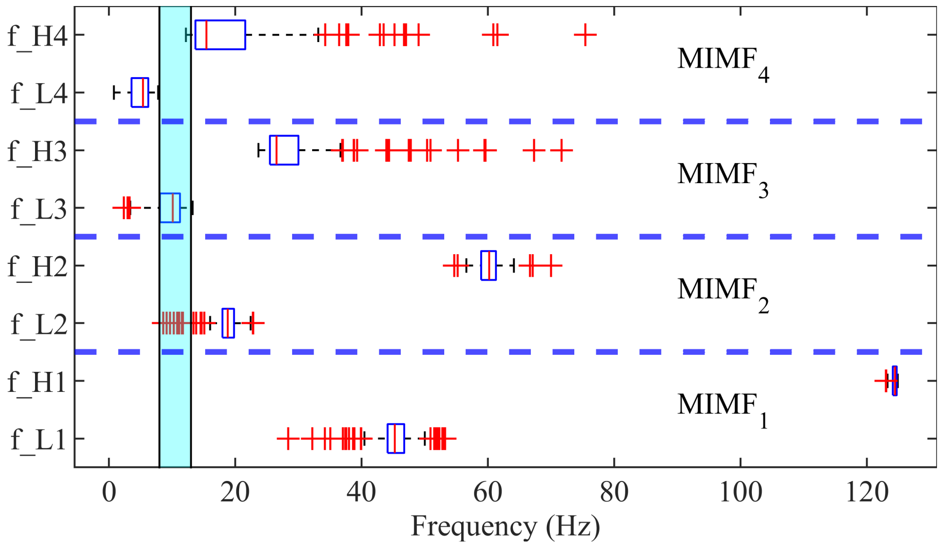

Figure 5.7: Frequency ranges of the MIMFs. (f_Li and f_Hi are lower and higher frequency range of i^{th} MIMF, respectively.)

In Fig. 5.8, CSP spatial filters corresponding to different MIMFs for subject A03T (L&R MI task) are shown. It can be observed that spatial filters, corresponding to the fourth MIMF, show distinct activation patterns in SMC area for L&R MI task, but other MIMFs' spatial filters do not have well-distinguishable activity patterns. For the right hand MI task, CSP features from the fourth MIMF have higher values in the SMC area of the right hemisphere. Similarly, for the left hand MI task a higher value is obtained in the left hemisphere SMC area. MI movement and activation occur on the same side of the body, which shows an ipsilateral relation. For visual representation, most significant two features corresponding to different MIMFs are shown in Fig. 5.8. Features obtained from the fourth MIMFs are linearly well separable, which confirms our previous finding that spatial filters corresponding to the fourth MIMF have distinct activity patterns.

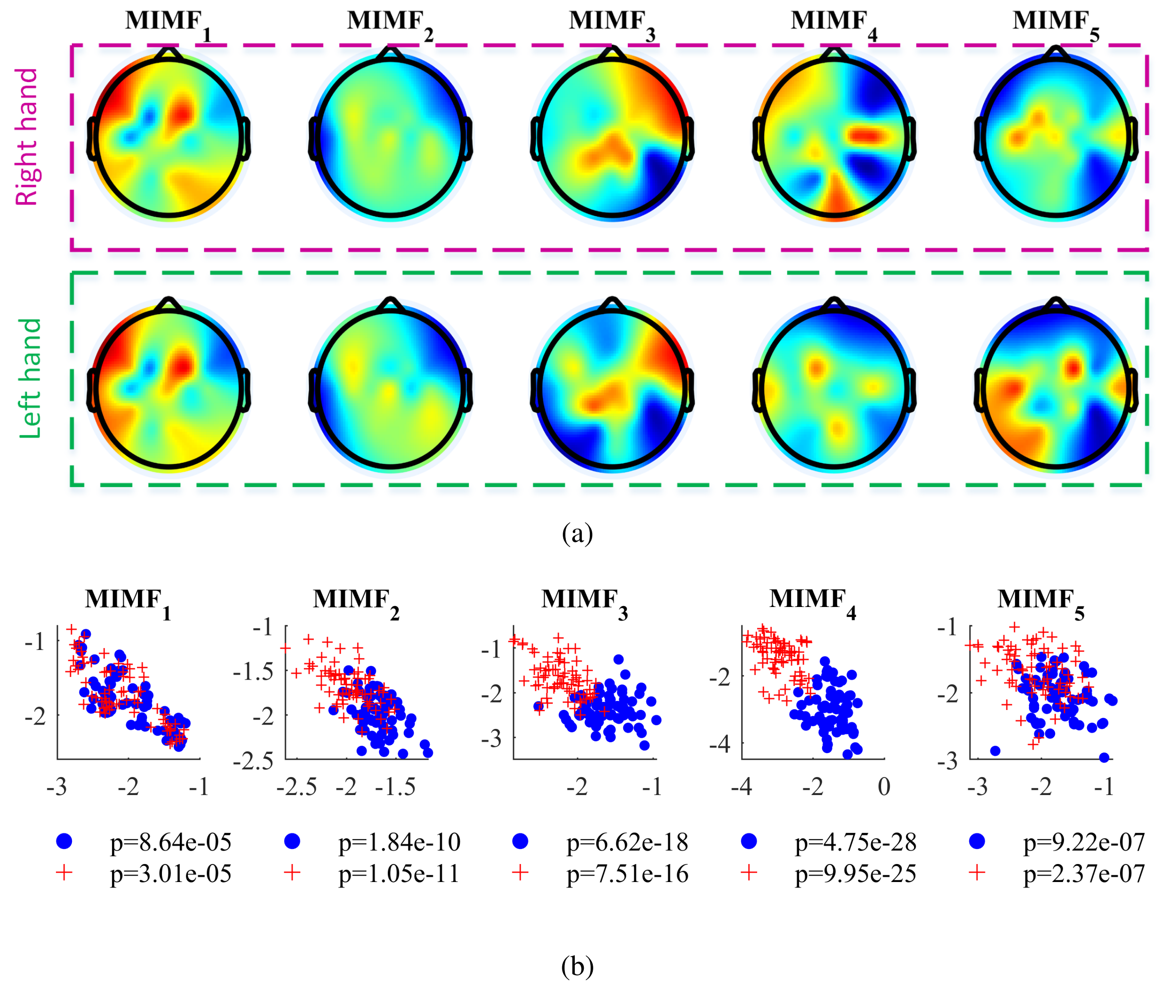

Figure 5.8: (a) CSP filters corresponding to different MIMFs and (b) feature space corresponding to the most significant two features extracted from the first five MIMFs.

Real-time implementation of MI BCI application and user convenience will directly depend on the latency or prediction time, which further depends on the computational complexity of the algorithm. EMD-based algorithm for MI BCI application suffers from the uniqueness problem of IMF across different bands and is prone to noise [63]. Using EEMD [104], stable IMFs can be generated in noisy conditions, but EEMD fails to address the uniqueness problem for multichannel data. Park *et al.* [69] proposed an MI BCI classification method, where they have used noise assisted MEMD (NA-MEMD), in which both the uniqueness problem and instability due to noisy conditions are successfully addressed. Both these EEMD and NA-MEMD-based methods demand very large computational resources due to the complexity of these decomposition techniques. We have used MIF for data-adaptive decomposition, which is computationally much more efficient compared to other existing multivariate decomposition techniques like MEMD, and MVMD [25].

Fig. 5.9 presents a comparative performance based on decomposition time taken by MIF and other multivariate signal decomposition algorithms when three channel EEG signal of length 500 are considered for decomposition (signal is shown in Fig. 5.4). The decomposition time for the MIF algorithm, being very small, is not properly visible for that, we have shown an enlarged version for clear visualization. Parameters for MVMD were kept as the default settings, which are as follows: $\alpha = 2000$, DC = 0, init = 1, tol = 10^{-7}. The number of modes to be extracted in MVMD was set to $K = 10$ to get the same number of modes as MEMD. For NA-MEMD, two additional channels of white Gaussian noise of 20 dB are added during simulation [69].

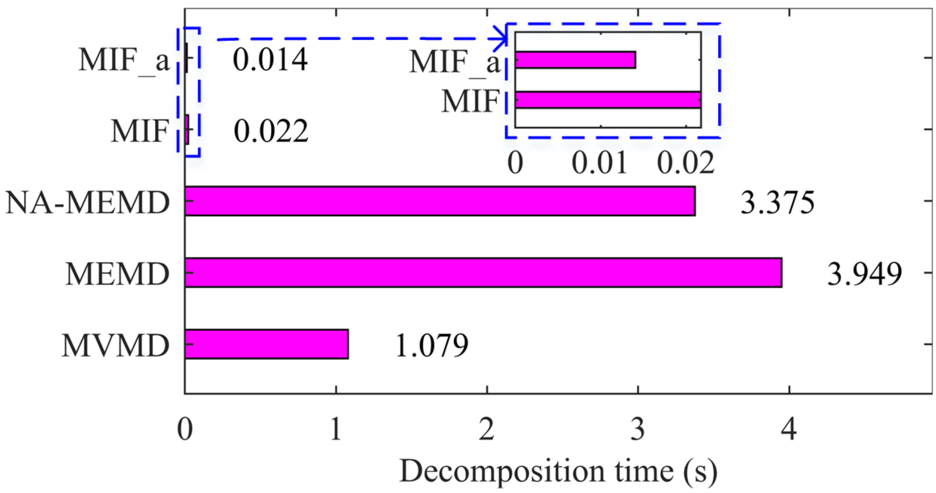

Figure 5.9: Comparison of decomposition time of MIF with other multivariate algorithms.

The usefulness of the MIF algorithm for MI BCI classification is shown by presenting a comparative study when MEMD and MVMD (with default parameters as defined in the previous paragraph) are used instead of MIF by keeping all other parameters the same as MIF-CSP. The classification accuracies for MI BCI are showcased in Fig. 5.10. For MEMD, we have used 15 channels (channels are chosen based on the MEMD-based MI BCI method proposed by Gaur *et al.* [208]) EEG signal out of 22 channels as MEMD code can capable of decomposing a maximum of 16 channels signal. The proposed MIF-CSP method outperforms by 5-15% for all six MI BCI classification tasks as compared to MVMD and

MEMD-based methods.

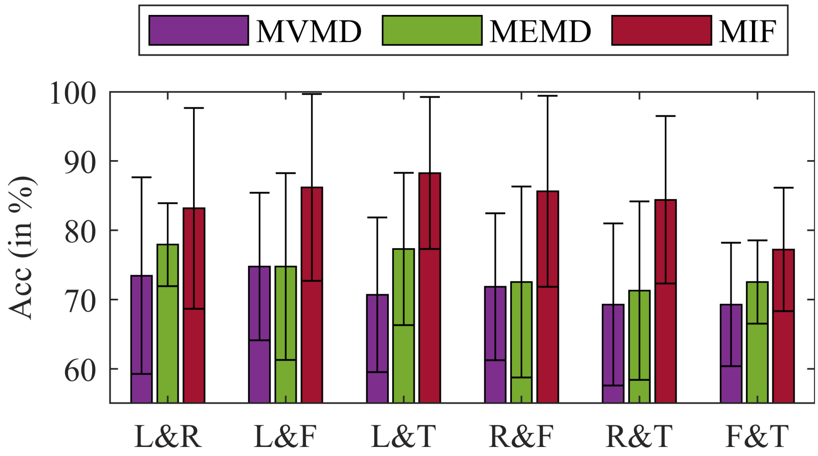

Figure 5.10: Classification accuracies of MVMD, MEMD based MI BCI and MIF-CSP method.

Automatic selection of features is achieved using student t-test based ranking. We have observed that for all the participants, the most significant CSP features are provided by the second MIMF to the fourth MIMF. Based on this observation, we have used features from the first four MIMFs only for feature extraction to classify MI BCI tasks. So, we can stop the extraction of further lower frequency MIMFs after extracting four or five MIMFs using the MIF algorithm, which will reduce the computational time without affecting the performance. The decomposition time for decomposing using MIF up to five MIMFs is shown in Fig. 5.9, which is denoted as MIF_a. Whereas, without limiting the number of MIMFs, MIF gives 8 MIMFs.

We can extend the binary MI classification algorithm for the multiclass MI BCI problem based on fusion at the decision level or feature level. Multiclass CSP [209] can alternatively be used for designing multiclass MI BCI classification in the future. Peng *et al.* [210] proposed an emotion detection algorithm from EEG signal based on a framework, namely, graph regularized least square regression with feature importance learning for adaptively select features according to their contributions, frequency bands, and channels. An auto weighting variable is used in least square regression classifier in order to achieve automatic selection of important features, frequency bands, and channels. In proposed MIF-CSP method, both critical frequency bands and features are adaptively chosen based on MIF and student t-test.

5.5 Summary

In the history of BCI technology, machine learning emerged as a revolutionary tool; the advancement of computational technology makes real-time implementation possible. Different approaches have been proposed to reduce the subject training time and prediction time of the classifier simultaneously increase the classification accuracy of the MI BCI algorithm. However, choosing appropriate frequency bands, in which ERD/ERS patterns corresponding to sensory-motor activation and deactivation are prominent, is a challenging task due to high-frequency variability across different subjects and even for different trials of the same subject. In literature, researchers heuristically chose narrowband signal obtained using band-pass filtering of the data, or a broadband signal for classification.

In this chapter, we proposed a novel MIF based framework to extract the oscillatory modes present in the signal adaptively without any previous assumption of fixed frequency bands. Using the spatial filtering technique, CSP, discriminant features are computed for classification. We have shown that our proposed method outperforms by 1-15% state-of-the-art technology with the help of the MI BCI EEG database, namely BCI competition IV 2a. To show the generality, we also validated MIF-CSP using another publicly available dataset. The superior accuracy provided by the MIF-CSP algorithm proved that it is a promising candidate for MI BCI application.

Chapter 6

SSVEP Detection in Mobile Environment for Brain-computer Interface

6.1 Introduction

The intricate process of human movement requires complex coordination and integration of both the central and peripheral nervous systems. Electroencephalogram (EEG) has emerged as the predominant choice for measuring brain activity for brain-computer interface (BCI) applications due to its high time resolution, portability, and ease of use [5, 70]. The ongoing process for human movement in the central nervous system may be affected due to the mobile environment, which will be reflected in EEG signals. The mobile environment also has the potential to introduce artifacts and signal distortion, ultimately compromising accuracy and signal quality. A framework should be robust enough to handle the effects arising from the mobile environment.

6.1.1 Related Works

In recent decades, numerous frameworks have been developed for detecting steady-state visual evoked potential (SSVEP) from EEG signals [211]. The SSVEP detection framework can be broadly classified into Fourier transform-based spectrum analysis, signal decomposition-based analysis, spatial filtering-based, canonical correlation analysis (CCA)-

based, and deep learning-based methods [84].

The widely used power spectral density (PSD) analysis for detecting SSVEP target frequency faces problems like PSD can be easily affected by noise and demand EEG signal of longer duration to provide good frequency resolution [212]. Lin *et al.* [213] have suggested CCA for SSVEP detection for BCI applications, which gives improved performance and draws the attention of many researchers. CCA uses sine-cosine reference signal, defined according to the stimulation frequency. Due to the inter-trial and inter-subject variance, using the same reference signal affects the performance of the SSVEP detection. To address this issue, several researchers have optimized the reference signals [214].

The performance of the SSVEP framework also depends on the noise present in the EEG signals, selecting specific bands from EEG signals. Chen *et al.* [215] have proposed an SSVEP detection framework termed as filter bank CCA (FBCCA) based on applying CCA on subband components of EEG signals. A filter bank, designed using zero-phase Chebyshev type I infinite impulse response filters, is used to decompose the EEG signals into subbands. The pass band of the filter banks has been identified based on choosing equally spaced bands, according to the individual harmonic frequency or multiple harmonic frequencies in a single band. The SSVEP components will vary in different subjects, trials, and channels; hence, selecting predefined bands like FBCCA may be ineffective. Therefore, various methods have attempted to choose the bands adaptively. Empirical mode decompositio (EMD) has been widely used to analyze nonstationary EEG signals [28]. Zheng *et al.* [216] have explored EMD techniques and other variants of EMD, like ensemble EMD (EEMD), improved complete EEMD with adaptive noise, and variational mode decomposition (VMD) for SSVEP frequency detection. This study uses a single-channel EEG for the detection of SSVEP frequency. Noise can easily affect a single-channel SSVEP; hence, more than one channel is preferred to increase the robustness of the framework. Chen *et al.* [217] used MEMD and CCA to detect SSVEP frequency, where they added white noise channels to ensure the consistency of the decomposed multivariate intrinsic mode functions (MIMFs) of EEG signals of different trials and subjects. Chang *et al.* [218] have proposed a MVMD-based framework for SSVEP detection. The decomposed modes obtained from multivariate VMD (MVMD) are weighted to reconstruct the EEG signals. Sparrow search algorithm is used to decide the weight for reconstruction. The CCA algorithm is used for classifying the reconstructed EEG signal. The multivariate decomposition techniques are computationally complex, adding more latency in SSVEP frequency predictions. Moreover, these techniques mainly aim at EEG signal denoising using multivariate mode decomposition. While multivariate adaptive signal decomposition techniques have significantly improved SSVEP detection, challenges remain. These include the computational complexity of real-time implementation, the need for parameter optimization, and the handling of inter-subject variability.

6.1.2 Key Contributions

This letter has addressed the aforementioned problems by proposing a multivariate iterative filtering (MIF)-based CCA (MIF-CCA) framework for SSVEP detection. Multivariate signal decomposition is performed using MIF in [70] for motor-imagery BCI applications from multichannel EEG signals. Here, the MIF algorithm is explored to analyze SSVEP EEG signals. In the literature, CCA-based studies have used CCA algorithm for classification of the SSVEP frequency [217, 218]. The proposed MIF-CCA framework uses CCA for feature extraction. The time complexity of the MIF is much less as compared to multivariate EMD (MEMD), MVMD, EEMD techniques, which will reduce the prediction time [70]. Moreover, the MIF decomposition can be stopped after extracting a certain number of MIMFs, which will save additional decomposition time [70].

6.1.3 Database

The proposed method has been evaluated using a real-time EEG database for SSVEP detection. The EEG signals have been collected during visual gazing at flickering visual stimuli. This experiment shows three different flickering frequencies (5.45, 8.57, and 12 Hz) for 5 s. These frequencies are selected, as 5-30 Hz are suitable for SSVEP frequency detection, and the frequency below 12 Hz is significantly affected by the movement artifacts [219]. Subjects were asked to walk at different speeds (standing (speed: 0 m/s), slow walking (speed: 0.8 m/s), walking (speed: 1.6 m/s), and slow running (speed: 2.0 m/s)) on a treadmill set up during the SSVEP experiment to incorporate the effect of movement on SSVEP performance [219].

The EEG data were collected from 23 participants (male: 14 and female: 9, mean age of 24.6 ± 3.0 years) without any history of neurological disorders. Only 17 participants took part in the experiment in slow-running conditions for personal reasons.

EEG signals were recorded using a 32-channel EEG acquisition device (BrainAmp, Brain Product GmbH) at a sampling rate of 500 Hz. The electrodes are placed according to 10-20 international standards of EEG electrode placement. FPz and FCz electrodes are used as ground and reference electrodes, respectively. The electrode impedance was maintained below 50 kΩ to ensure the signal quality.

Gazing at flickering visual stimuli evokes SSVEP over the occipital lobe of the human brain. The EEG channels in the occipital lobe (O1, Oz, and O2) and nearby electrodes (PO7, PO3, POz, PO4, and PO8) are chosen to identify the SSVEP target in this study. The selection of specific channels and downsampling EEG data to 128 Hz will reduce the computation complexity of the framework as well as increase performance by rejecting irrelevant information.

6.2 Methodology

The proposed SSVEP detection framework is comprised of MIF-based decomposition of EEG signals to get the oscillatory modes, CCA-based feature extraction, and a machine learning classifier for the identification of three flickering frequencies. The proposed SSVEP frequency detection framework is presented using a block diagram in Fig. 6.1. Each of the blocks is described in the following sections.

6.2.1 Multivariate Iterative Filtering

The acquisition of EEG signals often involves multiple electrodes to enhance spatial resolution. However, the inherent randomness and low signal-to-noise ratio in EEG signals present challenges for univariate decomposition techniques. Univariate signal decomposition techniques provide varying numbers of IMFs and frequency properties across chan-

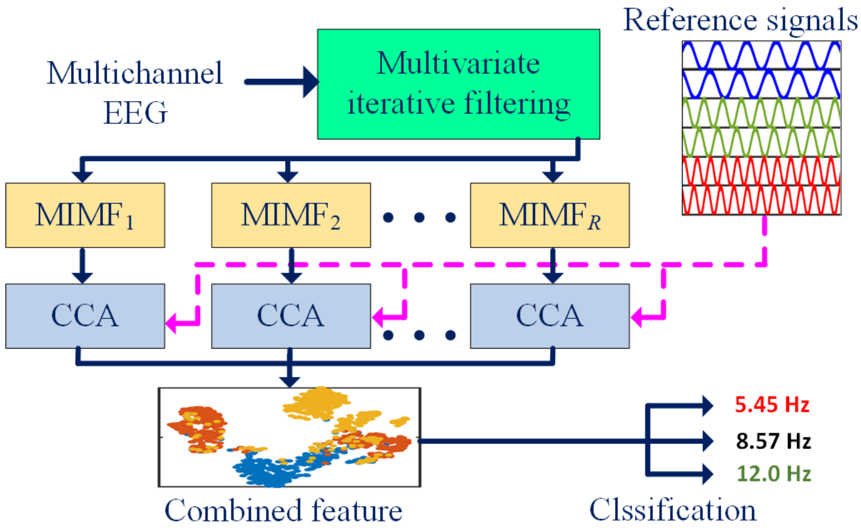

Figure 6.1: The block diagram of the proposed framework for SSVEP frequency detection.

nels, which can significantly degrade the performance of multichannel signal analysis. To address this issue, we have decomposed the multichannel EEG signals using the proposed MIF method.

6.2.2 Canonical Correlation Analysis

CCA has been widely used to find the underlying correlation between two sets of variables $u(t) \in \mathbb{R}^{I_1 \times N}$ and $r(t) \in \mathbb{R}^{I_2 \times N}$, where N is the number of samples in both the variables [220]. CCA computes a set of two linear transforms $\kappa \in \mathbb{R}^{I_1}$ and $\Lambda \in \mathbb{R}^{I_2}$ which aims to maximize the correlation between the transformed variables, $\hat{u} = \kappa^T u$ and $\hat{r} = \kappa^T r$. CCA solves an optimization problem based on a generalized eigenvalue problem to find the linear transforms.

In SSVEP-based BCI paradigms, CCA has been widely used to find the correlation between the multichannel EEG signals and the stimulus or reference signals [213]. Let us consider there are P stimulus frequencies to be detected in the SSVEP paradigm. EEG signals are represented as variable $u(t)$, where I_1 is the number of channels, and N is the number of samples. The reference signals $r(t)$ can be constructed using sine-cosine waves of P stimulus frequencies f_p $(p = 1, 2, \ldots, P)$ as [213],

$$r_P = \begin{bmatrix} \sin(2\pi f_p t) \\ \cos(2\pi f_p t) \\ \vdots \\ \sin(2\iota\pi f_p t) \\ \cos(2\iota\pi f_p t) \end{bmatrix}; \quad t = \frac{1}{f_s}, \frac{2}{f_s}, \ldots, \frac{N}{f_s} \tag{6.1}$$

ι denotes the number of harmonics and f_s is the sampling frequency. The correlation between the EEG signals and the reference signal of each frequency is computed. The correlation coefficients from different MIMFs are combined and used as feature.

6.2.3 Classification

The CCA-based features from MIMFs are classified using k-nearest neighbors (KNN), support vector machine (SVM), and linear discriminant analysis (LDA) classifiers [221]. As a supervised and non-parametric classifier, KNN categorizes a given data point by examining the majority of its neighboring data points. SVM classifier employs a linear decision surface to discriminate within a high-dimensional feature space. LDA classifier finds a linear boundary so that the mean of the two classes should be separated maximally and variance after projection on the boundary should be minimum.

6.3 Results and Discussion

This section presents the results obtained for the proposed MIF-CCA-based SSVEP framework for BCI applications. Additionally, we have discussed the results and compared the performance with baseline CCA methods.

The multichannel EEG signals are decomposed into MIMFs using MIF methods. MIF starts to extract the modes from the highest frequency; hence, the first MIMF will have the mode with the highest frequency content. The subsequent MIMFs will have lower frequency contents. The CCA of each MIMF is computed, and the maximum correlation coefficients for each stimulation frequency are used as a feature. Here, three different stimulation frequencies were there. So, each MIMF provides three correlation values corresponding to three stimulation frequencies. The features from different MIMFs are combined to obtain a feature vector. The t-distributed stochastic neighbor embedding (t-SNE) plots of the feature spaces obtained from different numbers of MIMFs are shown in Fig. 6.2. Each column in Fig. 6.2 represents feature spaces corresponding to a specific speed at which the subject was moving during the SSVEP experiment.

Three different classifiers, KNN, SVM, and LDA, were used to evaluate the proposed feature extraction method. Five-fold cross-validation was performed to compute the statistical performance parameter. The evaluation of five-fold cross-validation accuracy for KNN, SVM, and LDA classifiers when different numbers of MIMF are used for feature extraction are shown in Fig. 6.3.

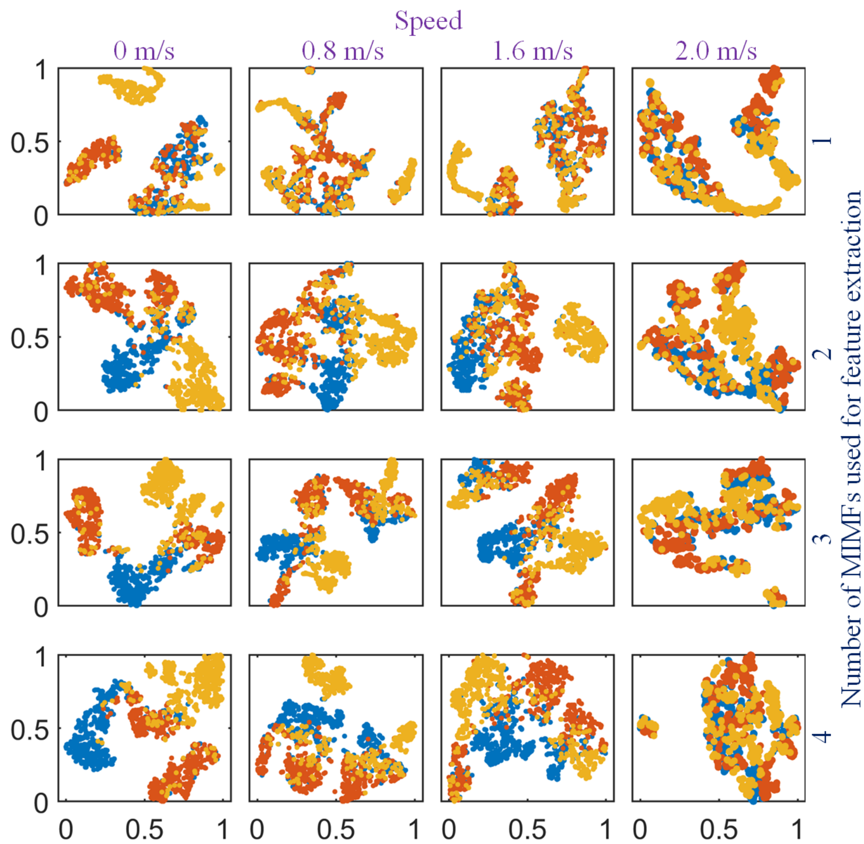

Figure 6.2: t-SNE plot for feature space obtained when the subject was moving at different speeds and different number MIMFs are used for feature extraction.

The mean and standard deviation (SD) of the accuracy obtained for the subject-wise classifier design paradigm are showcased in Tables 6.1-6.3 for KNN, LDA, and SVM, re-

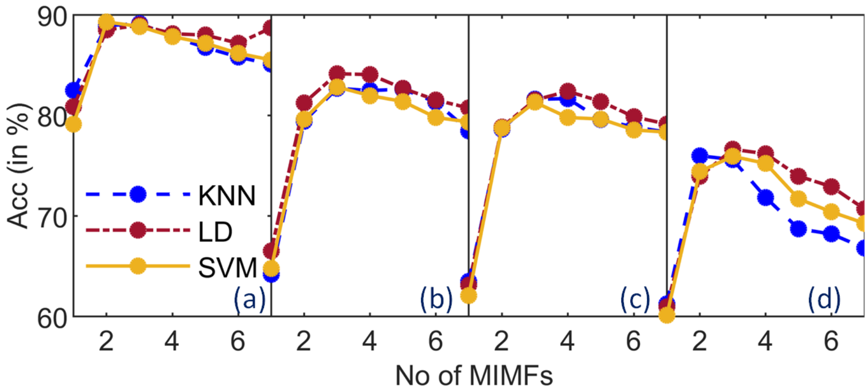

Figure 6.3: The SSVEP detection accuracy for varying the number of MIMFs used for feature extraction, different classifiers when the subject was moving at a speed of (a) 0 m/s, (b) 0.8 m/s, 1.6 m/s, and 2.0 m/s.

spectively. We also developed a subject-independent classifier for SSVEP frequency detection. In which the features extracted from different subjects are combined and used to develop a single classifier for all the subjects. The classification performance for the subject-independent MIF-CCA system is showcased in Table 6.4.

In Fig. 6.2, the t-SNE plots for features extracted from the first MIMF do not provide a discriminant feature space for different classes of stimulation frequency. Combining features from more MIMFs improves the separation in the feature space. When the speed of the subject increases, the feature discrimination in the feature space is adversely affected.

Including more MIMFs from higher frequency modes helps to increase the SSVEP target frequency prediction accuracy. Adding more than four MIMFs does not improve the accuracy; rather, the accuracy starts to decrease. This finding shows that the fifth and higher MIMFs are irrelevant to SSVEP frequency detection. This supports the intuitive understanding that the stimulation frequency will affect the EEG signals at the stimulation and harmonic frequencies. When the speed of the subject increases, the accuracy decreases. All the stimulation frequencies and harmonics will be greater than 5.45 Hz. So, the low-frequency MIMFs having frequency content less than 5.45 Hz will be irrelevant for SSVEP detection.

The subject-wise LDA classifier provides the best performance as compared to the other two classifiers. The average accuracies for the LDA classifier are 88.99%, 84.13%, 81.52%, and 76.62% for 0, 0.8, 1.6, and 2.0 m/s movement speeds, respectively.

Table 6.1: Accuracy (in %) of the MIF-CCA based SSVEP frequency detection when subject-wise KNN classifier is designed.

Subject \ Speed	0 m/s	0.8 m/s	1.6 m/s	2.0 m/s
1	98.33	98.33	96.67	100.00
2	100.00	100.00	98.33	98.33
3	98.33	95.00	93.33	86.67
4	100.00	98.33	100.00	98.33
5	95.00	91.67	93.33	56.67
6	98.33	86.67	83.33	85.00
7	100.00	100.00	96.67	95.00
8	95.00	90.00	70.00	40.00
9	93.33	73.33	96.67	68.33
10	100.00	81.67	81.67	30.00
11	100.00	90.00	93.33	68.33
12	98.33	96.67	90.00	78.33
13	91.67	53.33	90.00	88.33
14	100.00	91.67	95.00	59.57
15	98.33	100.00	98.33	100.00
16	91.67	100.00	95.00	-
17	81.67	60.00	45.00	-
18	88.33	71.67	48.33	56.67
19	43.33	45.00	33.33	-
20	40.00	43.33	50.00	-
21	100.00	95.00	96.67	-
22	100.00	100.00	98.33	-
23	38.33	40.00	33.33	-
Mean	89.13	82.68	81.59	75.60
SD	19.79	20.39	22.60	19.79

Customizing the classifier for every individual for a subject-wise classification system may be difficult. For that, a subject-independent classifier will be a better choice. The proposed MIF-CCA method provides similar accuracy for the subject-independent framework.

The performance of the presented MIF-CCA method for SSVEP detection is compared with the conventional CCA technique. The CCA provides 88.70$\pm$ 19.52%, 83.12$\pm$18.68%, 80.65$\pm$20.38%, and 54.76$\pm$25.84% accuracy for four different speeds [213, 219]. The accuracy for MIF-CCA methods is slightly higher for standing, slow, and fast walking for the MIF-CCA framework. For slow running at a speed of 2.0 m/s, MIF-CCA provides 21.86% higher accuracy as compared to conventional CCA.

Table 6.2: Accuracy (in %) of the MIF-CCA based SSVEP frequency detection when subject-wise LDA classifier is designed.

Subject \ Speed	0 m/s	0.8 m/s	1.6 m/s	2.0 m/s
1	98.33	96.67	98.33	100.00
2	100.00	96.67	98.33	98.33
3	98.33	93.33	95.00	95.00
4	100.00	98.33	100.00	98.33
5	98.33	96.67	93.33	41.67
6	100.00	90.00	85.00	91.67
7	100.00	100.00	95.00	95.00
8	95.00	86.67	73.33	55.00
9	93.33	73.33	100.00	70.00
10	98.33	80.00	86.67	35.00
11	100.00	91.67	91.67	66.67
12	95.00	95.00	93.33	83.33
13	88.33	61.67	86.67	88.33
14	100.00	95.00	96.67	65.96
15	100.00	100.00	98.33	100.00
16	96.67	100.00	100.00	-
17	78.33	66.67	55.00	-
18	90.00	76.67	46.67	41.67
19	51.67	41.67	33.33	-
20	33.33	53.33	28.33	-
21	100.00	96.67	95.00	-
22	100.00	100.00	95.00	-
23	31.67	45.00	30.00	-
Mean	88.99	84.13	81.52	76.62
SD	20.76	18.51	24.37	23.12

SSVEP-based BCI may open avenues to greatly enhance the quality of life for disabled individuals beyond clinical settings. These advancements can significantly increase their independence, autonomy, mobility, and overall capabilities, reducing social costs.

6.4 Summary

The study introduced the MIF-CCA framework for the detection of SSVEP for BCI applications. The proposed framework is evaluated using an EEG database recorded in a mobile environment to assess its robustness. The subject-wise MIF-CCA framework had

Table 6.3: Accuracy (in %) of the MIF-CCA based SSVEP frequency detection when subject-wise SVM classifier is designed.

Subject \ Speed	0 m/s	0.8 m/s	1.6 m/s	2.0 m/s
1	98.33	98.33	91.67	95.00
2	93.33	96.67	98.33	93.33
3	96.67	93.33	81.67	90.00
4	98.33	96.67	100.00	95.00
5	96.67	91.67	90.00	50.00
6	100.00	85.00	81.67	86.67
7	98.33	100.00	95.00	88.33
8	96.67	85.00	71.67	48.33
9	98.33	81.67	95.00	73.33
10	96.67	88.33	78.33	33.33
11	100.00	86.67	93.33	75.00
12	98.33	95.00	93.33	78.33
13	91.67	53.33	93.33	90.00
14	100.00	91.67	95.00	68.09
15	100.00	98.33	98.33	100.00
16	96.67	100.00	96.67	-
17	83.33	63.33	50.00	-
18	81.67	73.33	60.00	50.00
19	40.00	45.00	36.67	-
20	45.00	43.33	41.67	-
21	98.33	93.33	96.67	-
22	100.00	96.67	98.33	-
23	35.00	48.33	33.33	-
Mean	88.84	82.83	81.30	75.92
SD	19.98	18.77	21.61	20.45

Table 6.4: Accuracy (in %) of the MIF-CCA based SSVEP frequency detection when the classifier is developed independent of subject for SSVEP based BCI paradigm.

Classifier \ Speed	0 m/s	0.8 m/s	1.6 m/s	2.0 m/s
KNN	87.97	80.36	80.22	69.69
LDA	89.49	85.00	84.20	69.90
SVM	87.61	83.26	82.46	72.97

achieved mean accuracies of 88.99%, 84.13%, 81.52%, and 76.62% when the subjects were running at a speed of 0.0 m/s, 0.8 m/s, 1.6 m/s, and 2.0 m/s, respectively using LDA classifier. Similarly, for the subject-independent framework, the proposed framework provides accuracies of 89.49%, 85.00%, 84.20%, and 69.90% for four different speeds. The improvement in the detection accuracy for MIF-CCA shows the usefulness of the proposed feature. The proposed MIF-CCA method provides high accuracy as compared to conventional CCA in moving conditions, which shows the high potential of MIF-CCA in BCI applications.

Chapter 7

Joint Time-frequency Analysis of EEG Signal for Drowsiness Detection

7.1 Introduction

Driver drowsiness detection is one of the key technologies for road safety that can prevent deadly accidents due to drowsiness. Several studies have described methods to detect drowsiness in the literature, and each technique has its advantages and drawbacks. These methods can be broadly classified into three categories: behavioral, vehicular, and physiological parameter-based [222, 223].

Behavioral parameter-based techniques use drivers' eye closer ratio, eye blinking rate, eye fixation (region of interest), head position, yawning, facial expression [222, 223], etc., extracted through various image processing techniques to measure the different level of fatigue. Vehicular parameter-based techniques for drowsiness detection were developed based on lane detection, frequent changing of the lane, steering wheel angle, angular velocity or grip force, [223, 224], etc. Both the above-mentioned categories achieved good accuracy in predicting drowsiness, but these methods can be easily affected by several external factors like environmental changes, lighting conditions, illumination, geometric shape changes of roads, the disparity in road infrastructure, etc. [222, 224]. Moreover, the initial stage of drowsiness or disengagement does not affect the behavioral or vehicular parameters. So, the above methods will have a high probability of missing the onset of the non-focused mode.

Physiological parameters-based techniques are more reliable and accurate as they are based on biological parameters like heart rate [225], breathing pattern, pulse rate, electroencephalogram (EEG) [182, 226], electrocardiogram (ECG) [227], photoplethysmogram (PPG), body temperature, etc. which are not affected by external parameters easily.

EEG signals present a landscape of the human brain with very high temporal resolution. Any change in the focus level can be detected from EEG signals. In the literature, several research articles described methods for detecting drowsiness level, focused or non-focused state of mind from EEG signals [228]. The advantages of EEG signals for drowsiness detection are ease of acquiring EEG, lower cost, portability, and reliability, as well as the well-established nature of EEG technology.

7.1.1 Related Works

In this section, we have discussed recently developed EEG-based drowsiness detection methods. Arico *et al.* [229] developed a system to detect the mental workload of an air traffic controller using passive EEG brain-computer interface (BCI). Djamal *et al.* [226] proposed a method for recognizing attention and inattention state using wavelet filter and support vector machine (SVM). They have reported an accuracy of 77-83% for four subjects. Yin *et al.* [230] proposed a fatigue detection method based on the fuzzy entropy feature and SVM classifier. Tuncer *et al.* [231] extract dynamic center based binary pattern and multi threshold ternary pattern as features where discrete wavelet transform is used as the pooling method. The k-nearest neighbors (KNN) is used to classify the fatigue state. Latreche *et al.* [232] and Lee *et al.* [233] used convolutional neural network (CNN) and long short-term memory (LSTM) models for developing drowsiness detection framework. Chaudhuri and Routray [234] proposed a fatigue detection based on sample entropy, approximate entropy, and modified sample entropy embedded with the SVM classifier. Min *et al.* [235] developed a fatigue detection method from EEG signals based on several entropies like spectral entropy, sample entropy, approximate entropy, and autoregressive modeling. Li *et al.* [236] used multimodal data consisting of EEG and head movement measurement data for drowsiness detection. They have achieved accuracies of 93.67% and 96.15% for five-level and two-level drowsiness detection. Authors in [237] suggested a CNN with a global average puling layer for drowsiness detection. An accuracy of 73.22% for two-class classification of drowsiness and normal has been archived. Subasi *et al.* [238] proposed a fatigue detection technique using flexible analytic wavelet transform. EEG signals are decomposed into several subbands using flexible analytic wavelet transform. Statistical parameters like mean absolute value, average power of the flexible analytic wavelet transform coefficients are computed from each subband as features, which are further classified using machine learning classifiers. They have reported accuracies of 97.90% and 97.10% for fatigue and rest classes, respectively.

Aci *et al.* [239] developed a method for classifying different mental states (i.e., focused, non-focused, and drowsy) based on seven-channel EEG signals. The band power of EEG signals in different frequency bands was calculated using short-time Fourier transform (STFT) and used as features. With the SVM classifier, they achieved the highest accuracy of 96.70% (best) and 91.72% (average) for the subject-specific paradigm when the experiment was performed on seven participants.

In the literature, the reported methods used manually extracted various time-domain and frequency-domain features from EEG signals for mental state detection. Additionally, most of the developed methods used EEG signals using many electrodes, but more electrodes or multimodal data will add further complications and additional costs in system design.

We have proposed a multivariate iterative filtering (MIF) and discrete energy separation algorithm (DESA)-based approach for drowsiness (MIF-Drowsy) detection from multichannel EEG signals. Being nonlinear and nonstationary, EEG signals can not be properly represented in the frequency domain using the Fourier spectrum representation. Joint time-frequency representation (JTFR) can be proved to be a better option in this scenario [2]. So, we have represented the EEG signal in the joint time-frequency domain with the help of MIF [25] and DESA [240]. The joint marginal spectrum is obtained from the JTFR, which has been classified using an artificial neural network (ANN) into different mental states. Figure 7.1 presents the block diagram of the proposed automatic mental fatigue detection method.

The major contributions of the present study are as follows:

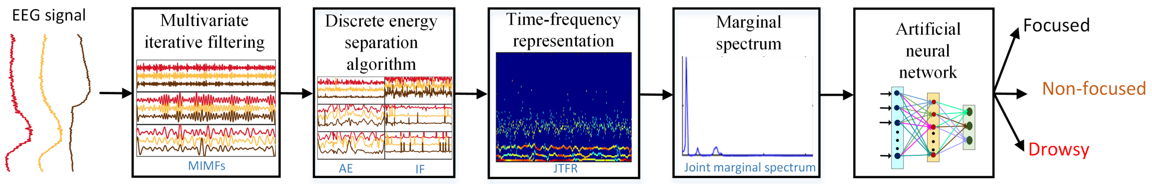

Figure 7.1: Block diagram of the proposed EEG-based mental state detection framework.

(1) Explore the nonstationary properties of EEG signals using MIF in the drowsiness detection scenario.

(2) Defined time-frequency representation (TFR) using amplitude envelope (AE) and instantaneous frequency (IF) of MIF-based oscillatory modes obtained from DESA.

(3) Proposed joint time-frequency distribution and marginal spectrum for multichannel signals.

(4) Developed a mental state detection framework based on MIF and DESA-derived joint marginal spectrum of multichannel EEG signals and ANN.

(5) Based on the developed MIF-Drowsy framework, the effects of drowsiness on different locations of the brain and EEG rhythms are analyzed.

7.2 EEG Dataset

We have used two publicly available EEG datasets to evaluate our proposed method for mental state detection. Dataset 1 [239] is used for detailed analysis and finding the optimum setting of the parameters, and the second dataset [235] is used for proving the efficacy of the developed method. The summary of the experimental setup is presented in Table 7.1.

7.2.1 Dataset 1

Dataset 1 contains approximately 25 hours of EEG recording of 5 participants, performing low-intensity control tasks. Participants were asked to virtually drive a train in the ”Microsoft Train Simulator” program for 35 min to 55 min, over a primarily featureless route. Each of the participants participated in 7 experiments. At most, one experiment was

Table 7.1: Dataset summary

Details	Dataset 1	Dataset 2
Participants	5	12
Recording duration	35-55 min	1-2 hours
Experimental session	7	1
Driving simulator	Microsoft train	Highway driving
Number of classes	3	2
Sampling frequency	128 Hz	1000 Hz
Number of EEG channels	7	32 (7 channels have been selected)

performed per day. The initial two experiments were for habituating the participants, so we have excluded these trials from our study. The fifth participant could not perform the last trial, so we have only four trials for the fifth participant.

This database consists of EEG recordings corresponding to three different mental states: focused, non-focused, and drowsy. In the focused state, the participant was controlling the train with focus and attention. After 10 minutes of focused state, the participant controlled the train without focusing much or in disengaged supervision mode. The last segment of the EEG signal corresponds to a drowsy state. In the first two states, the subjects were not allowed to drowse or close their eyes. The subjects were carefully monitored by the instructor. Additionally, the video was captured to check and ensure whether the experiment complied with the stated structure.

EEG signals were acquired during the driving simulation task using EPOC+ device with a modified head cap, at a sampling rate of 128 Hz, bandwidth between 0.2-43 Hz, and 0.51 voltage resolution. EEG electrodes were placed in the following locations F3, Fz, F4, C3, Cz, C4, and Pz, according to the 10-20 international system for EEG electrode placement.

7.2.2 Dataset 2

Dataset 2 consists of EEG recordings from 12 subjects participating in a driving simulation task inside a controlled lab environment. A 5 min practice session followed by a 10 min break was provided to each participant before starting the experiment to be habituated with the experiment protocol. The subjects were asked to control the car for approximately 1-2 hours. The Chalder fatigue scale and Li's subjective fatigue scale are used to confirm the fatigue state [235].

The EEG signal was recorded using a 32-channel electrode cap at a sampling rate of 1000 Hz. The signal is filtered using a 50 Hz notch and 0.15-45 Hz bandpass filters to improve the signal quality. After 20 min of driving, the EEG signal corresponding to the last five minutes is recorded and labeled as normal state EEG. Similarly, the last 5 min segments were recorded from 40-100 min of driving when the subject was in a fatigue state, indicated by above-mentioned scales.

7.3 Methodology

This section describes the proposed joint time-frequency analysis-based mental state detection method from EEG signal. The following subsections discuss the different parts in detail.

7.3.1 Data Segmentation

The continuous EEG signal is segmented into 5 s non-overlapping epochs. Additionally, the mean of the signal is subtracted from the signal, given by $\hat{x}[n] = x[n] - \frac{1}{L}\sum_{n=0}^{L-1} x[n]$, where L is the length of the signal.

7.3.2 Multivariate Iterative Filtering

The multivariate decomposition of time-series $x[n]$ can be expressed in expanded form as,

$$x[n] = \begin{bmatrix} I_1^1[n] & I_2^1[n] & \cdots & I_P^1[n] \\ I_1^2[n] & I_2^2[n] & \cdots & I_P^2[n] \\ \vdots & \vdots & \ddots & \vdots \\ I_1^C[n] & I_2^C[n] & \cdots & I_P^C[n] \end{bmatrix} \tag{7.1}$$

where $I_p^c[n]$ is the p^{th} multivariate intrinsic mode function (MIMF) corresponding to c^{th} channel and P is the number of MIMFs. Each column in the matrix in Eq. (7.1) will have similar oscillatory modes in terms of frequency contents due to the mode alignment property of MIF.

7.3.3 Discrete Energy Separation Algorithm

The MIMFs extracted using MIF show the amplitude and frequency modulation structures. The time-varying amplitude and frequency of the MIMFs are computed using the Teager nonlinear energy-tracking operator $\Gamma(\cdot)$ [28, 240, 241]. The $\Gamma(\cdot)$ operator can be defined mathematically for signal $y[n]$ as,

$$\Gamma(y[n]) = y^2[n] - y[n+1]y[n-1] \tag{7.2}$$

The IF $\Omega[n]$ and AE $a[n]$ of signal $y[n]$ is computed using DESA as [28],

$$\Omega[n] = \cos^{-1}\left[1 - \frac{\Gamma(\nu[n]) - \Gamma(\nu[n])}{4\Gamma(y[n])}\right], \quad 0 \leq \Omega[n] \leq \pi \tag{7.3}$$

$$|a[n]| = \sqrt{\frac{\Gamma(y[n])}{1 - \left(1 - \frac{\Gamma(\nu[n]) - \Gamma(\nu[n])}{4\Gamma(y[n])}\right)^2}} \tag{7.4}$$

where $\nu[n] = y[n] - y[n-1]$. It should be noted that if, for any sample n, $\Gamma(y[n])$ becomes zero, DESA fails to estimate the $\Omega[n]$ [240]. For such scenarios, $a[n]$ can be assigned with zeros, and IF $\Omega[n]$ can be estimated from its previous sample $(n-1)$ as, $\Omega[n] = \Omega[n-1]$ [240].

Now, the multivariate time series signal $x[n]$ can be represented with IF $\Omega_p^c[n]$ and AE $a_p^c[n]$ of the MIMF $I_p^c[n]$ as follows:

$$\Omega[n] = \begin{bmatrix} \Omega_1^1[n] & \Omega_2^1[n] & \cdots & \Omega_P^1[n] \\ \Omega_1^2[n] & \Omega_2^2[n] & \cdots & \Omega_P^2[n] \\ \vdots & \vdots & \ddots & \vdots \\ \Omega_1^C[n] & \Omega_2^C[n] & \cdots & \Omega_P^C[n] \end{bmatrix} \tag{7.5}$$

$$a[n] = \begin{bmatrix} a_1^1[n] & a_2^1[n] & \cdots & a_P^1[n] \\ a_1^2[n] & a_2^2[n] & \cdots & a_P^2[n] \\ \vdots & \vdots & \ddots & \vdots \\ a_1^C[n] & a_2^C[n] & \cdots & a_P^C[n] \end{bmatrix} \tag{7.6}$$

The evaluation of frequency and amplitude with respect to time can be seen from Eqs. (7.5) and (7.6), respectively, for individual channels. For predicting IF and AE for a particular sample, DESA needs the signal value corresponding to that sample and values of two consecutive previous and future samples. For example, to estimate IF and AE at n^{th} sample, the signal values at $(n-2)^{\text{th}}$, $(n-1)^{\text{th}}$, n^{th}, $(n+1)^{\text{th}}$, and $(n+2)^{\text{th}}$ samples are required. Due to this, the sample length of AE and IF will be less by four samples than the sample length of the signal. We can append two samples at both ends of the signals to obtain AE and IF of the same length as the signal. Spline extrapolation has been used to predict the values for extending the signal, which introduces errors in the few samples at the edge of the signals. In literature, Hilbert spectral analysis has been used for estimating AE and IF, which requires all the samples to compute the same [28]. In contrast, DESA only uses five samples for estimating IF and AE, which helps to obtain localized information and real-time implementation.

7.3.4 Joint Time-frequency Representation

The TFR is the distribution of signal energy over the 2-D time-frequency plane. The MIF provides similar oscillatory components across different channels due to its mode alignment property [25]. The AE and IF of all channels can be combined to obtain a JTFR for all the channels. The joint IF $\Omega_p^{\mathfrak{J}}[n]$ and AE $a_p^{\mathfrak{J}}[n]$ for p^{th} MIMF can be obtained using following equations [2]:

$$\Omega_p^{\mathfrak{J}}[n] = \frac{\sum_{c=1}^{C} (a_p^c[n])^2 \Omega_p^c[n]}{\sum_{c=1}^{C} (a_p^c[n])^2} \tag{7.7}$$

$$a_p^{\mathfrak{J}}[n] = \sqrt{\sum_{c=1}^{C} (a_p^c[n])^2} \tag{7.8}$$

The JTFR $\mathrm{TF}^{\mathfrak{J}}(n, \Omega)$ for multivariate time series can be obtained by considering all the oscillatory levels as follows:

$$\mathrm{TF}^{\mathfrak{J}}(n, \Omega) = (a_p^{\mathfrak{J}}[n])^2 \delta(\Omega - \Omega_p^{\mathfrak{J}}[n]) \text{ for } p = 1, 2, \cdots, P \tag{7.9}$$

where $\delta(\cdot)$ represents Kronecker delta function. The proposed concept of JTFR based on MIF and DESA is verified using synthetic and multichannel EEG signals.

7.3.4.1 Multivariate Synthetic Signal

In this section, we have presented the performance of the proposed MIF-based JTFR for synthetic signal. Let us consider the three-channel synthetic signal given as,

$$x_s(t) = \begin{bmatrix} x_{s_1}(t) + 0.5x_{s_2}(t) \\ x_{s_2}(t) + x_{s_3}(t) \\ x_{s_1}(t) + x_{s_3}(t) \end{bmatrix} \tag{7.10}$$

where $x_{s_1}(t)$, $x_{s_2}(t)$, and $x_{s_3}(t)$ are defined as follows:

$$\begin{aligned} x_{s_1}(t) &= 2\sin(70\pi t + 0.8\pi \sin(2\pi t)) \\ x_{s_2}(t) &= (1 + 0.6\sin(2\pi t))\cos(40\pi t) \\ x_{s_3}(t) &= \begin{cases} 0, & 0.67 \le t \le 1.35 \\ \sin(10\pi t), & \text{otherwise} \end{cases} \end{aligned} \tag{7.11}$$

For simulation purposes, a sampling frequency of 100 Hz has been considered for the synthetic signal $x_s(t)$. The multivariate synthetic signal $x_s(t)$ is shown in Figs. 7.2 (a)-(c). The JTFR of $x_s(t)$ obtained using MIF and DESA algorithm is shown in Fig. 7.2 (d).

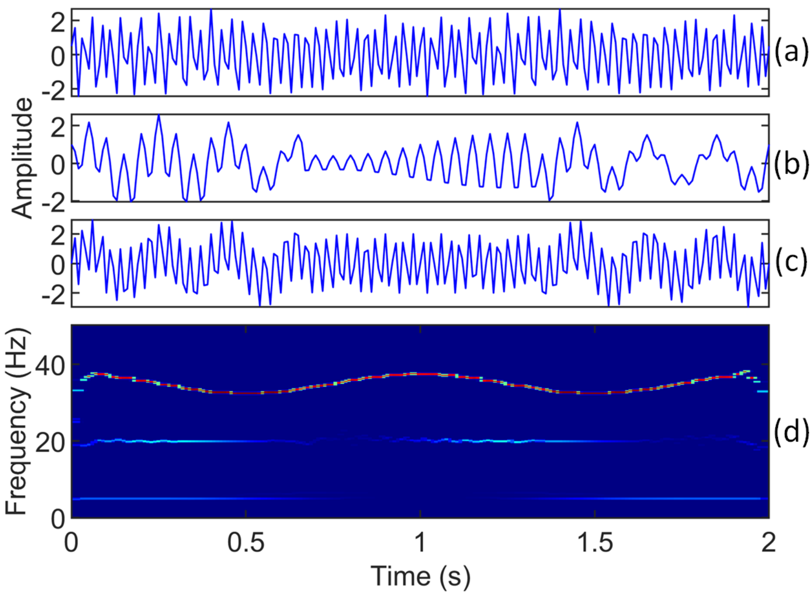

Figure 7.2: Multivariate synthetic signal: (a) channel 1, (b) channel 2, (c) channel 3, and (d) JTFR of $x_s(t)$.

7.3.4.2 Multichannel EEG Signal

To obtain the JTFR, the proposed model has been applied to the multichannel EEG signals. The JTFRs of EEG signals corresponding to focused, non-focused, and drowsy states of the brain (Fig. 7.4) based on the proposed MIF-DESA method are shown in Fig. 7.4 (middle).

7.3.5 Segmentation of Time-frequency Representation

EEG signals lie in the frequency band of 0.1 Hz to 100 Hz [25]. It can be further classified into different rhythms based on frequency, delta (δ), theta (θ), alpha (α), beta (β), and gamma (γ); their corresponding frequency bands are 0.5-4 Hz, 4-8 Hz, 8-13 Hz, 13-32 Hz, and 32-100 Hz, respectively. Different brain activities impact these rhythms in various ways. EEG signal has been analyzed at different rhythmic scales to study the effect of drowsiness on different EEG rhythms. The JTFRs are segmented depending on the frequency bands of rhythms into different levels: L1 (δ: 0.5-4 Hz), L2 ($\delta - \theta$: 0.5-8 Hz), L3 ($\delta - \theta - \alpha$: 0.5-13 Hz), L4 ($\delta - \theta - \alpha - \beta$: 0.5-32 Hz), and L5 ($\delta - \theta - \alpha - \beta - \gamma$: 0.5-64 Hz). Here, we have considered the upper-frequency limit for γ rhythm as half of the sampling frequency (128 Hz) of EEG signals.

7.3.6 Joint Marginal Spectrum

The Fourier transform is suitable for representing stationary signals but fails to represent nonstationary signals properly. EEG signal is nonstationary and complex in nature. The marginal spectrum obtained from TFR has been proven more suitable for the analysis of EEG signals [242, 243]. A joint marginal spectrum has been defined for multichannel EEG signals $x[n]$ from the JTFR $\mathrm{TF}^{\Im}(n, \Omega)$ as follows:

$$X^{\Im}(\Omega) = \sum_{n=0}^{N-1} \mathrm{TF}^{\Im}(n, \Omega) \tag{7.12}$$

The marginal spectrum for the synthetic signal defined in Eq. (7.10) is shown in Fig. 7.3 (a). For comparison, the average Fourier spectrum of the same signal is shown in Fig. 7.3 (b). The average Fourier spectrum is obtained by taking an average of magnitudes of the Fourier spectrum of the individual channels.

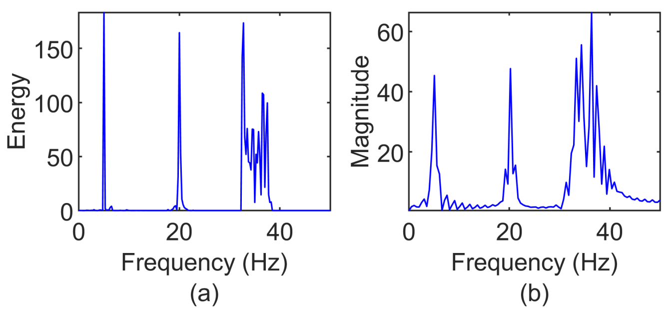

Figure 7.3: (a) Joint marginal spectrum and (b) average Fourier spectrum of $x_s(t)$.

For different rhythmic scales, a proper range of Ω has to be selected to obtain the spectrum corresponding to that scale. For example, L4 consists of $\delta - \theta - \alpha - \beta$ rhythms, so Ω corresponding to 0.5 to 32 Hz is chosen for obtaining the joint marginal spectrum L4. The marginal spectrum has been used as feature for classifying the different states of the brain.

7.3.7 Artificial Neural Network

This study uses a shallow ANN to classify different mental states from the feature vector computed in the previous steps. Cross-entropy between true outputs and predicted outputs is used as a loss function. Cross entropy of true class (y) and predicted class ($\hat{y}$) is given by equation [244],

$$J(y,\hat{y}) = -\frac{1}{M}\sum_{i=1}^{M}\sum_{j=1}^{C_L} y_{ij}\ln(\hat{y}_{ij}) + \frac{\lambda_L}{2}||W||_2^2 \tag{7.13}$$

where M is number of observations and C_L is number of classes. W and λ_L are the weight matrix between the input and hidden layers and regularization parameter, respectively. Here, λ_L is set to 0.0001. The developed ANN comprises an input layer, one hidden layer consisting of 100 neuron units with rectified linear unit (ReLU) activation function, and an output layer with softmax function for classifying different mental states.

7.4 Results and Discussion

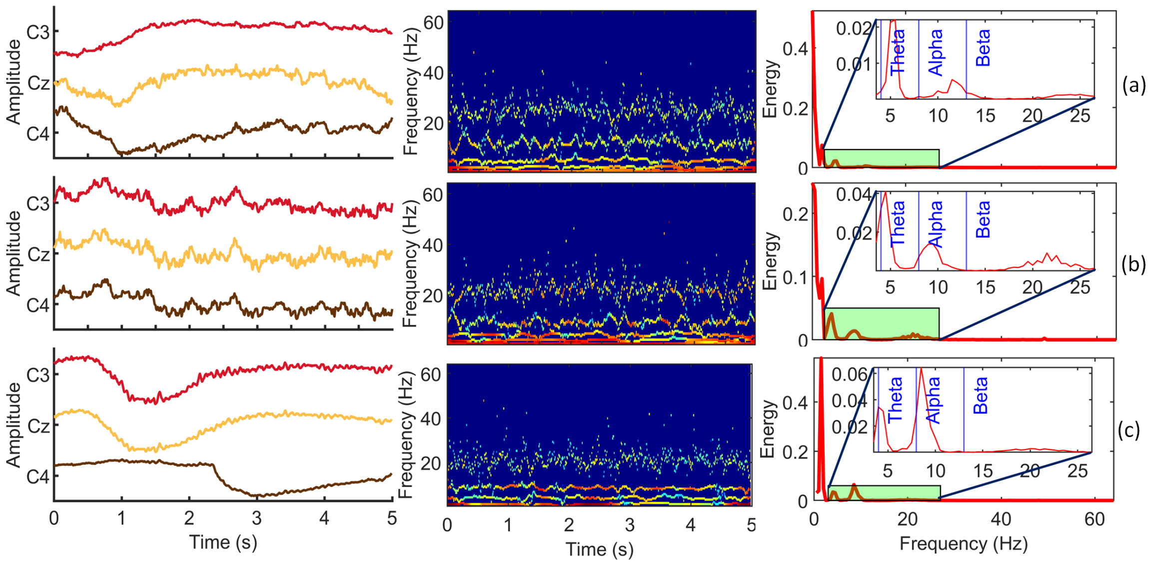

Figure 7.4: EEG signals, JTFR, and joint marginal spectrum (left-to-right) correspond to three different mental states: (a) focused, (b) non-focused, and (c) drowsy. (The inset figure in the joint marginal spectrum shows a magnified version of the green highlighted box for clear visualization. The theta, alpha, and beta rhythms are separated using lines (blue) in the inset figure.)

The proposed MIF-Drowsy framework for mental state detection is extensively analyzed and evaluated using database 1. Further, to prove the efficacy of the proposed method, we have also validated using another database for mental fatigue detection from EEG during car driving. Results and discussions of the same are presented in this section.

Based on MIF and DESA, the JTFR of the EEG signal is obtained. Fig. 7.4 shows sample EEG signals (C3, Cz, and C4 channels), JTFR, and joint marginal spectrum corresponding to three different mental states from dataset 1. The proposed JTFR shows clear separation of the frequency bands of EEG signal. Joint marginal spectrums are used as input to ANN for automatically classifying different mental states. For rejecting unwanted fluctuation, a moving average operator of a window length of three is applied on the joint marginal spectrums [245].

The performance of the proposed drowsiness detection framework is evaluated in terms of accuracy, given by, Accuracy = Number of correct predictions/Number of predictions. We randomly divided the total available samples into five mutually exclusive parts for five-fold cross-validation. The framework was developed and tested on MATLAB 2022b installed on a desktop having Windows 10 Education 64-bit operating system, intel i7 processor, and 28 GB RAM.

To find how drowsiness affects different regions of the brain and choose the most effective EEG electrodes for drowsiness detection, an experiment has been performed based on the three sets of EEG signals from different regions of the brain: frontal lobe (FL) (electrodes: F3, Fz, and F4), frontal and parietal lobe (FPL) (electrodes: C3, Cz, and C4), and the midline sagittal plane (MSP) (electrodes: Fz, Cz, and Pz). The joint marginal spectrums from FL, FPL, and MSP regions are used for classification individually. Also, the marginal spectrums from these three regions are concatenated to obtain a feature vector for all seven EEG channels, which has been used to develop a seven-channel-based mental state detection framework.

To determine the suitable rhythmic scale for drowsiness detection, the framework is studied for different rhythmic scales by choosing joint marginal spectrum corresponding to different rhythmic scales: L1, L2, L3, L4, and L5. The joint marginal spectrums at different levels correspond to the EEG signal (Fig. 7.4 (c)) are shown in Fig. 7.5.

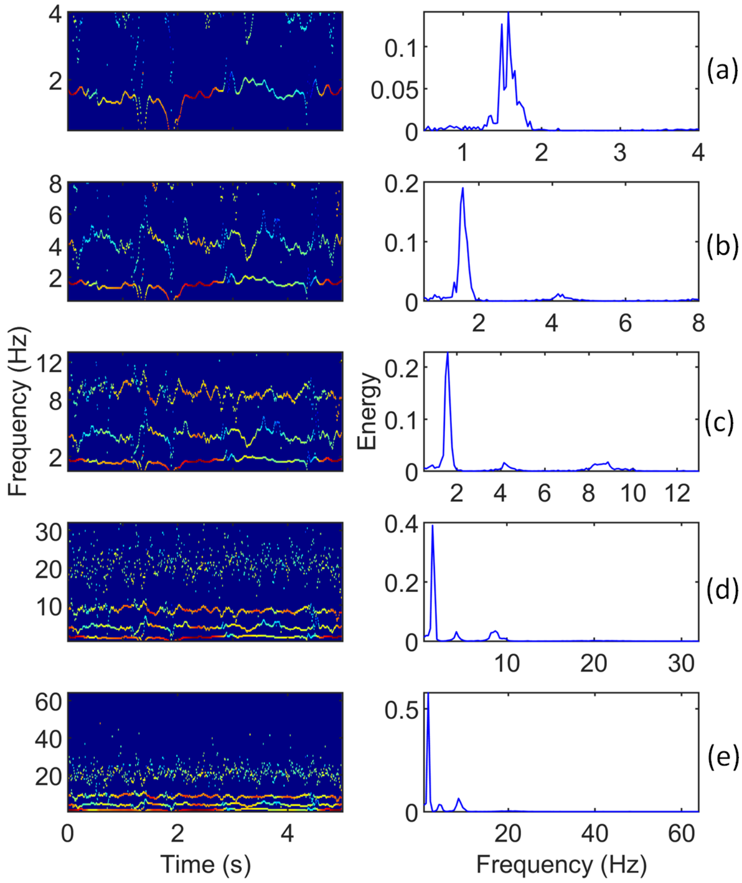

Figure 7.5: JTFRs and marginal spectrums at different rhythmic scales: (a) L1, (b) L2, (c) L3, (d) L4, and (e) L5.

Table 7.2 presents the subject-wise validation accuracy of the proposed MIF-Drowsy framework for dataset 1 in distinguishing mental states when the joint marginal spectrums corresponding to different rhythmic scales and brain regions are used as input. The average and standard deviation (SD) of classification accuracies for all subjects are mentioned at the bottom of the table.

We achieved higher accuracy when joint marginal spectrum corresponding to L4 rhythmic scale is used for classification in most of the cases. The use of joint marginal spectrum corresponding to the L5 rhythmic scale does not significantly improve the results; even for a few observations, the accuracy has dropped slightly. Previous research articles also claimed that drowsiness affects the alpha and beta rhythms of EEG. Depending on our findings and previous studies, we choose joint marginal spectrum-L4 for developing a mental state detection algorithm. In the remaining article, we have shown the results corresponding to L4

Table 7.2: Subject-wise classification Acc (in %) obtained from joint marginal spectrum corresponding to different levels of JTFR and regions of the brain for dataset 1.

Subject	Level	Brain region			
		FL	FPL	MSP	All regions
	L1	77.44	75.11	78.56	89.83
	L2	85.67	83.00	84.56	91.56
1	L3	87.83	84.61	87.39	92.89
	L4	88.33	88.33	87.17	94.06
	L5	85.78	86.17	85.94	91.67
	L1	77.33	78.39	78.61	88.28
	L2	84.11	84.56	83.17	93.33
2	L3	85.22	88.22	85.39	93.39
	L4	88.33	90.39	89.78	94.44
	L5	86.50	91.11	89.56	94.28
	L1	78.22	78.94	78.83	88.72
	L2	84.50	83.72	85.00	91.94
3	L3	87.83	90.28	89.39	93.94
	L4	89.78	91.56	92.11	94.94
	L5	88.67	90.33	91.28	94.22
	L1	78.20	78.76	77.18	88.73
	L2	84.11	82.54	84.23	93.46
4	L3	87.04	83.38	87.27	94.76
	L4	89.13	86.20	91.77	**96.85**
	L5	89.46	84.51	90.31	96.28
	L1	79.10	81.32	81.25	90.07
	L2	84.17	87.01	86.74	92.08
5	L3	86.74	89.79	89.93	94.79
	L4	89.03	89.93	90.07	94.86
	L5	88.13	89.03	88.96	93.61
	L1	78.06±0.71	78.50±2.22	78.89±1.47	89.35±0.78
Average	L2	84.51±0.67	84.17±1.77	84.74±1.31	92.48±0.87
± SD	L3	86.93±1.07	87.26±3.10	87.87±1.82	93.95±0.84
	L4	88.92±0.61	89.28±2.08	**90.18±1.97**	**95.03±1.08**
	L5	87.71±1.53	88.23±2.81	89.21±2.02	94.01±1.65

Note: Bold entries denote the highest values of Acc.

rhythmic scale only.

The proposed mental state detection framework has also been validated using another multichannel EEG database for the generality. For a fair comparison, EEG signals from the same set of channels, as chosen for dataset 1, are also used for dataset 2. The classification accuracy obtained for dataset 2 is showcased in Table 7.3. The seven-channel MIF-Drowsy framework achieves a classification accuracy of 98.33±1.51%.

Table 7.3: Subject-wise classification accuracy (in %) obtained from the joint marginal spectrum of L4 rhythmic scale corresponding to different regions of the brain for dataset 2.

Subject	Brain region			
	FL	FPL	MSP	All regions
1	99.17	100.00	100.00	100.00
2	99.17	100.00	100.00	100.00
3	98.33	99.17	97.50	98.33
4	99.17	99.17	100.00	100.00
5	97.50	99.17	94.17	98.33
6	95.83	92.50	94.17	95.83
7	99.17	98.33	97.50	99.17
8	97.50	92.50	95.00	95.83
9	98.33	97.50	95.83	96.67
10	98.33	97.50	99.17	99.17
11	99.17	94.17	97.50	98.33
12	96.67	97.50	99.17	98.33
Average± SD	98.19±1.11	97.29±2.73	97.50±2.25	98.33±1.51

Table 7.4: Subject-wise classification accuracy (in %) obtained from average Fourier spectrum for L4 rhythmic scale for dataset 1.

Subject	Brain region			
	FP	FPL	MSP	All regions
1	70.00	72.94	68.72	81.50
2	67.22	69.94	67.06	81.78
3	67.56	76.22	69.83	81.28
4	56.90	67.49	56.23	71.27
5	64.38	74.38	72.36	80.21
Average±SD	65.21±5.06	72.20±3.49	66.84±6.24	79.21±4.48

The joint marginal spectrum at L4 rhythmic scale from MSP regions gives slightly higher accuracy than the other two regions. Results in Table 7.2 show that EEG signal from the MSP brain region is best suitable for mental state detection based on 3-channel EEG data and achieves an accuracy of 91.20% for dataset 1. When the joint marginal spectrum from all channels is used, the accuracy has improved significantly to 95.82% for dataset 1.

The effectiveness of joint marginal spectrum over conventional Fourier spectrum is studied here with the help of both synthetic signal and EEG signal in the drowsiness detection framework. The multichannel synthetic signal defined in Eq. (7.10) contained frequency-modulated, amplitude-modulated, and sinusoidal components. The amplitude-modulated and sinusoidal components have constant frequency content centered around 20 Hz and 5 Hz, respectively. The joint marginal spectrum shows two peaks corresponding to amplitude-modulated and sinusoidal components without much spectral leakage. On the other hand, the Fourier spectrum in Fig. 7.3 (b) shows significant spectral leakage for amplitude-modulated and sinusoidal components.

The marginal spectrum-based drowsiness detection framework is compared with the conventional Fourier spectrum in the mental state detection scenario. The obtained results for the Fourier spectrum at L4 rhythmic scale are presented in Table 7.4. The average accuracy for the FFT-based spectrum is 79.21%, which is inferior to the average accuracy of 95.03% of the proposed framework for dataset 1. The presented results suggest the marginal spectrum is more suitable to represent the frequency contents of nonstationary EEG signals.

The existing literature presents a plethora of EEG changes associated with fatigue; however, the results exhibit considerable variability [239, 246, 247]. From Fig. 7.5, two prominent peaks in the joint marginal spectrum can be observed in the theta and alpha rhythm regions. For the non-focused mode, signal energy has slightly increased in alpha rhythm as compared to the focused mode. It also can be observed that the marginal spectral peak in alpha rhythm appears at the higher range of alpha in focused mode. From Fig. 7.4, it can be noticed that signal energy rises around alpha rhythm and suppression of theta rhythm energy for the drowsy state [239, 246]. With sleepiness, the beta band power shows a slight reduction [248]. Several studies in literature reported the changes in energy in theta, alpha, and beta bands of EEG signal due to drowsiness, which supports our findings [182, 239, 249].

The performance of the proposed MIF-Drowsy framework is evaluated for four different EEG segment lengths L of 1 s, 3 s, 5 s, and 10 s to find the effect of EEG segment length on performance. The average and SD of accuracies for all subjects for different window lengths are shown in Fig. 7.6. For dataset 1, the window of length 5 s gives the highest accuracy of 95.03$\pm$1.08%. A statistical significance test is performed to assess the change in accuracies due to different segment lengths of EEG. Student t-test based p-value is computed for the group of validation accuracies (for five folds and all subjects) belonging to different segment lengths. The p-values are shown in Fig. 7.6. The significance test shows that 5 s segment length provides significantly higher performance for dataset 1 as compared to 1 s ($p = 2.0 \times 10^{-20}$) and 3 s ($p = 1.5 \times 10^{-6}$) EEG segments. However, the performance obtained using the 10 s EEG segment does not have any statistically significant difference ($p = 0.23$) with the performance of the 5 s EEG segment. For dataset 2, the 5 s segment of EEG provides an accuracy of 98.3%, which is slightly lower (by 0.8%) than the accuracy for the 3 s EEG segment. However, the performance between 5 s and 3 s EEG segments is not significantly different ($p = 0.10$). So, the EEG segment of duration 5 s can be used for the effective detection of drowsiness. Moreover, a higher length of EEG segment will be more computationally expensive and add extra latency in prediction time. So, we did not go for a segment with a length higher than 5 s.

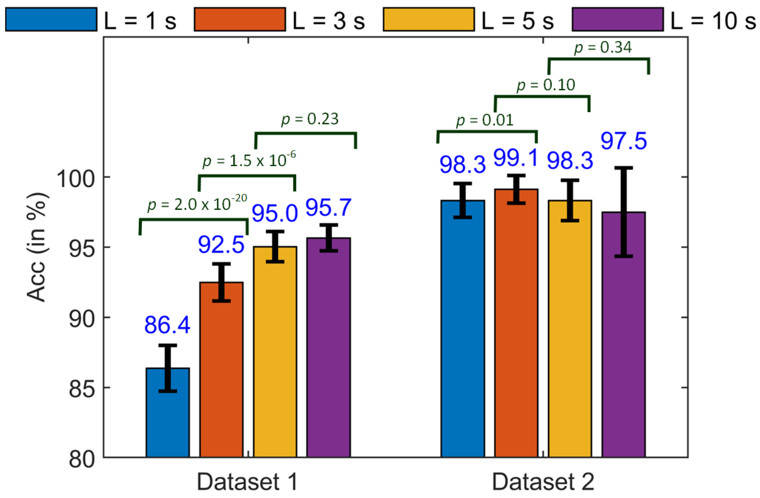

Figure 7.6: Effect of different EEG segment lengths on classification accuracy.

Figure 7.7 shows the confusion matrix of the proposed MIF-Drowsy framework for dataset 1. For an alertness monitoring system, detection of a non-focused or drowsy state is important as probable risks are associated with these states. The misclassified samples (non-focused or drowsy mode as a focused mode) are marked as hazardous detection in Fig. 7.7. From the confusion matrix, it is clearly visible that the number of hazardous predictions is negligible (less than 1.52% of total observations). Also, the number of false alarms is negligible (1.42% of total observations).

In this study, the mental state of the human subject is distinguished based on EEG sig-

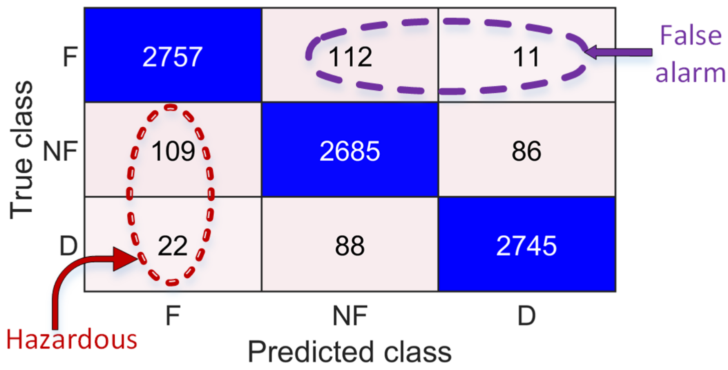

Figure 7.7: Confusion matrix of the proposed MIF-Drowsy framework for dataset 1. (F: Focused, NF: Non-focused, and D: Drowsy)

nals. The obtained results show that our method can classify the three mental states with appreciable performance. In the literature, many studies also aim to point out the problem of discriminating between a drowsy state and an attentive state based on EEG data in the context of car driving. Our study differed from such studies in that we tried to separate the focused state from the detached or unfocused state where participants do not explicitly doze, but due to lower attention levels, quick responding ability is hindered. This non-focused state can cause fatal accidents and is difficult to detect. The proposed method shows good performance in discriminating such non-focused states.

Many past studies with a similar objective of differentiating the focused and drowsy state of car drivers based on behavioral or vehicular parameters, e.g., eye fixation, lane detection, video monitoring, etc., were employed. Although they have achieved good accuracy, the performance of many such studies relies on many external conditions like road infrastructure, light conditions, etc. Also, methods based on movements or videos face a special challenge in detecting passive present or non-focused states, as these states do not significantly affect behavioral or vehicular parameters. EEG-based alertness monitoring systems directly monitor the neural activity of the brain, which carries important signatures related to mental state. In this way, pitfalls associated with other physiological, behavioral, or vehicular parameter-based methods can be avoided.

Results of previous studies carried out on drowsiness detection are summarized in Table 7.5. Several methods have used different entropy measures for developing a drowsiness detection framework [230, 234, 235]. Subasi *et al.* [238] extracted low-order statistical features from subband EEG obtained from flexible analytic wavelet transform for the classification of drowsiness. Deep learning-based classification techniques for the identification of drowsiness have been reported by Latreche *et al.* [232] and Lee *et al.* [233].

Table 7.5: Comparison of previous studies with the proposed method.

Author (Year)	Methods	Database (Subject, Number of classes)	Accuracy (in %)
Djamal *et al.* (2016) [226]	Wavelet based filters and SVM	4, 2	80.00
Yin *et al.* (2017) [230]	Fuzzy entropy and SVM	12, 2	95.00
Min *et al.* (2017) [235]	Spectral entropy, approximate entropy, sample entropy, and fuzzy entropy	12, 2	98.30
Chaudhuri and Routray (2019) [234]	Sample entropy, approximate entropy, and modified sample entropy with SVM classifier	12, 11	86.00
Aci *et al.* (2019) [239]	EEG signal energy in different frequency bands and SVM classifier	5, 3	91.72
Tuncer *et al.* (2021) [231]	Discrete wavelet transform, dynamic center based binary pattern and multi threshold ternary pattern for feature extraction and KNN classifier	16, 2	97.29
Latreche *et al.* (2022) [232]	1D-CNN and LSTM	11, 2	75.55
Subasi *et al.* (2022) [238]	Flexible analytic wavelet transform based low order statistical feature extraction and SVM classifier	16, 2	97.50
Lee *et al.* (2023) [233]	LSTM and CNN with 1 s window length for selecting EEG	19, 3	86.00
This work	MIF and DESA based JTFR, joint marginal spectrum derived from JTFR, and ANN	5, 3 12, 2	95.03 98.33

Aci *et al.* [239] reported accuracy of 90.72% (best) and 87.13% (average) subject-specific paradigm based on three-channel EEG. The proposed MIF-Drowsy three-channel EEG-based method achieved an accuracy of 96.85% (best) and 90.18±1.97% (average). Handcrafted feature-based techniques are normally tedious due to the manual finding of the appropriate features. Here, we use joint marginal spectrum for classification using ANN.

Latreche *et al.* [232] and Lee *et al.* [233] used CNN and LSTM on EEG signal for the classification of drowsiness. The multichannel EEG-based approach gives superior performance, which can be shown in Table. 7.5.

Different parameters of the EEG acquisition subsystem, like bandwidth, sampling rate, number of electrodes, etc., may affect the overall performance of the mental state detection system. These parameters also affect the design cost, user comfort, etc. We have used joint marginal spectrum L4 for classification, the frequency of which is limited to 32 Hz. Performance of more than 90.0% can be recovered using the three electrodes lying on the MSP region of the brain. These findings indicate that we can use an EEG acquisition system with a relatively lower sampling rate of around 80 Hz and only three channels to develop a mental state detector.

With all the previously mentioned advantages of the EEG-based mental state detection method, it also suffers from a few complications. EEG acquisition will be affected by different kinds of artifacts like motion and muscle artifacts. Any electrical or electronic devices in the surroundings may interfere with EEG acquisition, which may lead to deterioration of performance. These are not serious problems for a controlled indoor environment as we can take different measures to minimize them, but outside of the laboratory, it is difficult to avoid such interference. Incorporating EEG artifact removal techniques [250] as a preprocessing step can be helpful in such scenarios. Extensive research is required to develop a more robust EEG acquisition system, which will increase the effectiveness and reliability of EEG-based mental state detectors.

7.5 Summary

In this chapter, we have demonstrated a subject-specific mental state detection framework using MIF and DESA-based time-frequency analysis techniques and ANN. The multichannel EEG signals are decomposed into MIMFs using MIF. AE and IF of MIMFs are calculated with the help of DESA, which are used to obtain JTFR and joint marginal spectrum. An ANN is developed to distinguish different mental states. We evaluated the proposed method using two EEG databases. Dataset 1 is extensively analyzed to find suitable parameters like segment length of EEG, rhythmic scale, and EEG electrodes for identifying mental states. The proposed MIF-Drowsy framework shows promising results in distinguishing different mental states, namely, focused, non-focused, and drowsy modes. For dataset 1, the accuracy of the proposed method reached 96.85% (best) and 95.03$\pm$1.08% (average) using multichannel EEG data when joint marginal spectrum L4 is used. Dataset 2 is used to show the generality of the algorithm. For the second database, the MIF-Drowsy framework provides 98.33$\pm$1.51% accuracy. Comparison to other existing techniques reveals the superiority of the method described in this chapter in discriminating different mental states. Significant improvement in performance is showing the usefulness of joint time-frequency analysis of EEG signals in drowsiness detection.

Chapter 8

Conclusion and Future Works

8.1 Conclusion

We have proposed a novel extension of univariate iterative filtering for multichannel signals. The proposed multivariate iterative filtering (MIF)-based framework extracts the common oscillatory modes present in the multichannel signal adaptively without any previous assumption of fixed frequency bands. Compared to other multivariate decomposition techniques, MIF consumed much less time for the decomposition of the same signal. Having much lower computational time is a great advantages of the proposed MIF algorithm over other multivariate decomposition algorithms like multivariate empirical mode decomposition (MEMD), multivariate variational mode decomposition (MVMD).

We have developed an automated schizophrenia detection framework based on multivariate electroencephalogram (EEG) rhythms obtained from MIF. The extracted feature, namely the Hjorth parameters of each rhythm along with the support vector machine (SVM) classifier, have provided 98.9% accuracy (99.0% sensitivity and 98.8% specificity). The proposed schizophrenia detection method based on MIF has shown significant improvement (approximately 5% higher) in accuracy over existing machine learning based algorithms and similar performance like the deep learning-based method. Deep learning based methods are computationally very expensive compared to machine learning based approach. The proposed adaptive rhythm separation will be useful for EEG rhythm analysis for other neuroscience applications.

The development and implementation of an automated Parkinson's disease detection system represent a significant advancement in addressing diagnostic challenges associated with Parkinson's disease. By bridging healthcare gaps in both rural and urban settings, this technology has the potential to revolutionize Parkinson's disease management, leading to earlier diagnosis, improved patient outcomes, and more efficient healthcare delivery. The proposed method for classifying Parkinson's disease based on the phase-space representation (PSR) of multivariate intrinsic mode function (MIMF) has been found to be suitable. The proposed feature, the area under the Euclidean distance curve, can be used as a visualization tool to discriminate Parkinson's disease and healthy EEG signals. We have observed that the feature values are higher for Parkinson's disease EEG signals. This feature can be used as a diagnostic feature. We have evaluated the framework based on raw EEG signals, univariate iterative filtering-based intrinsic mode function (IMF), and MIF-based MIMF. The proposed framework based on the MIMF obtained using MIF provides the highest performance, which shows the usefulness of the MIF method for the analysis of multichannel EEG signals.

We have developed an motor imagery (MI) brain-computer interface (BCI) framework using multichannel EEG signals. The proposed method is a combination of MIF, common spatial pattern (CSP), and linear discriminant analysis (LDA) classifiers. CSP is used to extract the features from properly aligned MIMFs across different channels. The proposed framework is also evaluated by replacing the MIF with other existing multivariate decomposition algorithms. namely, MEMD and MVMD. The MIF-CSP framework provides higher accuracy as compared to both the multivariate signal decomposition approach. Moreover, due to the less time complexity of MIF, the computational time for the MIF-CSP framework will be less.

We have proposed a framework to detect the flickering frequency of steady-state visual evoked potential (SSVEP) from EEG signals. The properly aligned multivariate mode provided by the MIF method enabled us to use Canonical correlation analysis (CCA) for feature extraction in an efficient manner. The LDA classifier is used to identify different frequencies based on CCA-based features. The effectiveness of the feature are shown using t-distributed stochastic neighbor embedding (t-SNE) plot. The framework has been evaluated using an

EEG database recorded in a mobile environment. The performance of the proposed MIF-CCA-based framework is similar to the baseline methods when the subject was standing or moving at a slower speed. When the subject was running at a speed of 2 m/s, the proposed SSVEP identification framework achieved 21.8% higher accuracy as compared to the conventional CCA-based method. This shows the robustness of the proposed framework in the mobile environment.

We have developed a drowsiness detection framework using MIF, discrete energy separation algorithm (DESA)-based joint time-frequency representation (JTFR), and artificial neural network (ANN). The joint marginal spectrum obtained from MIF-based JTFR of EEG signals is proposed as a feature for the classification of drowsy EEG. We have evaluated the proposed drowsiness detection framework using two publicly available databases. The MIF-Drowsy framework provides accuracies of 95.0% and 98.3% for the two databases. The framework for MIF and DESA-based JTFR can be used for other physiological signal analyses and classifications.

8.2 Future Work

The proposed method for EEG signal processing using MIF is found suitable for identifying neurological disorders and BCI applications. The presented algorithms and framework in the thesis address several issues like improper mode alignment in multichannel signal decomposition, variability in the number of modes in different channels' signals, high computation complexity, feature extraction, feature processing and selection, and classification of EEG signals.

However, the presented work in the thesis can be improved and extended further. The developed framework can be implemented on stand-alone dedicated hardware for real-time application. We manually chose the different parameters for MIF and classifiers throughout the work. An optimization technique can be chosen to automate this step and choose the best set of parameters. The developed frameworks have been validated using one or two publicly available databases with EEG signals from a limited number of subjects. In the future, the performance of the proposed frameworks can be tested on a large set of available data. EEG signals have a wide range of applications. The MIF method can be used to develop other applications based on EEG signals. The proposed framework is only used for the analysis of EEG signals. Other imaging techniques like magnetoencephalography (MEG), near-infrared spectroscopy (NIRS) signals can also be used to understand the different states of the brain. The MIF can be used to study these signals related to the brain. More discriminated and visually separable diagnostic features can be developed using MIF for EEG signal representation and classification. Brain connectivity is an important measure for understanding the states of the brain. MIF can be used for the analysis of brain connectivity at different scales.

The proposed MIF method can be used to study other multichannel physiological signals like electrocardiogram (ECG), electromyogram (EMG), Electrooculogram (EOG), etc. EEG signals together with other physiological signals, can be studied for a multimodal framework to access the common oscillatory information across different modalities.

MIF decomposes the signals into narrowband components. MIF provides high-frequency resolution for lower-frequency components and low-frequency resolution for higher-frequency components. That means the higher frequency components will have a wider band as compared to the lower frequency components. The MIF can be modified to improve the separation of oscillatory components at higher frequencies. The MIF method is found to be suitable for EEG signal analysis as the related information lies in the lower frequency range in EEG signals. The computation time of the proposed MIF algorithm can be further reduced by proper optimization of the algorithmic steps. Detail theoretical assessment and analysis of the robustness of the proposed MIF algorithm need to be carried out in future.

Bibliography

[1] D. L. Schomer and F. L. Da Silva, *Niedermeyer's Electroencephalography: Basic Principles, Clinical Applications, and Related Fields*. Lippincott Williams & Wilkins, 2012.

[2] A. Bhattacharyya and R. B. Pachori, "A multivariate approach for patient-specific EEG seizure detection using empirical wavelet transform," *IEEE Transactions on Biomedical Engineering*, vol. 64, no. 9, pp. 2003–2015, 2017.

[3] L.-M. Sánchez-Reyes, J. Rodríguez-Reséndiz, G. N. Avecilla-Ramírez, M.-L. García-Gomar, and J.-B. Robles-Ocampo, "Impact of EEG parameters detecting dementia diseases: A systematic review," *IEEE Access*, vol. 9, pp. 78 060–78 074, 2021.

[4] J. A. Urigüen and B. Garcia-Zapirain, "EEG artifact removal state-of-the-art and guidelines," *Journal of Neural Engineering*, vol. 12, no. 3, p. 031001, 2015.

[5] K. Das, V. K. Singh, and R. B. Pachori, "Introduction to EEG signal recording and processing," in *Artificial Intelligence Enabled Signal Processing based Models for Neural Information Processing*. CRC Press, 2024, pp. 1–19.

[6] S. Sanei and J. A. Chambers, *EEG Signal Processing*. John Wiley & Sons, 2013.

[7] I. J. Rampil, "A primer for EEG signal processing in anesthesia," *The Journal of the American Society of Anesthesiologists*, vol. 89, no. 4, pp. 980–1002, 1998.

[8] M. X. Cohen, "Where does EEG come from and what does it mean?" *Trends in Neurosciences*, vol. 40, no. 4, pp. 208–218, 2017.

[9] M. X. Cohen, *Analyzing Neural Time Series Data: Theory and Practice*. MIT Press, 2014.

[10] N. Phukan, M. S. Manikandan, and R. B. Pachori, “AFibri-Net: A lightweight convolution neural network based atrial fibrillation detector,” *IEEE Transactions on Circuits and Systems I: Regular Papers*, vol. 70, no. 12, pp. 4962–4974, 2023.

[11] R. Dubey, M. Kumar, A. Upadhyay, and R. B. Pachori, “Automated diagnosis of muscle diseases from EMG signals using empirical mode decomposition based method,” *Biomedical Signal Processing and Control*, vol. 71, p. 103098, 2022.

[12] S. Calder, G. O’Grady, L. K. Cheng, and P. Du, “A theoretical analysis of electrogastrography (EGG) signatures associated with gastric dysrhythmias,” *IEEE Transactions on Biomedical Engineering*, vol. 64, no. 7, pp. 1592–1601, 2016.

[13] S. I. Khan and R. B. Pachori, “Automated eye movement classification based on EMG of EOM signals using FBSE-EWT technique,” *IEEE Transactions on Human-Machine Systems*, vol. 53, no. 2, pp. 346–356, 2023.

[14] S. Sanei, *Adaptive Processing of Brain Signals*. John Wiley & Sons, 2013.

[15] M. Soufineyestani, D. Dowling, and A. Khan, “Electroencephalography (EEG) technology applications and available devices,” *Applied Sciences*, vol. 10, no. 21, p. 7453, 2020.

[16] M. A. Frankel, M. J. Lehmkuhle, M. C. Spitz, B. J. Newman, S. V. Richards, and A. M. Arain, “Wearable reduced-channel EEG system for remote seizure monitoring,” *Frontiers in Neurology*, vol. 12, pp. 1–13, 2021.

[17] J. H. Shin, J. Kwon, J. U. Kim, H. Ryu, J. Ok, S. Joon Kwon, H. Park, and T.-i. Kim, “Wearable EEG electronics for a brain–AI closed-loop system to enhance autonomous machine decision-making,” *npj Flexible Electronics*, vol. 6, no. 1, p. 32, 2022.

[18] M. Mahmood, D. Mzurikwao, Y.-S. Kim, Y. Lee, S. Mishra, R. Herbert, A. Duarte, C. S. Ang, and W.-H. Yeo, "Fully portable and wireless universal brain–machine interfaces enabled by flexible scalp electronics and deep learning algorithm," *Nature Machine Intelligence*, vol. 1, no. 9, pp. 412–422, 2019.

[19] EEG (electroencephalogram). [Online]. Available: https://www.mayoclinic.org/tests-procedures/eeg/about/pac-20393875

[20] K. Das, P. Verma, and R. B. Pachori, "Assessment of chanting effects using EEG signals," in *2022 24th International Conference on Digital Signal Processing and its Applications (DSPA)*. IEEE, 2022, pp. 1–5.

[21] X. Jiang, G.-B. Bian, and Z. Tian, "Removal of artifacts from EEG signals: A review," *Sensors*, vol. 19, no. 5, p. 987, 2019.

[22] A. de Cheveigné, "ZapLine: A simple and effective method to remove power line artifacts," *NeuroImage*, vol. 207, p. 116356, 2020.

[23] A. Nishad, A. Upadhyay, G. Ravi Shankar Reddy, and V. Bajaj, "Classification of epileptic EEG signals using sparse spectrum based empirical wavelet transform," *Electronics Letters*, vol. 56, no. 25, pp. 1370–1372, 2020.

[24] S. Dash, R. K. Tripathy, G. Panda, and R. B. Pachori, "Automated recognition of imagined commands from EEG signals using multivariate fast and adaptive empirical mode decomposition based method," *IEEE Sensors Letters*, vol. 6, no. 2, pp. 1–4, 2022.

[25] K. Das and R. B. Pachori, "Schizophrenia detection technique using multivariate iterative filtering and multichannel EEG signals," *Biomedical Signal Processing and Control*, vol. 67, p. 102525, 2021.

[26] S. V. Bhalerao and R. B. Pachori, "Sparse spectrum based swarm decomposition for robust nonstationary signal analysis with application to sleep apnea detection from EEG," *Biomedical Signal Processing and Control*, vol. 77, p. 103792, 2022.

[27] A. Anuragi, D. S. Sisodia, and R. B. Pachori, "Epileptic-seizure classification using phase-space representation of FBSE-EWT based EEG sub-band signals and ensemble learners," *Biomedical Signal Processing and Control*, vol. 71, p. 103138, 2022.

[28] R. B. Pachori, *Time-frequency Analysis Techniques and Their Applications*. CRC Press, 2023.

[29] R. R. Sharma and R. B. Pachori, "Time–frequency representation using IEVDHM–HT with application to classification of epileptic EEG signals," *IET Science, Measurement & Technology*, vol. 12, no. 1, pp. 72–82, 2018.

[30] V. Gupta and R. B. Pachori, "FBDM based time-frequency representation for sleep stages classification using EEG signals," *Biomedical Signal Processing and Control*, vol. 64, p. 102265, 2021.

[31] A. Bhattacharyya, A. Verma, R. Ranta, and R. B. Pachori, "Ocular artifacts elimination from multivariate EEG signal using frequency-spatial filtering," *IEEE Transactions on Cognitive and Developmental Systems*, vol. 15, pp. 1547–1559, 2022.

[32] P. Gajbhiye, R. K. Tripathy, and R. B. Pachori, "Elimination of ocular artifacts from single channel EEG signals using FBSE-EWT based rhythms," *IEEE Sensors Journal*, vol. 20, no. 7, pp. 3687–3696, 2019.

[33] P. Gajbhiye, R. K. Tripathy, A. Bhattacharyya, and R. B. Pachori, "Novel approaches for the removal of motion artifact from EEG recordings," *IEEE Sensors Journal*, vol. 19, no. 22, pp. 10 600–10 608, 2019.

[34] V. Paliwal, K. Das, S. M. Doesburg, G. Medvedev, P. Xi, U. Ribary, R. B. Pachori, and V. A. Vakorin, "Classifying routine clinical electroencephalograms with multivariate iterative filtering and convolutional neural networks," *IEEE Transactions on Neural Systems and Rehabilitation Engineering*, vol. 32, pp. 2038–2048, 2024.

[35] A. Nalwaya, K. Das, and R. B. Pachori, "Automated emotion identification using Fourier–Bessel domain-based entropies," *Entropy*, vol. 24, no. 10, p. 1322, 2022.

[36] V. K. Singh and R. B. Pachori, "Sliding eigenvalue decomposition for non-stationary signal analysis," in *2020 International Conference on Signal Processing and Communications (SPCOM)*. IEEE, 2020, pp. 1–5.

[37] V. K. Singh and R. B. Pachori, "Iterative eigenvalue decomposition of Hankel matrix: An EMD like tool," 2022.

[38] S. P. Kamaraju, K. Das, and R. B. Pachori, "EEG based biometric authentication system using multivariate FBSE entropy," 2023.

[39] S. I. Khan and R. B. Pachori, "Empirical wavelet transform-based framework for diagnosis of epilepsy using EEG signals," in *AI-Enabled Smart Healthcare Using Biomedical Signals*. IGI Global, 2022, pp. 217–239.

[40] A. Anuragi, D. S. Sisodia, and R. B. Pachori, "Automated FBSE-EWT based learning framework for detection of epileptic seizures using time-segmented EEG signals," *Computers in Biology and Medicine*, vol. 136, p. 104708, 2021.

[41] S. Madhavan, R. K. Tripathy, and R. B. Pachori, "Time-frequency domain deep convolutional neural network for the classification of focal and non-focal EEG signals," *IEEE Sensors Journal*, vol. 20, no. 6, pp. 3078–3086, 2019.

[42] R. Boostani, F. Karimzadeh, and M. Nami, "A comparative review on sleep stage classification methods in patients and healthy individuals," *Computer Methods and Programs in Biomedicine*, vol. 140, pp. 77–91, 2017.

[43] P. Moridian, A. Shoeibi, M. Khodatars, M. Jafari, R. B. Pachori, A. Khadem, R. Alizadehsani, and S. H. Ling, "Automatic diagnosis of sleep apnea from biomedical signals using artificial intelligence techniques: Methods, challenges, and future works," *Wiley Interdisciplinary Reviews: Data Mining and Knowledge Discovery*, vol. 12, no. 6, p. e1478, 2022.

[44] A. Nalwaya, K. Das, and R. B. Pachori, "Emotion identification from TQWT-based EEG rhythms," in *AI-Enabled Smart Healthcare Using Biomedical Signals*. IGI Global, 2022, pp. 195–216.

[45] A. Anuragi, D. S. Sisodia, and R. B. Pachori, “EEG-based cross-subject emotion recognition using Fourier-Bessel series expansion based empirical wavelet transform and NCA feature selection method,” *Information Sciences*, vol. 610, pp. 508–524, 2022.

[46] A. Bhattacharyya, R. K. Tripathy, L. Garg, and R. B. Pachori, “A novel multivariate-multiscale approach for computing EEG spectral and temporal complexity for human emotion recognition,” *IEEE Sensors Journal*, vol. 21, no. 3, pp. 3579–3591, 2020.

[47] Y. Zhou, S. Huang, Z. Xu, P. Wang, X. Wu, and D. Zhang, “Cognitive workload recognition using EEG signals and machine learning: A review,” *IEEE Transactions on Cognitive and Developmental Systems*, vol. 14, no. 3, pp. 799–818, 2021.

[48] Y. Zhu, Q. Wang, and L. Zhang, “Study of EEG characteristics while solving scientific problems with different mental effort,” *Scientific Reports*, vol. 11, no. 1, pp. 1–12, 2021.

[49] S. Dash, R. K. Tripathy, D. K. Dash, G. Panda, and R. B. Pachori, “Multiscale domain gradient boosting models for the automated recognition of imagined vowels using multichannel EEG signals,” *IEEE Sensors Letters*, vol. 6, no. 11, pp. 1–4, 2022.

[50] A. T. Gifford, K. Dwivedi, G. Roig, and R. M. Cichy, “A large and rich EEG dataset for modeling human visual object recognition,” *NeuroImage*, vol. 264, p. 119754, 2022.

[51] N. Dijkstra, S. E. Bosch, and M. A. van Gerven, “Shared neural mechanisms of visual perception and imagery,” *Trends in Cognitive Sciences*, vol. 23, no. 5, pp. 423–434, 2019.

[52] S. Xie, D. Kaiser, and R. M. Cichy, “Visual imagery and perception share neural representations in the alpha frequency band,” *Current Biology*, vol. 30, no. 13, pp. 2621–2627, 2020.

[53] B. R. Cahn and J. Polich, “Meditation states and traits: EEG, ERP, and neuroimaging studies,” *Psychological Bulletin*, vol. 132, no. 2, p. 180, 2006.

[54] Y. Yang, X. Dong, Z. Peng, W. Zhang, and G. Meng, “Component extraction for non-stationary multi-component signal using parameterized de-chirping and band-pass filter,” *IEEE Signal Processing Letters*, vol. 22, no. 9, pp. 1373–1377, 2014.

[55] I. Orovi, S. Stanković, and A. Draganić, “Time-frequency nalysis and singular value decomposition applied to the highly multicomponent musical signals,” *Acta Acustica United with Acustica*, vol. 100, no. 1, pp. 93–101, 2014.

[56] L. Stankovic, M. Daković, and T. Thayaparan, *Time-frequency Signal Analysis with Applications*. Artech House, 2014.

[57] V. Katkovnik and L. Stankovic, “Instantaneous frequency estimation using the Wigner distribution with varying and data-driven window length,” *IEEE Transactions on Signal Processing*, vol. 46, no. 9, pp. 2315–2325, 1998.

[58] J. B. Allen and L. R. Rabiner, “A unified approach to short-time Fourier analysis and synthesis,” *Proceedings of the IEEE*, vol. 65, no. 11, pp. 1558–1564, 1977.

[59] D. Griffin and J. Lim, “Signal estimation from modified short-time Fourier transform,” *IEEE Transactions on Acoustics, Speech, and Signal Processing*, vol. 32, no. 2, pp. 236–243, 1984.

[60] L. Cohen, *Time-frequency Analysis*. Prentice Hall New Jersey, 1995, vol. 778.

[61] S. Mallat, *A Wavelet Tour of Signal Processing*. Elsevier, 1999.

[62] I. Daubechies, *Ten Lectures on Wavelets*. SIAM, 1992.

[63] N. E. Huang, Z. Shen, S. R. Long, M. C. Wu, H. H. Shih, Q. Zheng, N.-C. Yen, C. C. Tung, and H. H. Liu, “The empirical mode decomposition and the Hilbert spectrum for nonlinear and non-stationary time series analysis,” *Proceedings of the Royal Society of London. Series A: Mathematical, Physical and Engineering sciences*, vol. 454, no. 1971, pp. 903–995, 1998.

[64] L. Lin, Y. Wang, and H. Zhou, "Iterative filtering as an alternative algorithm for empirical mode decomposition," *Advances in Adaptive Data Analysis*, vol. 1, no. 04, pp. 543–560, 2009.

[65] K. Dragomiretskiy and D. Zosso, "Variational mode decomposition," *IEEE Transactions on Signal Processing*, vol. 62, no. 3, pp. 531–544, 2013.

[66] A. Bhattacharyya, L. Singh, and R. B. Pachori, "Fourier–Bessel series expansion based empirical wavelet transform for analysis of non-stationary signals," *Digital Signal Processing*, vol. 78, pp. 185–196, 2018.

[67] J. Gilles, "Empirical wavelet transform," *IEEE Transactions on Signal Processing*, vol. 61, no. 16, pp. 3999–4010, 2013.

[68] A. Mert and A. Akan, "Emotion recognition from EEG signals by using multivariate empirical mode decomposition," *Pattern Analysis and Applications*, vol. 21, pp. 81–89, 2018.

[69] C. Park, D. Looney, N. ur Rehman, A. Ahrabian, and D. P. Mandic, "Classification of motor imagery BCI using multivariate empirical mode decomposition," *IEEE Transactions on Neural Systems and Rehabilitation Engineering*, vol. 21, no. 1, pp. 10–22, 2012.

[70] K. Das and R. B. Pachori, "Electroencephalogram based motor imagery brain computer interface using multivariate iterative filtering and spatial filtering," *IEEE Transactions on Cognitive and Developmental Systems*, vol. 15, pp. 1408 – 1418, 2022.

[71] L. Stanković, D. Mandić, M. Daković, and M. Brajović, "Time-frequency decomposition of multivariate multicomponent signals," *Signal Processing*, vol. 142, pp. 468–479, 2018.

[72] A. Ahrabian, D. Looney, L. Stanković, and D. P. Mandic, "Synchrosqueezing-based time-frequency analysis of multivariate data," *Signal Processing*, vol. 106, pp. 331–341, 2015.

[73] J. M. Lilly and S. C. Olhede, “Bivariate instantaneous frequency and bandwidth,” *IEEE Transactions on Signal Processing*, vol. 58, no. 2, pp. 591–603, 2009.

[74] J. M. Lilly and S. C. Olhede, “Analysis of modulated multivariate oscillations,” *IEEE Transactions on Signal Processing*, vol. 60, no. 2, pp. 600–612, 2011.

[75] “Schizophrenia.” [Online]. Available: https://www.who.int/news-room/fact-sheets/detail/schizophrenia

[76] “What is Schizophrenia?” [Online]. Available: https://www.psychiatry.org/patients-families/schizophrenia/what-is-schizophrenia

[77] T. M. Laursen, M. Nordentoft, and P. B. Mortensen, “Excess early mortality in schizophrenia,” *Annual Review of Clinical Psychology*, vol. 10, pp. 425–448, 2014.

[78] M. Olfson, T. Gerhard, C. Huang, S. Crystal, and T. S. Stroup, “Premature mortality among adults with schizophrenia in the united states,” *JAMA Psychiatry*, vol. 72, no. 12, pp. 1172–1181, 2015.

[79] Parkinson’s disease. [Online]. Available: https://www.mayoclinic.org/diseases-conditions/parkinsons-disease/symptoms-causes/syc-20376055

[80] What is Parkinson’s? [Online]. Available: https://www.parkinson.org/understanding-parkinsons/what-is-parkinsons

[81] P. Gaur, H. Gupta, A. Chowdhury, K. McCreadie, R. B. Pachori, and H. Wang, “A sliding window common spatial pattern for enhancing motor imagery classification in EEG-BCI,” *IEEE Transactions on Instrumentation and Measurement*, vol. 70, pp. 1–9, 2021.

[82] P. Chholak, G. Niso, V. A. Maksimenko, S. A. Kurkin, N. S. Frolov, E. N. Pitsik, A. E. Hramov, and A. N. Pisarchik, “Visual and kinesthetic modes affect motor imagery classification in untrained subjects,” *Scientific Reports*, vol. 9, no. 1, pp. 1–12, 2019.

[83] R. Foong, K. K. Ang, C. Quek, C. Guan, K. S. Phua, C. W. K. Kuah, V. A. Deshmukh, L. H. L. Yam, D. K. Rajeswaran, N. Tang *et al.*, "Assessment of the efficacy of EEG-based MI-BCI with visual feedback and EEG correlates of mental fatigue for upper-limb stroke rehabilitation," *IEEE Transactions on Biomedical Engineering*, vol. 67, no. 3, pp. 786–795, 2019.

[84] Y. Zhang, S. Q. Xie, H. Wang, and Z. Zhang, "Data analytics in steady-state visual evoked potential-based brain–computer interface: A review," *IEEE Sensors Journal*, vol. 21, no. 2, pp. 1124–1138, 2020.

[85] National highway traffic safety administration (NHTSA). distracted driving 2018. [Online]. Available: https://crashstats.nhtsa.dot.gov/Api/Public/ViewPublication/812926

[86] C. Park, D. Looney, P. Kidmose, M. Ungstrup, and D. P. Mandic, "Time-frequency analysis of EEG asymmetry using bivariate empirical mode decomposition," *IEEE Transactions on Neural Systems and Rehabilitation Engineering*, vol. 19, no. 4, pp. 366–373, 2011.

[87] N. Rehman and D. P. Mandic, "Multivariate empirical mode decomposition," *Proceedings of the Royal Society A: Mathematical, Physical and Engineering Sciences*, vol. 466, no. 2117, pp. 1291–1302, 2010.

[88] N. Ur Rehman and H. Aftab, "Multivariate variational mode decomposition," *IEEE Transactions on Signal Processing*, vol. 67, no. 23, pp. 6039–6052, 2019.

[89] D. Gabor, "Theory of communication," *Proceedings of the Institution of Electrical Engineers*, vol. 93, pp. 429–457, 1946.

[90] D. Vakman, "On the analytic signal, the Teager-Kaiser energy algorithm, and other methods for defining amplitude and frequency," *IEEE Transactions on Signal Processing*, vol. 44, no. 4, pp. 791–797, 1996.

[91] B. Picinbono, "On instantaneous amplitude and phase of signals," *IEEE Transactions on Signal Processing*, vol. 45, no. 3, pp. 552–560, 1997.

[92] L. Stanković, M. Brajović, M. Daković, and D. Mandic, "On the decomposition of multichannel nonstationary multicomponent signals," *Signal Processing*, vol. 167, p. 107261, 2020.

[93] T. Tanaka and D. P. Mandic, "Complex empirical mode decomposition," *IEEE Signal Processing Letters*, vol. 14, no. 2, pp. 101–104, 2007.

[94] G. Rilling, P. Flandrin, P. Gonçalves, and J. M. Lilly, "Bivariate empirical mode decomposition," *IEEE Signal Processing Letters*, vol. 14, no. 12, pp. 936–939, 2007.

[95] M. U. B. Altaf, T. Gautama, T. Tanaka, and D. P. Mandic, "Rotation invariant complex empirical mode decomposition," in *2007 IEEE International Conference on Acoustics, Speech and Signal Processing-ICASSP'07*, vol. 3. IEEE, 2007, pp. III–1009.

[96] N. ur Rehman and D. P. Mandic, "Empirical mode decomposition for trivariate signals," *IEEE Transactions on Signal Processing*, vol. 58, no. 3, pp. 1059–1068, 2009.

[97] X. Lang, Q. Zheng, Z. Zhang, S. Lu, L. Xie, A. Horch, and H. Su, "Fast multivariate empirical mode decomposition," *IEEE Access*, vol. 6, pp. 65 521–65 538, 2018.

[98] J. Schroeder, "Signal processing via Fourier-Bessel series expansion," *Digital Signal Processing*, vol. 3, pp. 112–124, 1993.

[99] P. K. Chaudhary, V. Gupta, and R. B. Pachori, "Fourier-Bessel representation for signal processing: A review," *Digital Signal Processing*, vol. 135, p. 103938, 2023.

[100] A. Anuragi, D. S. Sisodia, and R. B. Pachori, "Automated alcoholism detection using Fourier-Bessel series expansion based empirical wavelet transform," *IEEE Sensors Journal*, vol. 20, no. 9, pp. 4914–4924, 2020.

[101] R. B. Pachori and P. Sircar, "EEG signal analysis using FB expansion and second-order linear TVAR process," *Signal Processing*, vol. 88, no. 2, pp. 415–420, 2008.

[102] D. Zosso, K. Dragomiretskiy, A. L. Bertozzi, and P. S. Weiss, "Two-dimensional compact variational mode decomposition: Spatially compact and spectrally sparse

image decomposition and segmentation," *Journal of Mathematical Imaging and Vision*, vol. 58, pp. 294–320, 2017.

[103] S. Liu and K. Yu, "Successive multivariate variational mode decomposition," *Multidimensional Systems and Signal Processing*, vol. 33, no. 3, pp. 917–943, 2022.

[104] Z. Wu and N. E. Huang, "Ensemble empirical mode decomposition: A noise-assisted data analysis method," *Advances in Adaptive Data Analysis*, vol. 1, no. 01, pp. 1–41, 2009.

[105] J. S. Smith, "The local mean decomposition and its application to EEG perception data," *Journal of the Royal Society Interface*, vol. 2, no. 5, pp. 443–454, 2005.

[106] R. Vautard and M. Ghil, "Singular spectrum analysis in nonlinear dynamics, with applications to paleoclimatic time series," *Physica D: Nonlinear Phenomena*, vol. 35, no. 3, pp. 395–424, 1989.

[107] J. Harmouche, D. Fourer, F. Auger, P. Borgnat, and P. Flandrin, "The sliding singular spectrum analysis: A data-driven nonstationary signal decomposition tool," *IEEE Transactions on Signal Processing*, vol. 66, no. 1, pp. 251–263, 2017.

[108] D. S. Broomhead and G. P. King, "Extracting qualitative dynamics from experimental data," *Physica D: Nonlinear Phenomena*, vol. 20, no. 2-3, pp. 217–236, 1986.

[109] J. Zheng, J. Cheng, and Y. Yang, "A rolling bearing fault diagnosis approach based on LCD and fuzzy entropy," *Mechanism and Machine Theory*, vol. 70, pp. 441–453, 2013.

[110] M. G. Frei and I. Osorio, "Intrinsic time-scale decomposition: time–frequency–energy analysis and real-time filtering of non-stationary signals," *Proceedings of the Royal Society A: Mathematical, Physical and Engineering Sciences*, vol. 463, no. 2078, pp. 321–342, 2007.

[111] P. J. Schmid, "Dynamic mode decomposition of numerical and experimental data," *Journal of Fluid Mechanics*, vol. 656, pp. 5–28, 2010.

[112] D. Iatsenko, P. V. McClintock, and A. Stefanovska, “Nonlinear mode decomposition: A noise-robust, adaptive decomposition method,” *Physical Review E*, vol. 92, no. 3, p. 032916, 2015.

[113] A. Cicone, J. Liu, and H. Zhou, “Adaptive local iterative filtering for signal decomposition and instantaneous frequency analysis,” *Applied and Computational Harmonic Analysis*, vol. 41, no. 2, pp. 384–411, 2016.

[114] P. Singh, S. D. Joshi, R. K. Patney, and K. Saha, “The Fourier decomposition method for nonlinear and non-stationary time series analysis,” *Proceedings of the Royal Society A: Mathematical, Physical and Engineering Sciences*, vol. 473, no. 2199, p. 20160871, 2017.

[115] Q. Chen, L. Xie, and H. Su, “Multivariate nonlinear chirp mode decomposition,” *Signal Processing*, vol. 176, p. 107667, 2020.

[116] J. Huang, C. Li, X. Xiao, T. Yu, X. Yuan, and Y. Zhang, “Adaptive multivariate chirp mode decomposition,” *Mechanical Systems and Signal Processing*, vol. 186, p. 109897, 2023.

[117] R. Mahmoudvand, P. C. Rodrigues, and M. Yarmohammadi, “Forecasting daily exchange rates: A comparison between SSA and MSSA,” *REVSTAT-Statistical Journal*, vol. 17, no. 4, pp. 601–616, 2019.

[118] P. C. Rodrigues and R. Mahmoudvand, “The benefits of multivariate singular spectrum analysis over the univariate version,” *Journal of the Franklin Institute*, vol. 355, no. 1, pp. 544–564, 2018.

[119] Q. Zhang, R. Yuan, Y. Lv, Z. Li, and H. Wu, “Multivariate dynamic mode decomposition and its application to bearing fault diagnosis,” *IEEE Sensors Journal*, vol. 23, no. 7, pp. 7514–7524, 2023.

[120] A. S. S. Reddy and R. B. Pachori, “Multivariate dynamic mode decomposition for automatic imagined speech recognition using multichannel EEG signals,” *IEEE Sensors Letters*, vol. 8, p. 6001604, 2024.

[121] T. Matsuda and F. Komaki, “Multivariate time series decomposition into oscillation components,” *Neural Computation*, vol. 29, no. 8, pp. 2055–2075, 2017.

[122] L. Lin, Y. Wang, and H. Zhou, “Iterative filtering as an alternative algorithm for empirical mode decomposition,” *Advances in Adaptive Data Analysis*, vol. 1, no. 04, pp. 543–560, 2009.

[123] A. Cicone, C. Garoni, and S. Serra-Capizzano, “Spectral and convergence analysis of the discrete ALIF method,” *Linear Algebra and its Applications*, vol. 580, pp. 62–95, 2019.

[124] A. Cicone and P. Dell’Acqua, “Study of boundary conditions in the iterative filtering method for the decomposition of nonstationary signals,” *Journal of Computational and Applied Mathematics*, vol. 373, p. 112248, 2020.

[125] A. Cicone, “Iterative filtering as a direct method for the decomposition of nonstationary signals,” *Numerical Algorithms*, vol. 85, no. 3, pp. 811–827, 2020.

[126] A. Cicone and E. Pellegrino, “Multivariate fast iterative filtering for the decomposition of nonstationary signals,” *IEEE Transactions on Signal Processing*, vol. 70, pp. 1521–1531, 2022.

[127] D. Sulzer, C. Cassidy, G. Horga, U. J. Kang, S. Fahn, L. Casella, G. Pezzoli, J. Langley, X. P. Hu, F. A. Zucca *et al.*, “Neuromelanin detection by magnetic resonance imaging (MRI) and its promise as a biomarker for Parkinson’s disease,” *npj Parkinson’s Disease*, vol. 4, no. 1, pp. 1–13, 2018.

[128] U. R. Acharya, S. L. Fernandes, J. E. WeiKoh, E. J. Ciaccio, M. K. M. Fabell, U. J. Tanik, V. Rajinikanth, and C. H. Yeong, “Automated detection of Alzheimer’s disease using brain MRI images–a study with various feature extraction techniques,” *Journal of Medical Systems*, vol. 43, no. 9, p. 302, 2019.

[129] N. Salamon, J. Kung, S. Shaw, J. Koo, S. Koh, J. Wu, J. Lerner, R. Sankar, W. Shields, J. Engel *et al.*, “FDG-PET/MRI coregistration improves detection of cortical dysplasia in patients with epilepsy,” *Neurology*, vol. 71, no. 20, pp. 1594–1601, 2008.

[130] V. Gupta and R. B. Pachori, "Epileptic seizure identification using entropy of FBSE based EEG rhythms," *Biomedical Signal Processing and Control*, vol. 53, p. 101569, 2019.

[131] V. Joshi, R. B. Pachori, and A. Vijesh, "Classification of ictal and seizure-free EEG signals using fractional linear prediction," *Biomedical Signal Processing and Control*, vol. 9, pp. 1–5, 2014.

[132] R. B. Pachori and V. Gupta, "Biomedical engineering fundamentals," in *Intelligent Internet of Things*. Springer, 2020, pp. 547–605.

[133] J. W. Kim, Y. S. Lee, D. H. Han, K. J. Min, J. Lee, and K. Lee, "Diagnostic utility of quantitative EEG in un-medicated schizophrenia," *Neuroscience Letters*, vol. 589, pp. 126–131, 2015.

[134] Z. Dvey-Aharon, N. Fogelson, A. Peled, and N. Intrator, "Schizophrenia detection and classification by advanced analysis of EEG recordings using a single electrode approach," *PloS One*, vol. 10, no. 4, p. e0123033, 2015.

[135] L. Santos-Mayo, L. M. San-José-Revuelta, and J. I. Arribas, "A computer-aided diagnosis system with EEG based on the P3b wave during an auditory odd-ball task in schizophrenia," *IEEE Transactions on Biomedical Engineering*, vol. 64, no. 2, pp. 395–407, 2016.

[136] A. J. Ibáñez-Molina, V. Lozano, M. Soriano, J. Aznarte, C. J. Gómez-Ariza, M. Bajo *et al.*, "EEG multiscale complexity in schizophrenia during picture naming," *Frontiers in Physiology*, vol. 9, p. 1213, 2018.

[137] V. Jahmunah, S. L. Oh, V. Rajinikanth, E. J. Ciaccio, K. H. Cheong, N. Arunkumar, and U. R. Acharya, "Automated detection of schizophrenia using nonlinear signal processing methods," *Artificial Intelligence in Medicine*, vol. 100, p. 101698, 2019.

[138] S. L. Oh, J. Vicnesh, E. J. Ciaccio, R. Yuvaraj, and U. R. Acharya, "Deep convolutional neural network model for automated diagnosis of schizophrenia using EEG signals," *Applied Sciences*, vol. 9, no. 14, p. 2870, 2019.

[139] P. T. Krishnan, A. N. J. Raj, P. Balasubramanian, and Y. Chen, "Schizophrenia detection using multivariate empirical mode decomposition and entropy measures from multichannel EEG signal," *Biocybernetics and Biomedical Engineering*, vol. 40, pp. 1124 – 1139, 2020.

[140] E. Olejarczyk and W. Jernajczyk, "Graph-based analysis of brain connectivity in schizophrenia," *PLoS One*, vol. 12, no. 11, p. e0188629, 2017.

[141] J. S. Kumar and P. Bhuvaneswari, "Analysis of electroencephalography (EEG) signals and its categorization–A study," *Procedia Engineering*, vol. 38, pp. 2525–2536, 2012.

[142] P. Welch, "The use of fast Fourier transform for the estimation of power spectra: A method based on time averaging over short, modified periodograms," *IEEE Transactions on Audio and Electroacoustics*, vol. 15, no. 2, pp. 70–73, 1967.

[143] A. Cicone and H. Zhou, "Numerical analysis for iterative filtering with new efficient implementations based on FFT," *Numerische Mathematik*, vol. 147, no. 1, pp. 1–28, 2021.

[144] P. Singh and R. B. Pachori, "Classification of focal and nonfocal EEG signals using features derived from Fourier-based rhythms," *Journal of Mechanics in Medicine and Biology*, vol. 17, no. 07, p. 1740002, 2017.

[145] A. Rényi *et al.*, "On measures of entropy and information," in *Proceedings of the Fourth Berkeley Symposium on Mathematical Statistics and Probability, Volume 1: Contributions to the Theory of Statistics*. The Regents of the University of California, 1961.

[146] J. S. Richman and J. R. Moorman, "Physiological time-series analysis using approximate entropy and sample entropy," *American Journal of Physiology-Heart and Circulatory Physiology*, vol. 278, no. 6, pp. H2039–H2049, 2000.

[147] M. T. Rosenstein, J. J. Collins, and C. J. De Luca, "A practical method for calculating

largest Lyapunov exponents from small data sets," *Physica D: Nonlinear Phenomena*, vol. 65, no. 1-2, pp. 117–134, 1993.

[148] B. Hjorth, "EEG analysis based on time domain properties," *Electroencephalography and Clinical Neurophysiology*, vol. 29, no. 3, pp. 306–310, 1970.

[149] C. Bishop, *Pattern recognition and machine learning*, ser. Information science and statistics. Springer New York, NY, 2006.

[150] C. Cortes and V. Vapnik, "Support-vector networks," *Machine Learning*, vol. 20, pp. 273–297, 1995.

[151] J. A. Suykens and J. Vandewalle, "Least squares support vector machine classifiers," *Neural Processing Letters*, vol. 9, no. 3, pp. 293–300, 1999.

[152] E. Fix, *Discriminatory analysis: nonparametric discrimination, consistency properties*. USAF School of Aviation Medicine, 1985, vol. 1.

[153] D. S. Sisodia, R. B. Pachori, and L. Garg, *Handbook of Research on Advancements of Artificial Intelligence in Healthcare Engineering*. IGI Global, 2020.

[154] R. A. Fisher, "The use of multiple measurements in taxonomic problems," *Annals of Eugenics*, vol. 7, no. 2, pp. 179–188, 1936.

[155] L. Breiman, J. Friedman, C. J. Stone, and R. A. Olshen, *Classification and Regression Trees*. CRC Press, 1984.

[156] A. T. Azar and S. A. El-Said, "Performance analysis of support vector machines classifiers in breast cancer mammography recognition," *Neural Computing and Applications*, vol. 24, no. 5, pp. 1163–1177, 2014.

[157] T. Fawcett, "An introduction to ROC analysis," *Pattern Recognition Letters*, vol. 27, no. 8, pp. 861–874, 2006.

[158] L. E. DeLisi, K. U. Szulc, H. C. Bertisch, M. Majcher, and K. Brown, "Understanding structural brain changes in schizophrenia," *Dialogues in Clinical Neuroscience*, vol. 8, no. 1, pp. 71–78, 2006.

[159] A. Shalbaf, S. Bagherzadeh, and A. Maghsoudi, “Transfer learning with deep convolutional neural network for automated detection of schizophrenia from EEG signals,” *Physical and Engineering Sciences in Medicine*, vol. 43, pp. 1229–1239, 2020.

[160] F. S. Racz, O. Stylianou, P. Mukli, and A. Eke, “Multifractal and entropy-based analysis of delta band neural activity reveals altered functional connectivity dynamics in schizophrenia,” *Frontiers in Systems Neuroscience*, vol. 14, p. 49, 2020.

[161] Z. Aslan and M. Akin, “Automatic detection of schizophrenia by applying deep learning over spectrogram images of EEG signals.” *Traitement du Signal*, vol. 37, no. 2, pp. 235–244, 2020.

[162] K. Singh, S. Singh, and J. Malhotra, “Spectral features based convolutional neural network for accurate and prompt identification of schizophrenic patients,” *Proceedings of the Institution of Mechanical Engineers, Part H: Journal of Engineering in Medicine*, vol. 235, pp. 167–184, 2021.

[163] A. N. Chandran, K. Sreekumar, and D. Subha, “EEG-based automated detection of schizophrenia using long short-term memory (LSTM) network,” in *Advances in Machine Learning and Computational Intelligence*. Springer, 2020, pp. 229–236.

[164] N. Jackson, S. R. Cole, B. Voytek, and N. C. Swann, “Characteristics of waveform shape in Parkinson’s disease detected with scalp electroencephalography,” *eNeuro*, vol. 6, no. 3, 2019.

[165] D.-H. Jeong, Y.-D. Kim, I.-U. Song, Y.-A. Chung, and J. Jeong, “Wavelet energy and wavelet coherence as EEG biomarkers for the diagnosis of Parkinson’s disease-related dementia and Alzheimer’s disease,” *Entropy*, vol. 18, no. 1, p. 8, 2016.

[166] G. Liu, Y. Zhang, Z. Hu, X. Du, W. Wu, C. Xu, X. Wang, and S. Li, “Complexity analysis of electroencephalogram dynamics in patients with Parkinson’s disease,” *Parkinson’s Disease*, vol. 2017, no. 1, p. 8701061, 2017.

[167] E. Naghsh, M. F. Sabahi, and S. Beheshti, “Spatial analysis of EEG signals for

Parkinson's disease stage detection," *Signal, Image and Video Processing*, vol. 14, no. 2, pp. 397–405, 2020.

[168] N. Betrouni, A. Delval, L. Chaton, L. Defebvre, A. Duits, A. Moonen, A. F. Leentjens, and K. Dujardin, "Electroencephalography-based machine learning for cognitive profiling in Parkinson's disease: Preliminary results," *Movement Disorders*, vol. 34, no. 2, pp. 210–217, 2019.

[169] S. L. Oh, Y. Hagiwara, U. Raghavendra, R. Yuvaraj, N. Arunkumar, M. Murugappan, and U. R. Acharya, "A deep learning approach for Parkinson's disease diagnosis from EEG signals," *Neural Computing and Applications*, vol. 32, pp. 10 927–10 933, 2020.

[170] H. W. Loh, C. P. Ooi, E. Palmer, P. D. Barua, S. Dogan, T. Tuncer, M. Baygin, and U. R. Acharya, "GaborPDNet: Gabor transformation and deep neural network for Parkinson's disease detection using EEG signals," *Electronics*, vol. 10, no. 14, p. 1740, 2021.

[171] M. F. Anjum, S. Dasgupta, R. Mudumbai, A. Singh, J. F. Cavanagh, and N. S. Narayanan, "Linear predictive coding distinguishes spectral EEG features of Parkinson's disease," *Parkinsonism & Related Disorders*, vol. 79, pp. 79–85, 2020.

[172] J. S. George, J. Strunk, R. Mak-McCully, M. Houser, H. Poizner, and A. R. Aron, "Dopaminergic therapy in Parkinson's disease decreases cortical beta band coherence in the resting state and increases cortical beta band power during executive control," *NeuroImage: Clinical*, vol. 3, pp. 261–270, 2013.

[173] K. Li, B. Ao, X. Wu, Q. Wen, E. Ul Haq, and J. Yin, "Parkinson's disease detection and classification using EEG based on deep CNN-LSTM model," *Biotechnology and Genetic Engineering Reviews*, pp. 1–20, 2023.

[174] S. Qiu, H. Zhao, N. Jiang, Z. Wang, L. Liu, Y. An, H. Zhao, X. Miao, R. Liu, and G. Fortino, "Multi-sensor information fusion based on machine learning for real applications in human activity recognition: State-of-the-art and research challenges," *Information Fusion*, vol. 80, pp. 241–265, 2022.

[175] A. Delorme and S. Makeig, "EEGLAB: An open source toolbox for analysis of single-trial EEG dynamics including independent component analysis," *Journal of Neuroscience Methods*, vol. 134, no. 1, pp. 9–21, 2004.

[176] L. D. Iasemidis, J. Chris Sackellares, H. P. Zaveri, and W. J. Williams, "Phase space topography and the Lyapunov exponent of electrocorticograms in partial seizures," *Brain Topography*, vol. 2, pp. 187–201, 1990.

[177] R. Sharma and R. B. Pachori, "Classification of epileptic seizures in EEG signals based on phase space representation of intrinsic mode functions," *Expert Systems with Applications*, vol. 42, no. 3, pp. 1106–1117, 2015.

[178] S. I. Khan and R. B. Pachori, "Automated classification of lung sound signals based on empirical mode decomposition," *Expert Systems with Applications*, vol. 184, p. 115456, 2021.

[179] F. Takens, "Detecting strange attractors in turbulence," in *Dynamical Systems and Turbulence, Warwick 1980: Proceedings of a symposium held at the University of Warwick 1979/80*. Springer, 2006, pp. 366–381.

[180] K. Atkinson, *An Introduction to Numerical Analysis*. John Wiley & Sons, 1991.

[181] R. B. Pachori and K. Das, "System and method for predicting Parkinson's disease," 2022, Indian Patent, Application no: 202221027358.

[182] M. V. Yeo, X. Li, K. Shen, and E. P. Wilder-Smith, "Can SVM be used for automatic EEG detection of drowsiness during car driving?" *Safety Science*, vol. 47, no. 1, pp. 115–124, 2009.

[183] A. G. Lalkhen and A. McCluskey, "Clinical tests: sensitivity and specificity," *Continuing Education in Anaesthesia Critical Care & Pain*, vol. 8, no. 6, pp. 221–223, 2008.

[184] T. Hanakawa, M. A. Dimyan, and M. Hallett, "Motor planning, imagery, and execution in the distributed motor network: a time-course study with functional MRI," *Cerebral Cortex*, vol. 18, no. 12, pp. 2775–2788, 2008.

[185] P. Gaur, R. B. Pachori, H. Wang, and G. Prasad, "An automatic subject specific intrinsic mode function selection for enhancing two-class EEG-based motor imagery-brain computer interface," *IEEE Sensors Journal*, vol. 19, no. 16, pp. 6938–6947, 2019.

[186] H.-L. Halme and L. Parkkonen, "Across-subject offline decoding of motor imagery from MEG and EEG," *Scientific Reports*, vol. 8, no. 1, pp. 1–12, 2018.

[187] S. Izumi, T. W. Findley, T. Ikai, J. Andrews, M. Daum, and N. Chino, "Facilitatory effect of thinking about movement on motor-evoked potentials to transcranial magnetic stimulation of the brain," *American Journal of Physical Medicine & Rehabilitation*, vol. 74, no. 3, pp. 207–213, 1995.

[188] H. Boecker, A. O. Ceballos-Baumann, P. Bartenstein, A. Dagher, K. Forster, B. Haslinger, D. J. Brooks, M. Schwaiger, and B. Conrad, "A H215O positron emission tomography study on mental imagery of movement sequences—the effect of modulating sequence length and direction," *Neuroimage*, vol. 17, no. 2, pp. 999–1009, 2002.

[189] V. V. Nikouline, K. Linkenkaer-Hansen, H. Wikström, M. Kesäniemi, E. V. Antonova, R. J. Ilmoniemi, and J. Huttunen, "Dynamics of mu-rhythm suppression caused by median nerve stimulation: a magnetoencephalographic study in human subjects," *Neuroscience Letters*, vol. 294, no. 3, pp. 163–166, 2000.

[190] G. Pfurtscheller and F. L. Da Silva, "Event-related EEG/MEG synchronization and desynchronization: basic principles," *Clinical Neurophysiology*, vol. 110, no. 11, pp. 1842–1857, 1999.

[191] H. Ramoser, J. Muller-Gerking, and G. Pfurtscheller, "Optimal spatial filtering of single trial EEG during imagined hand movement," *IEEE Transactions on Rehabilitation Engineering*, vol. 8, no. 4, pp. 441–446, 2000.

[192] K. K. Ang, Z. Y. Chin, H. Zhang, and C. Guan, "Filter bank common spatial pattern (FBCSP) in brain-computer interface," in *2008 IEEE International Joint Conference*

on Neural Networks (IEEE World Congress on Computational Intelligence). IEEE, 2008, pp. 2390–2397.

[193] N. ur Rehman and H. Aftab, "Multivariate variational mode decomposition," *IEEE Transactions on Signal Processing*, vol. 67, no. 23, pp. 6039–6052, 2019.

[194] P. Gaur, R. B. Pachori, H. Wang, and G. Prasad, "A multi-class EEG-based BCI classification using multivariate empirical mode decomposition based filtering and Riemannian geometry," *Expert Systems with Applications*, vol. 95, pp. 201–211, 2018.

[195] K. Wang, M. Xu, Y. Wang, S. Zhang, L. Chen, and D. Ming, "Enhance decoding of pre-movement EEG patterns for brain–computer interfaces," *Journal of Neural Engineering*, vol. 17, no. 1, p. 016033, 2020.

[196] J. Jin, Y. Miao, I. Daly, C. Zuo, D. Hu, and A. Cichocki, "Correlation-based channel selection and regularized feature optimization for mi-based bci," *Neural Networks*, vol. 118, pp. 262–270, 2019.

[197] P. Gaur, R. B. Pachori, H. Wang, and G. Prasad, "An empirical mode decomposition based filtering method for classification of motor-imagery EEG signals for enhancing brain-computer interface," in *2015 International Joint Conference on Neural Networks (IJCNN)*. IEEE, 2015, pp. 1–7.

[198] J. Jin, R. Xiao, I. Daly, Y. Miao, X. Wang, and A. Cichocki, "Internal feature selection method of CSP based on L1-norm and Dempster-Shafer theory," *IEEE Transactions on Neural Networks and Learning Systems*, 2020.

[199] J. Jin, H. Fang, I. Daly, R. Xiao, Y. Miao, X. Wang, and A. Cichocki, "Optimization of model training based on iterative minimum covariance determinant in motor-imagery bci," *International Journal of Neural Systems*, vol. 31, no. 07, p. 2150030, 2021.

[200] C. Brunner, R. Leeb, G. Müller-Putz, A. Schlögl, and G. Pfurtscheller, "BCI competition 2008–Graz data set a," *Institute for Knowledge Discovery (Laboratory of Brain-Computer Interfaces), Graz University of Technology*, vol. 16, pp. 1–6, 2008.

[201] A. Schlögl, F. Lee, H. Bischof, and G. Pfurtscheller, "Characterization of four-class motor imagery EEG data for the BCI-competition 2005," *Journal of Neural Engineering*, vol. 2, no. 4, p. L14, 2005.

[202] K. A. Ludwig, R. M. Miriani, N. B. Langhals, M. D. Joseph, D. J. Anderson, and D. R. Kipke, "Using a common average reference to improve cortical neuron recordings from microelectrode arrays," *Journal of Neurophysiology*, vol. 101, no. 3, pp. 1679–1689, 2009.

[203] B. Blankertz, R. Tomioka, S. Lemm, M. Kawanabe, and K.-R. Muller, "Optimizing spatial filters for robust EEG single-trial analysis," *IEEE Signal Processing Magazine*, vol. 25, no. 1, pp. 41–56, 2007.

[204] A. M. Azab, L. Mihaylova, K. K. Ang, and M. Arvaneh, "Weighted transfer learning for improving motor imagery-based brain–computer interface," *IEEE Transactions on Neural Systems and Rehabilitation Engineering*, vol. 27, no. 7, pp. 1352–1359, 2019.

[205] Y. Zhang, C. S. Nam, G. Zhou, J. Jin, X. Wang, and A. Cichocki, "Temporally constrained sparse group spatial patterns for motor imagery BCI," *IEEE Transactions on Cybernetics*, vol. 49, no. 9, pp. 3322–3332, 2018.

[206] J. Jin, Z. Wang, R. Xu, C. Liu, X. Wang, and A. Cichocki, "Robust similarity measurement based on a novel time filter for SSVEPs detection," *IEEE Transactions on Neural Networks and Learning Systems*, vol. 34, no. 8, pp. 4096–4105, 2021.

[207] Y. Li, F. Wang, Y. Chen, A. Cichocki, and T. Sejnowski, "The effects of audiovisual inputs on solving the cocktail party problem in the human brain: an fMRI study," *Cerebral Cortex*, vol. 28, no. 10, pp. 3623–3637, 2018.

[208] P. Gaur, R. B. Pachori, H. Wang, and G. Prasad, "A multivariate empirical mode decomposition based filtering for subject independent BCI," in *2016 27th Irish Signals and Systems Conference (ISSC)*. IEEE, 2016, pp. 1–7.

[209] M. Grosse-Wentrup and M. Buss, "Multiclass common spatial patterns and information theoretic feature extraction," *IEEE Transactions on Biomedical Engineering*, vol. 55, no. 8, pp. 1991–2000, 2008.

[210] Y. Peng, F. Qin, W. Kong, Y. Ge, F. Nie, and A. Cichocki, "GFIL: A unified framework for the importance analysis of features, frequency bands and channels in EEG-based emotion recognition," *IEEE Transactions on Cognitive and Developmental Systems*, vol. 14, no. 3, pp. 935 – 947, 2021.

[211] E. Erkan and M. Akbaba, "A study on performance increasing in SSVEP based BCI application," *Engineering Science and Technology, an International Journal*, vol. 21, no. 3, pp. 421–427, 2018.

[212] M. Cheng, X. Gao, S. Gao, and D. Xu, "Design and implementation of a brain-computer interface with high transfer rates," *IEEE Transactions on Biomedical Engineering*, vol. 49, no. 10, pp. 1181–1186, 2002.

[213] Z. Lin, C. Zhang, W. Wu, and X. Gao, "Frequency recognition based on canonical correlation analysis for SSVEP-based BCIs," *IEEE Transactions on Biomedical Engineering*, vol. 53, no. 12, pp. 2610–2614, 2006.

[214] Y. Zhang, G. Zhou, J. Jin, M. Wang, X. Wang, and A. Cichocki, "L1-regularized multiway canonical correlation analysis for SSVEP-based BCI," *IEEE Transactions on Neural Systems and Rehabilitation Engineering*, vol. 21, no. 6, pp. 887–896, 2013.

[215] X. Chen, Y. Wang, S. Gao, T.-P. Jung, and X. Gao, "Filter bank canonical correlation analysis for implementing a high-speed SSVEP-based brain–computer interface," *Journal of Neural Engineering*, vol. 12, no. 4, p. 046008, 2015.

[216] X. Zheng, X. Zhang, G. Xu, and R. Zhang, "Enhancing performance of single-channel SSVEP-based visual acuity assessment via mode decomposition," *IEEE Transactions on Neural Systems and Rehabilitation Engineering*, vol. 31, pp. 4203–4210, 2023.

[217] Y.-F. Chen, K. Atal, S.-Q. Xie, and Q. Liu, "A new multivariate empirical mode decomposition method for improving the performance of SSVEP-based brain–computer interface," *Journal of Neural Engineering*, vol. 14, no. 4, p. 046028, 2017.

[218] L. Chang, R. Wang, and Y. Zhang, "Decoding SSVEP patterns from EEG via multivariate variational mode decomposition-informed canonical correlation analysis," *Biomedical Signal Processing and Control*, vol. 71, p. 103209, 2022.

[219] Y.-E. Lee, G.-H. Shin, M. Lee, and S.-W. Lee, "Mobile BCI dataset of scalp-and ear-EEGs with ERP and SSVEP paradigms while standing, walking, and running," *Scientific Data*, vol. 8, no. 1, p. 315, 2021.

[220] T. Anderson, *An Introduction to Multivariate Statistical Analysis*. Wiley, 2003.

[221] E. Alpaydin, *Introduction to Machine Learning*. MIT press, 2020.

[222] M. Ramzan, H. U. Khan, S. M. Awan, A. Ismail, M. Ilyas, and A. Mahmood, "A survey on state-of-the-art drowsiness detection techniques," *IEEE Access*, vol. 7, pp. 61 904–61 919, 2019.

[223] S. Lee, M. Q. Khan, and M. N. Husen, "Continuous car driving intent detection using structural pattern recognition," *IEEE Transactions on Intelligent Transportation Systems*, vol. 22, pp. 1001–1013, 2020.

[224] W. S. Schinkel, T. P. van der Sande, and H. Nijmeijer, "Driver intervention detection via real-time transfer function estimation," *IEEE Transactions on Intelligent Transportation Systems*, vol. 22, pp. 772–781, 2019.

[225] J. A. Healey and R. W. Picard, "Detecting stress during real-world driving tasks using physiological sensors," *IEEE Transactions on Intelligent Transportation Systems*, vol. 6, no. 2, pp. 156–166, 2005.

[226] E. C. Djamal, D. P. Pangestu, and D. A. Dewi, "EEG-based recognition of attention state using wavelet and support vector machine," in *2016 International Seminar on Intelligent Technology and Its Applications (ISITIA)*. IEEE, 2016, pp. 139–144.

[227] K. T. Chui, K. F. Tsang, H. R. Chi, B. W. K. Ling, and C. K. Wu, “An accurate ECG-based transportation safety drowsiness detection scheme,” *IEEE Transactions on Industrial Informatics*, vol. 12, no. 4, pp. 1438–1452, 2016.

[228] T. G. Monteiro, C. Skourup, and H. Zhang, “Using EEG for mental fatigue assessment: A comprehensive look into the current state of the art,” *IEEE Transactions on Human-Machine Systems*, vol. 49, no. 6, pp. 599–610, 2019.

[229] P. Aricò, G. Borghini, G. Di Flumeri, A. Colosimo, S. Pozzi, and F. Babiloni, “A passive brain–computer interface application for the mental workload assessment on professional air traffic controllers during realistic air traffic control tasks,” *Progress in Brain Research*, vol. 228, pp. 295–328, 2016.

[230] J. Yin, J. Hu, and Z. Mu, “Developing and evaluating a mobile driver fatigue detection network based on electroencephalograph signals,” *Healthcare Technology Letters*, vol. 4, no. 1, pp. 34–38, 2017.

[231] T. Tuncer, S. Dogan, F. Ertam, and A. Subasi, “A dynamic center and multi threshold point based stable feature extraction network for driver fatigue detection utilizing EEG signals,” *Cognitive Neurodynamics*, vol. 15, no. 2, pp. 223–237, 2021.

[232] I. Latreche, S. Slatnia, and O. Kazar, “CNN-LSTM to identify the most informative EEG-based driver drowsiness detection brain region,” in *2022 International Symposium on Multidisciplinary Studies and Innovative Technologies (ISMSIT)*. IEEE, 2022, pp. 725–730.

[233] C. Lee and J. An, “LSTM-CNN model of drowsiness detection from multiple consciousness states acquired by EEG,” *Expert Systems with Applications*, vol. 213, p. 119032, 2023.

[234] A. Chaudhuri and A. Routray, “Driver fatigue detection through chaotic entropy analysis of cortical sources obtained from scalp EEG signals,” *IEEE Transactions on Intelligent Transportation Systems*, vol. 21, no. 1, pp. 185–198, 2019.

[235] J. Min, P. Wang, and J. Hu, “Driver fatigue detection through multiple entropy fusion analysis in an EEG-based system,” *PLoS One*, vol. 12, no. 12, p. e0188756, 2017.

[236] G. Li and W.-Y. Chung, “Combined EEG-gyroscope-tDCS brain machine interface system for early management of driver drowsiness,” *IEEE Transactions on Human-Machine Systems*, vol. 48, no. 1, pp. 50–62, 2017.

[237] J. Cui, Z. Lan, Y. Liu, R. Li, F. Li, O. Sourina, and W. Müller-Wittig, “A compact and interpretable convolutional neural network for cross-subject driver drowsiness detection from single-channel EEG,” *Methods*, vol. 202, pp. 173–184, 2022.

[238] A. Subasi, A. Saikia, K. Bagedo, A. Singh, and A. Hazarika, “EEG based driver fatigue detection using FAWT and multiboosting approaches,” *IEEE Transactions on Industrial Informatics*, vol. 18, no. 10, pp. 6602–6609, 2022.

[239] Ç. İ. Acı, M. Kaya, and Y. Mishchenko, “Distinguishing mental attention states of humans via an EEG-based passive BCI using machine learning methods,” *Expert Systems with Applications*, vol. 134, pp. 153–166, 2019.

[240] P. Maragos, J. F. Kaiser, and T. F. Quatieri, “Energy separation in signal modulations with application to speech analysis,” *IEEE Transactions on Signal Processing*, vol. 41, no. 10, pp. 3024–3051, 1993.

[241] R. B. Pachori and P. Sircar, “Analysis of multicomponent AM-FM signals using FB-DESA method,” *Digital Signal Processing*, vol. 20, no. 1, pp. 42–62, 2010.

[242] K. Fu, J. Qu, Y. Chai, and T. Zou, “Hilbert marginal spectrum analysis for automatic seizure detection in EEG signals,” *Biomedical Signal Processing and Control*, vol. 18, pp. 179–185, 2015.

[243] P. A. Bizopoulos, D. G. Tsalikakis, A. T. Tzallas, D. D. Koutsouris, and D. I. Fotiadis, “EEG epileptic seizure detection using k-means clustering and marginal spectrum based on ensemble empirical mode decomposition,” in *13th IEEE International Conference on Bioinformatics and Bioengineering*. IEEE, 2013, pp. 1–4.

[244] I. Goodfellow, Y. Bengio, A. Courville, and Y. Bengio, *Deep Learning*. MIT Press Cambridge, 2016.

[245] R.-N. Duan, J.-Y. Zhu, and B.-L. Lu, "Differential entropy feature for EEG-based emotion classification," in *2013 6th International IEEE/EMBS Conference on Neural Engineering (NER)*. IEEE, 2013, pp. 81–84.

[246] S. Arif, M. Arif, S. Munawar, Y. Ayaz, M. J. Khan, and N. Naseer, "EEG spectral comparison between occipital and prefrontal cortices for early detection of driver drowsiness," in *2021 International Conference on Artificial Intelligence and Mechatronics Systems (AIMS)*. IEEE, 2021, pp. 1–6.

[247] S. K. Lal and A. Craig, "A critical review of the psychophysiology of driver fatigue," *Biological Psychology*, vol. 55, no. 3, pp. 173–194, 2001.

[248] A. Matheus, G. Samer, W. Lu, H. Nengah, W. Samantha, S. Y. Carl, and M. Reena, "Machine learning polysomnographically-derived electroencephalography biomarkers predictive of Epworth sleepiness scale," *Scientific Reports*, vol. 13, no. 1, p. 9120, 2023.

[249] A. Hashemi, V. Saba, and S. N. Resalat, "Real time driver's drowsiness detection by processing the EEG signals stimulated with external flickering light," *Basic and Clinical Neuroscience*, vol. 5, no. 1, p. 22, 2014.

[250] Y. Zou, V. Nathan, and R. Jafari, "Automatic identification of artifact-related independent components for artifact removal in EEG recordings," *IEEE Journal of Biomedical and Health Informatics*, vol. 20, no. 1, pp. 73–81, 2014.

List of Publications

Outcomes from Ph.D. thesis work

In Refereed Journals

1. **K. Das** and R.B. Pachori. Multivariate iterative filtering based SSVEP detection in mobile environment for brain-computer interface application. *IEEE Sensors Letters*, volume 8(4), pages 6003604, IEEE, 2024. DOI: 10.1109/LSENS.2024.3375378.

2. **K. Das** and R.B. Pachori. Electroencephalogram based motor imagery brain computer interface using multivariate iterative filtering and spatial filtering. *IEEE Transactions on Cognitive and Developmental Systems*, volume 15(3), pages 1408-1418, IEEE, 2023. DOI: 10.1109/TCDS.2022.3214081.

3. **K. Das** and R.B. Pachori. Schizophrenia detection technique using multivariate iterative filtering and multichannel EEG signals. *Biomedical Signal Processing and Control*, volume 67(102525), pages 1-10, Elsevier, 2021. DOI: 10.1016/j.bspc.2021.102525.

4. **K. Das** and R.B. Pachori. Automated mental fatigue detection from EEG using joint time-frequency representation based on multivariate iterative filtering. *IEEE Transactions on Cognitive and Developmental Systems*. (Under review)

5. **K. Das** and R.B. Pachori. Multivariate iterative filtering enabled AI framework for Parkinson's disease identification from EEG. *IEEE Transaction on Artificial Intelligence*. (Under review)

In Book chapters

1. **K. Das**, V. K. Singh, and R.B. Pachori. Introduction to EEG signal recording and processing. *In Artificial Intelligence Enabled Signal Processing based Models for Neural Information Processing*. CRC Press, 2023.

2. **K. Das**, A. Mondal, N. Phukan, and R.B. Pachori. Multivariate adaptive signal decomposition techniques and their applications to EEG signal processing: An introduction. *In Handbook of Neural Engineering, Vol. 1: Signal Processing Strategies*. Elsevier, 2023.

Patent

1. R.B. Pachori and **K. Das**. System and method for predicting Parkinson's disease, 2022. Indian Patent, Application no: 202221027358.

Outcomes from other than Ph.D. thesis work

In Refereed Journals

1. A. Nalwaya, **K. Das**, and R.B. Pachori. Electroencephalogram rhythms-based automated emotion identification using multivariate variational mode decomposition. *IEEE Sensors Journal*, volume 24(13), pages 20920-20927, IEEE, 2024. DOI: 10.1109/JSEN.2024.3398050.

2. V. Paliwal, **K. Das**, S. M. Doesburg, G. Medvedev, P. Xi, U. Ribary, R.B. Pachori, and V. A. Vakorin. Brain age prediction from routine clinical electroencephalograms using multivariate iterative filtering and convolutional neural networks. *IEEE Transactions on Neural Systems and Rehabilitation Engineering*, volume 32, pages 2038-2048, IEEE, 2024. DOI: 10.1109/TNSRE.2024.3403198.

3. R. Krishna, **K. Das**, H. K. Meena, and R.B. Pachori. Spectral graph wavelet transform based feature representation for automated classification of emotions from EEG signal. *IEEE Sensors Journal*, volume 23(24), pages 31229-31236, IEEE, 2023. DOI: 10.1109/JSEN.2023.3330090.

4. A. Nalwaya, **K. Das**, and R.B. Pachori. Automated emotion identification using Fourier–Bessel domain-based entropies. *Entropy*, volume 24, page 1322, MDPI, 2022. DOI: 10.3390/e24101322.

5. A. Mahato, **K. Das**, and R.B. Pachori. A multivariate approach for drowsiness detection using empirical Fourier decomposition. *IEEE Transactions on Instrumentation and Measurement*. (Under review)

6. S. P. Kamaraju, **K. Das**, and R.B. Pachori. Electroencephalogram based biometric authentication system using multivariate Fourier-Bessel series expansion-based entropies. *IEEE Transactions on Biometrics, Behavior, and Identity Science*. (Under review)

7. P. K. Chaudhary, **K. Das**, and R.B. Pachori. Breast cancer diagnosis using iterative Fourier-Bessel decomposition method based CNN-kernel features. *IEEE Transactions*

on Artificial Intelligence. (Under review)

In refereed conferences

1. A. Mahato, **K. Das**, V. M. Gadre, D. D. Mahapatra, and R.B. Pachori. Investigating the impact of Rudram mantra listening on brain activity: A scientific exploration. In Mind Brain and Consciousness Conference: Perspectives from Indian Knowledge System, Mandi, India. Springer, 2023. (Accepted)

2. **K. Das**, P. Verma, and R.B. Pachori. Assessment of chanting effects using EEG signals. In 2022 24th International Conference on Digital Signal Processing and its Applications (DSPA), pages 1–5. Moscow, Russia, IEEE, 2022.

In Book chapters

1. **K. Das** and R.B. Pachori. Advanced signal processing and machine learning techniques for computer-aided medical diagnosis. *In Non-stationary and Nonlinear Data Processing for Automated Computer-aided Medical Diagnosis*, Elsevier, 2024. (Accepted)

2. A. Nalwaya, **K. Das**, and R.B. Pachori. Emotion identification from TQWT-based EEG rhythms. *In AI-Enabled Smart Healthcare Using Biomedical Signals*, IGI Global, 2022.

About The Author

Kritiprsanna Das was born in Hooghly, India, in January 1995. He received a Bachelor of Technology (B.Tech.) degree in Electronics and Communication Engineering from the Academy of Technology (Affiliated under Maulana Abul Kalam Azad University of Technology, formerly known as West Bengal University of Technology), India, in 2016 and Master of Technology (M.Tech.) degree in VLSI Design and Embedded Systems from the National Institute of Technology Arunachal Pradesh, India, in 2018. He joined the Ph.D. program in the Department of Electrical Engineering at the Indian Institute of Technology Indore, India, in July 2019. His research interests include nonstationary signal processing, time-frequency analysis, EEG signal processing, and neuroscience.